ELASTIC PLASTIC FRACTURE MECHANICS METHODOLOGY FOR SURFACE CRACKS

$\cancel{\text{No.}}$ NAG 8-243

SECOND SEMIANNUAL REPORT
CONTRACT MSFC CONTROL NO. 91-78

NASA MARSHALL SPACE FLIGHT CENTER
HUNTSVILLE, AL 35812

Project Monitor:

Mr. Wayne Gregg

Principal Investigator:

Dr. Hugo A. Ernst
Associate Professor

Researchers:

D. W. Boatwright
W. J. Curtin
D. M. Lambert

GEORGIA INSTITUTE OF TECHNOLOGY
THE GEORGE W. WOODRUFF SCHOOL OF MECHANICAL ENGINEERING
Atlanta, GA 30332-0405

August 1993

INDEX

1. Introduction

1.1 General

The safety and reliability of structures has always been a matter of vital concern to the aerospace industry. In this respect, fracture mechanics (FM) is a specially useful technology, since it can provide a quantitative description of the capability of structural parts to tolerate flaws. Initially, FM concepts covered quasi-linear elastic conditions (LEFM). Later, these methods were further developed to cover more general situations. Specifically, there was a need to extend these concepts to include cases where yielding was not necessarily contained in very small regions, for the case of new and tougher materials, higher loads, thinner sections, et cetera. This led to the development of the so-called Elastic Plastic Fracture Mechanics (EPFM) Methodology.

To apply these methods, two pieces of information are needed: the so-called material/specimen response to deformation, and the material response to crack extension. The former, obtained by finite element analysis or experimental calibration, consists of two expressions connecting the J-integral, load P, load-point displacement v, and crack length a for the specimen geometry of interest; the latter consists of a characterization of the way the material resists crack extension for the type of load applied: J, or a similar parameter, versus crack extension, for monotonic load, da/dN versus ΔK or ΔJ for cyclic loading, da/dt versus K, C^* or C_t for creep crack growth, et cetera. It

is assumed that within some limitations, these curves are specimen geometry independent, i.e., the curve obtained from a small laboratory specimen applies to the structural part under consideration, as well.

A simple computer program can be developed to combine the two pieces of information mentioned and assess the structural reliability of the structural part of interest.

It is very important to devote effort to guarantee that the curve of material response to crack extension is, in fact, geometry independent. That is, it is important to understand the limitations of the parameters and/or approaches used, identify clearly their limits of validity, and eventually improve the characterization of the phenomenon, proposing new parameters and methods to extend the range of applicability of existing models.

1.2 Elastic Plastic Fracture Mechanics

Specifically, for the case of EPFM applied to monotonic load, the mentioned limitations are expressed in terms of the amount of crack extension to ligament ratio, r, the ratio of ligament to applied J over the yield strength, m, and the ratio of logarithmic increase of J to logarithmic decrease in ligament, ω.

To overcome some of these limitations, particularly the one on r, Ernst [1.1] proposed a modified version of J called J_M. Resistance (R) curves plotted in terms of J_M were not subjected to the same limitations as those using J, and in general, showed

a better correlation between specimens of different size and geometry.

More recently, this methodology was further extended: general formulas were developed for J_M and J_D for growing cracks, criteria were proposed to identify the limits of applicability of both parameters, methods were presented to make use of the information of experimental points beyond this limit, and several schemes were proposed to extrapolate small laboratory specimen resistance curves to large amounts of crack extension, using J_M, J_D, or other parameters [1.2].

Although the progress made has been significant, and understanding has been gained on how to represent the R curve [1.2-1.6], there are still several very important points that need to be addressed before the method can be safely applied.

Among the most important ones, the need to extend this whole methodology to include cases involving three dimensions (3D) must be mentioned.

Specifically, it is mandatory to know how specimen thickness, constraint, and the possible dependence of the fracture mechanism on specimen thickness may affect the fracture resistance.

Ultimately, this knowledge gained from "2D" planar specimens should be used to explain and predict the behavior of real life 3D defects found in structures, i.e., surface or embedded cracks, et cetera.

1.3   The Leak Before Burst (LBB) Criterion

Pressure vessels containing surface flaws are often required to comply with the so-called LBB criterion. LBB is understood as the condition in which an assumed initial flaw will grow through the wall of a pressure vessel and cause leakage rather than bursting.

In particular, pressure vessels of interest to NASA have to comply to MIL-STD-1522A Standard General Requirements for Safe Design and Operation of Pressurized Missile and Space Systems. This document requires that: (1) a/2c (crack depth to total width ratio) needs to be in a range from 0.05 and 0.5, and (2) LBB will occur if $K_{Ic}/\sigma_{op} > 2\alpha B^{0.5}$ with $\alpha\sigma_{op} < \sigma_{ys}$ and $\alpha > 1$.

The rationale behind this expression is that the initial semi-elliptical flaw will grow in a self-similar manner, i.e., keeping a/2c constant until the crack depth a is exactly equal to the thickness B, as shown in Figure 1.1. At that time, it is considered that the flaw becomes a through crack with a total length of 2c, with $2c = (2c/a)_o B$, where the subscript 'o' stands for 'initial'. Finally, to prevent the crack from running unstably in the longitudinal direction, i.e., bursting, it is then required that the toughness K_{Ic} be bigger than the applied K given by $K_{app} = \sigma_{op}(\pi c)^{0.5}$.

The weaknesses of this Standard are these: (1) the above equation only holds for a/2c = 0.5, (2) the flaw shape is considered to always remain elliptical with constant a/2c, and (3) the whole analysis is based on LEFM concepts.

On the other hand, for the real materials, thicknesses, and typical flaws of interest, the situation is markedly different from the one assumed above, as can be seen in Figure 1.2. The cracks, clearly, do not grow in an elliptical self-similar manner, but rather in a very complex shape, with a dimension in the direction parallel to the surface, longer in the interior than on the surface. Moreover there is no guarantee that this dimension can be conservatively estimated by taking the original $(2c/a)_o$ and multiplying by B.

1.4 This Project

The EPFM Methodology has evolved significantly in the last several years. Nevertheless, some of these concepts need to be extended further before the whole methodology can be safely applied to structural parts. Specifically, there is a need to include the effect of constraint in the characterization of material resistance to crack growth and also to extend these methods to the case of 3D defects.

As a consequence, this project was started as a 36 month research program with the general objective of developing an elastic plastic fracture mechanics methodology to assess the structural reliability of pressure vessels and other parts of interest to NASA containing defects.

The project is divided into the following tasks.

Task 1. <u>Constraint</u> <u>and</u> <u>Thickness</u> <u>Effects</u>

This task includes the study of the problem of constraint and thickness effects, in different specimen sizes and geometries in materials of interest.

Specifically, the following subtasks will be performed:

a) The large body of available data from centers around the World will be gathered to study this effect in specimens of different size and geometry.

b) Resistance to crack growth tests will be conducted using specimens of different size and geometry, on at least one material of interest. The material will be provided by NASA; Georgia Tech will machine the lab specimens.

c) Characterization of fracture surfaces to determine mechanisms of fracture, and typical surface dimensions will be performed using modern quantitative metallographic techniques.

d) Using the information obtained, models will be developed to describe the effect of constraint on the growth of cracks under elastic plastic conditions.

Task 2.   Three Dimensional Cracks

The problem of applicability of EPFM concepts to 3D crack problems, in materials of interest, will be studied in this task. Specifically, the following subtasks will be performed:

a)   Plates containing surface cracks with different initial crack aspect ratios and relative crack to plate geometry dimension will be tested. The evolution of the crack shape (planar) and the crack surface displacement with loading will be determined.

b)   Analytical and numerical efforts will be devoted to determine values of J and constraint along the crack front.

c)   The models and information obtained from Task 1 will be used here to predict the behavior of these 3D cracks.

d)   Predictions and experimental resullts will be compared and, if necessary, refinement of the models will be made.

Task 3.   Leak Before Burst (LBB) Criterion

Finally, the body of information obtained in the previous tasks will be organized in a Methodology format to assess the structural integrity of parts containing defects, in the spirit of the current LBB criterion.

1.5 This Report

This report covers the activities of the period March 1993 through August 1993. In this period, full advantage was taken from the experience and knowledge gained in previous projects [1.6-1.9]. In particular, some efforts were devoted in this project to complete and extend previously obtained results.

The report is organized as follows: In Chapter 2, a computer modelling algorithm used to simulate the growth of a semi-elliptical surface crack is explained in detail. This is an excerpt from the thesis of D.W. Boatwright [1.9].

In Chapter 3, a finite element investigation is presented. This investigation, an excerpt of the thesis of W.J. Curtin [1.10], compared the theoretical (HRR) stress field to that produced by elastic and elastic-plastic models. The difference in these stress fields is the constraint effect.

In Chapter 4, experimental efforts to characterize three dimensional aspects of fracture present in "two dimensional", or planar configuration specimens have been continued. This discussion specifically contains a preliminary discussion

associated with the determination of, and use of, crack face

separation data.

1.6 References

[1.1]   Ernst, H. A., "Material Resistance and Instability beyond J-Controlled Crack Growth", *ASTM STP 803*, American Society for Testing and Materials, 1983.

[1.2]   Ernst, H. A. and Pollitz, E. T., "Fracture Toughness from Existing Surveillance Data", EPRI RP-2975-10, Preliminary Final Report, December 1988.

[1.3]   Landes, J. D., McCabe, D. E., and Ernst, H. A., "Elastic Plastic Methodology to Establish R-Curves and Instability Criteria", *EPRI Report RP-1238-2*, August 1982.

[1.4]   Kumar, V., German, M. D., and Shih, C. F., "An Engineering Approach for Elastic Plastic Fracture Analysis", *EPRI NP-1931*, July 1981.

[1.5]   Roos, E., Eisele, U., Silcher, H., and Spaeth, F., "The Influence of the Material Toughness and the State of Stress on Fracture of Large Scale Specimens", *Nuclear Engineering and Design* 102 (1987), Pp. 439-49.

[1.6]   Hiser, A., "Results of Testing A302", *private communications*, January 1988.

[1.7]   McCabe, D. E., and Ernst, H. A., "Predictive Methodology for Integrity of Tank Welds with Crack-like Defects:, *MEA Report*, November 1989.

[1.8]   Ernst, H. A., and Lambert, D. M., "Three Dimensional Aspects of Elastic Plastic Crack Growth", *NASA GSRP Grant, NGT-50641*.

[1.9]   Boatwright, D.W., *An Elastic-Plastic Fracrture Mechanics Analysis of Semi-Elliptical Surface Crack Growth*, Master's Thesis, Georgia Institute of Technology, April 1993.

[1.10]   Curtin, W.J., *An Investigation of a Two Parameter Elastic-Plastic Fracture Mechanics Methodology*, Master's Thesis, Georgia Institute of Technology, June 1993.
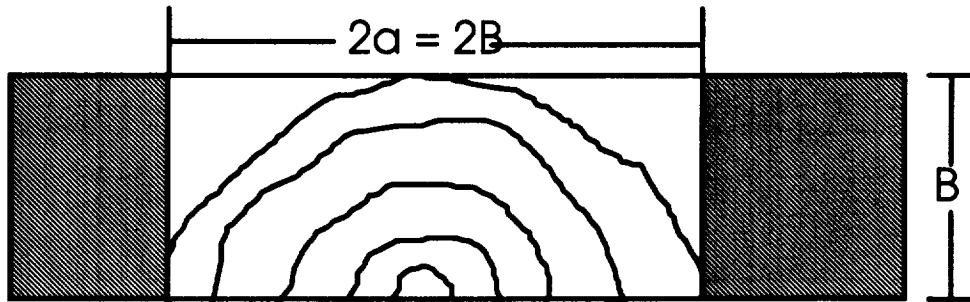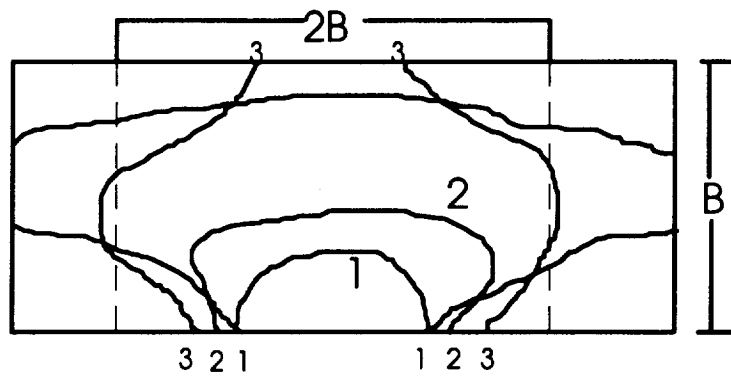
Figure 1 Simple Leak Criterion

Figure 2 Growth of a Part-Through Crack to Critical Size

CHAPTER III

COMPUTER MODELLING OF SURFACE CRACK GROWTH

Background

The best way to determine the physical response of a cracked body to a particular set of loading conditions is to run a test on the structure in question. Unfortunately, this is not a practical solution in many cases. One alternative to testing is to use a mathematical model that can predict the behavior of a test specimen in any given situation.

In order to use a mathematical model, it is first necessary to run a series of mechanical tests to characterize to behavior of the specimens. Once these tests have been run, it is then possible to use the test data to develop a valid model for the specimen in question. Today, libraries of functions exist that can be used to model most common fracture specimens given the material properties [18,22].

After developing a mathematical model that accurately predicts test results, the key parameters of the test can be changed to observe their influence on test results.

Currently, the only way to model a surface crack specimen is to run a three-dimensional finite element model. This modelling process is computationally intensive and very time consuming since a new finite element mesh must be constructed for each iteration in the solution process.

It would be far more efficient to develop a special purpose fracture mechanics based computer program designed to model surface crack behavior. One of the goals of this work was to do just that. This chapter covers the development and testing of a fracture mechanics based computer program for modelling the behavior of surface cracks.

The intent in the development of this computer program was to develop a program general enough to model any surface crack geometry in any material that is under J-dominant conditions. Given the material deformation and fracture properties, the program should accurately predict the distribution of crack growth along the front.

The program described in this chapter represents a continuation of the work begun by Sheldon and Ernst [14,15] in computer modelling of surface crack growth. The new version of the program attempts to overcome some of the problems that surfaced in the first program. There are also concepts integrated into the current program that were not in the original program.

One new feature that has been introduced into the current version of the program is displacement control rather than load control. The current version of the program uses plastic displacement as the evolutionary variable. In the first program, the load was increased in small increments to simulate a mechanical test. One problem that arose from the use of this method was that virtually all the crack growth occurred in the last few load steps. Use of displacement control corrected this problem because with displacement control the load increases very quickly at first and very slowly around maximum load which is where the majority of crack growth occurs. Another feature of displacement control is that the simulation can continue past the maximum load; that is, the applied load can decrease. This feature would be useful in leak-before-break analyses.

The program uses the key curve to calculate the load at each displacement step given the plastic displacement and the current crack geometry. The load and the crack geometry are then used to calculate the fracture variables along the crack front.

The incrementing of plastic displacement is not intended to directly parallel an actual mechanical test. Plastic displacement was chosen because it was a nondecreasing variable in the key curve equation. The other possible

evolutionary variables were load, the crack dimension a, and the crack dimension c.

The program does not use any component of displacement in the calculation of the conditions along the front. Although, it is possible to calculate the elastic and plastic components of displacement in a real mechanical test, through unloading compliance measurements, in order to relate the simulation to an actual test.

The original modelling technique used by Sheldon [15] divided the crack front into a collection of discrete points. Sheldon assigned values of a and c to each point along the front by fitting an ellipse to the point in question by using the position of the point, the position of the center of the ellipse, and the slope at that point as determined from the neighboring points. Sheldon then used these variables in a J calculation method as developed by McCabe, Ernst, and Newman [16] which was based on the Newman-Raju equations [7]. A value of J was calculated for each point along the front. A value of crack extension at each point was obtained from the material resistance curve, and the point was then advanced in the direction normal to the simulated crack front.

The original program would divide the crack front into two halves when the program detected that the surface crack was mushrooming, that is, when the crack started growing in a non-self-similar way. The program considered the crack to be

mushrooming when it detected a point with an approximately vertical slope. The section of the front from that point to the surface was modelled as a through crack with a crack length equal to the x coordinate of the point in question. The remainder of the crack front was modelled as a semi-elliptical crack as before.

While this scheme showed promise, there were some complications that could be avoided by the use of a different model. The main problem was that calculating J using two different models led to problems in establishing continuity of J and dJ/da along the front. The program scaled the J values in order to maintain continuity of J, but no consideration was given to continuity of dJ/da. The discontinuity in dJ/da led to excessive crack growth at the point of the discontinuity.

In part, the program developed in this chapter represents an evolutionary step forward. Modelling techniques that caused problems in the original program were modified. The use of two separate J estimation methods has been replaced by a single method that is used for all the points along the crack front. In addition to the evolutionary modifications, new features were added to the program to better model the fracture process. The primary addition to the program was the incorporation of constraint effects. The original version of the program as written by Sheldon [15] did not consider

constraint effects. The techniques used to model crack growth will be described in the following sections.

Computer Program Development

This program models the evolution of the crack front in a displacement controlled test of a rectangular surface crack panel in tension. The program requires prior knowledge of the material deformation properties, the plane strain resistance curve, and the key curve for the specimen. The plane strain resistance curve is intended to represent the material fracture properties for the most constrained state of stress, and the key curve for the specimen will be used to relate the plastic displacement and current crack geometry to the load. The key curve was obtained using the same material and specimen geometry under blunt notch, or non-growing crack, conditions as explained in Chapter II.

The program simulates a growing crack test by incrementing the plastic displacement. The user must enter the final plastic displacement along with the initial semi-elliptical crack geometry. The conditions along the crack front are recalculated and updated with each displacement step. The user is free to specify the number of displacement steps in any simulation.

In this model, the crack front is represented by discrete points. The user is free to specify the number of points along the crack front. Specifying a large number of points allows the user to see how the front evolves in detail, but the program takes longer to run. The solutions calculated are insensitive to the number of points along the front; so, there is no computational advantage gained by specifying a very large number of points.

It was sufficient to only consider one half of the front due to the symmetry of the problem. Boundary conditions on crack growth direction were applied at the surface and at the deepest point in order to enforce symmetry. Modelling only half the crack front halves the time it takes to run a simulation without affecting accuracy.

This program was written in GW-BASIC. A listing of the computer program is included in the Appendix.

J Estimation along the Crack Front

This program models the fracture process using a J resistance curve approach that incorporates constraint effects. This methodology was based on work done by McCabe, Ernst, and Newman [16]. In the first version of this program as developed by Sheldon and Ernst [14,15], a one-parameter approach to predicting fracture was used. In that program, J was calculated at each point along the crack front; then, the

crack extension was calculated from the material R-curve. This approach did not consider constraint effects. In the current version of the program, a two-parameter approach incorporating constraint was used to calculate crack extension at each point along the crack front. The first step in modelling the crack extension across the crack front was to calculate the value of J at each point on the front.

In Chapter I, it was shown that, given two cracked bodies subjected to the same loading history that differ in crack length by a small amount, the J integral can be defined as the difference in potential energy divided by the difference in cracked area. For a body where the crack only has a length dimension, the difference in cracked area, dA, is equal to the specimen thickness multiplied by the difference in crack lengths. It is not so simple for a geometry such as a surface crack that requires two length parameters. For example, a semi-elliptical surface crack requires the two length parameters a and c.

For a semi-elliptical surface crack, Ernst [23] showed that the expression for the global value of J is linked to the way the virtual crack extension is taken. Ernst examined three different ways for taking the virtual crack extension: 1) increasing c, keeping a constant, 2) increasing a, keeping c constant, and 3) increasing a and c, keeping a/c constant.

The following equations for the plastic portion of J were developed by Ernst. The only difference between the three cases is the expression for the coefficient η_{pl}.

$$J_{pl} = \frac{\eta_{pl}}{\left(\frac{\pi}{2}\right) a\, c} \int_0^{v_{pl}} P\, dv_{pl} \tag{3.1}$$

Taking the key curve equation, which relates load and plastic displacement, and substituting it for the variable P yields the following expression.

$$J_{pl} = \beta_o \frac{\eta_{pl}}{(\pi/2)\, a\, c} \frac{W t^2}{N+1} \left(\frac{a}{c}\right)^{-\frac{p}{N}} \left(\frac{a}{t}\right)^{-\frac{m}{N}} \left(\frac{P}{W t \beta_o}\right)^{\frac{N+1}{N}} \tag{3.2}$$

The expressions for η_{pl} turned out to be independent of the a/c and a/t ratios. These expressions are shown in Table 3.1.

Table 3.1: Expressions for η_{pl}

Variable Held Constant	η plastic Expression
a	-(p+m)/2
c	p/2
a/c	-m/2

At this point it was necessary to determine which method should be used to calculate the global J and how that global J relates to the values of J along the front. The following normalization scheme was developed for this purpose.

The total system energy in a cracked body can be expressed as follows.

$$W = E + U \qquad (3.3)$$

W = total energy supplied by external forces

E = energy spent growing the crack

U = strain energy

The energy release rate for an incremental crack extension can be written as follows.

$$\frac{\delta E}{\delta A} = \frac{1}{\delta A} \int_0^1 J \, ds \, dn \qquad (3.4)$$

The differential element ds represents an element along the crack front, and the differential element dn represents an element normal to the crack front. The above integral expression should be integrated along the entire crack front.

In addition, taking the derivative of the energy balance with respect to the virtual increase in cracked area yields the following relationship.

$$\frac{\delta W}{\delta A} = \frac{(\delta E + \delta U)}{\delta A} \qquad (3.5)$$

Replacing the incremental quantities in the above equation with experimentally measurable global quantities yields the following equations for constant displacement conditions.

$$\frac{\delta E}{\delta A} = -\left(\frac{\delta U}{\delta A}\right)_v \qquad (3.6a)$$

$$\frac{\delta E}{\delta A} = \frac{d}{dA}\int_0^v P\, dv \qquad (3.6b)$$

The above result is entirely independent of the geometry of the surface crack.

Now, for the case of growth of a semi-elliptical surface crack at a constant aspect ratio, Ernst shows that the following equations can be used to define ds,dn, and dA in terms of a, c, and elliptical angle, ϕ [23].

$$ds = \sqrt{(c\cos\phi)^2 + (a\sin\phi)^2}\, d\phi \qquad (3.7a)$$

$$dn = 2\, c\, \sqrt{(c\cos\phi)^2 + (a\sin\phi)^2}\, da \qquad (3.7b)$$

$$dA = \pi \, c \, da \qquad\qquad (3.7c)$$

Using these relationships allows the following definition of the energy release rate.

$$\frac{\delta E}{\delta A} = J_{avg} = (J)_{a/c \; constant} = \frac{2}{\pi} \int_0^{\frac{\pi}{2}} J(\phi) \, d\phi \qquad (3.8)$$

This result shows that the global J obtained by taking the virtual crack extension with a/c constant is numerically equal to the linear average of J along the crack front.

Since no assumptions were made regarding material behavior, the above equation applies for the elastic portion of J, the plastic portion of J, or the total J.

This J estimation technique uses the observation that the distribution of the plastic portion of J along the crack front follows the distribution of the elastic portion of J for moderate amount on deformation [24,25]. This relationship can be expressed as follows.

$$J_{pl}(\phi) = k \, G(\phi) \qquad\qquad (3.9)$$

Therefore,

$$J(\phi) = (1 + k) \, G(\phi) \qquad\qquad (3.10)$$

Following this line of reasoning the linear averages along the crack front should also be related as follows.

$$k = \frac{J_{pl,avg}}{G_{avg}}$$

(3.11)

Out of convenience, k was incorporated into a coefficient D that is independent of applied stress.

$$D = \frac{k}{\sigma^{(n+1)}}$$

(3.12)

By substitution, the value of D can be shown to be equal to the following expression.

$$D = \frac{0.224 \, n \, W}{\pi \, \beta_0 \, (n+1) \, (G_{avg}/\sigma^2)} \left(\frac{a}{c}\right)^{1-pn} \left(\frac{a}{t}\right)^{-2-mn}$$

(3.13)

The values of J along the crack front can be calculated using the following formula.

$$J(\phi) = G(\phi) \, (1 + D \, \sigma^{n-1})$$

(3.14)

Now, the linear elastic portion of J as predicted by the Newman-Raju equations can be used with the above equation to perform an elastic-plastic J analysis along the crack front.

Since the Newman-Raju equations are based on a semi-elliptical crack front, it was necessary to assign values of

a/c and a/t to each point. A value of a/c was assigned to each point based on the a/c of an ellipse centered at the origin that passed through the deepest point and the position of the point in question. The value of a/t was taken to be the depth of the central point divided by the thickness. This method is illustrated in Figure 3.1.

While this method of assigning values for a/c and a/t at each point is admittedly crude, the method was chosen because of its simplicity. The fact that this method is applicable at every point along the crack front prevents some of the problems that developed in the first attempt at simulating surface crack growth as developed by Sheldon [15].

Crack Growth Direction

For the purposes of this computer program, crack growth was assumed to occur normal to the local crack front as defined by the points that represent the evolving crack front. The normal direction was determined by taking a numerical derivative at the point in question.

As boundary conditions, the point at the front surface was constrained to growth along the surface, and the deepest point was constrained to growth through the depth.
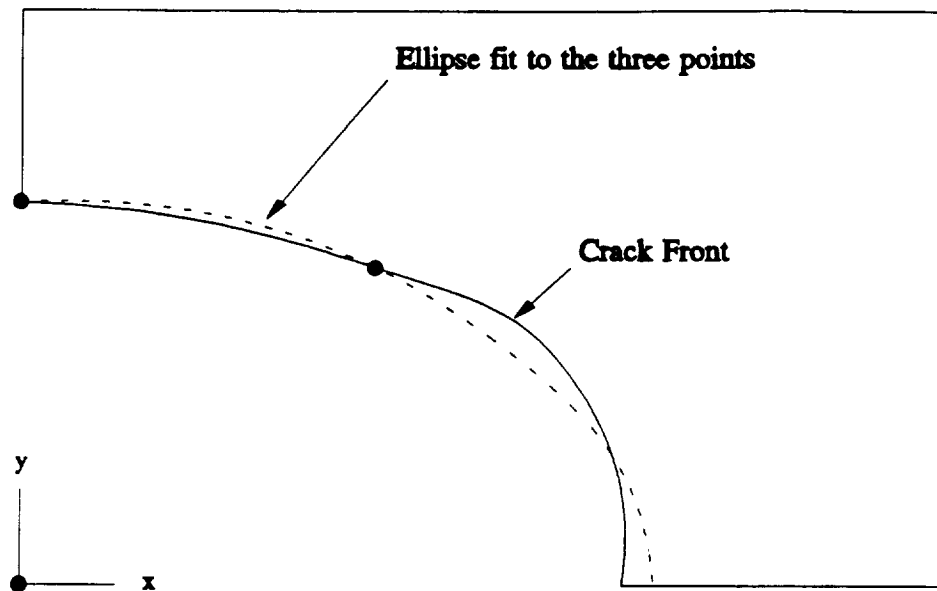
Figure 3.1: Procedure for Fitting an Ellipse

Crack Tip Constraint

Today, it is accepted that constraint influences the J R-Curve. ASTM acknowledged this idea in their recommendation of bend specimens for determining R-curves [17]. This recommendation was based on the fact that bend specimens exhibit more in-plane constraint than tension specimens, and, thus, produce a more conservative design specification. It should be noted here that two specimens with identical out-of-plane constraint, e.g. plane strain or plane stress, can exhibit different levels of in-plane constraint.

The typical differences in the R-Curves for bend and tension geometries illustrates how different levels of constraint affect the fracture properties of a material. The rate of change of the resistance curve slope is a function of constraint. Specimens under a high level of constraint have a slope that is lower than for low constraint configurations. Thus, the R-Curve for a high constraint situation would be below the R-Curve for a low constraint situation.

It has been widely shown that a one parameter approach to modelling surface crack growth is inadequate [26,27,28]. The incorporation of a measure of constraint into this computer program is an attempt to address the problems inherent in a one-parameter approach.

It has been shown by Ernst, Rush and McCabe [19] that there is a relationship between dJ/da and the level of constraint at the crack tip which they called $(\ell_{el})^{-1}$. The variable $(\ell_{el})^{-1}$ has been shown to characterize constraint. This variable was defined as follows.

$$(1_{el})^{-1} = \frac{\left(\frac{\partial G}{\partial a}\right)_P}{G} \qquad (3.15)$$

In calculating derivatives with respect to a virtual crack extension, a problem is again encountered in defining the manner that the virtual crack extension occurs. For the purpose of derivatives, the crack extension is assumed to

occur normal to the equivalent ellipse that is fit at the point in question. This convention was adopted in the interest of consistency since the values for J are calculated from the equivalent ellipses.

For the purposes of this computer simulation, dJ/da was chosen as a tool to incorporate constraint into the modelling of surface crack behavior. Briefly stated, the procedure calculates constraint effects by comparing dJ/da as calculated at a point on the crack front to dJ/da as calculated from the plane strain material resistance curve.

Constraint effects were calculated in the following manner. The value of dJ/da was calculated for each point on the crack front. These values were obtained by calculating the value of J a small distance ahead of the point in question. Another equivalent ellipse was fit through the new incrementally advanced point. The a/c and a/t obtained from the three point fit were then used to calculate J. The value of dJ/da was found by dividing the difference in J values by the distance between the points.

The methodology for incorporating constraint into the crack growth model began with the R-curve for $(\ell_{\theta 1})^{-1}$ equal to zero. This R-curve represents the most constrained situation possible and served as the reference for the fracture parameters calculated in the program. The following equation was used to model the R-curve.

$$\Delta \ a_{reference} = \alpha_o \ J^3 + \beta_o \ J^2 + \gamma_o \ J \qquad (3.16)$$

The R-curve for the side-grooved compact tension specimen was used in the computer program because the side-grooved compact tension specimen R-curve represented the most constrained geometry tested. The bend type loading and the side-grooves contributed to the high level of constraint in these specimens.

The derivative of Equation 3.16 served a reference to be compared to the values of dJ/da calculated in the program.

$$\left(\frac{dJ}{da} \right)_{reference} = \frac{1}{3 \ \alpha_o J^2 + 2 \ \beta_o J + \gamma_o} \qquad (3.17)$$

The factor F was defined as follows.

$$F = \frac{\left(\dfrac{dJ}{da} \right)}{\left(\dfrac{dJ}{da} \right)_{reference}} \qquad (3.18)$$

The prior assumption that constraint and dJ/da are related implies that constraint and the variable F are related. Substituting Equation 3.17 into Equation 3.18 yields the following.

$$\frac{dJ}{da} = \frac{F}{3\alpha_o J^2 + 2\beta J + \gamma_o} \tag{3.19}$$

Substitution of the above equation into the integral definition for crack extension yields the following expression.

$$\Delta a = \int_{a_o}^{a} \frac{3\alpha_o J^2 + 2\beta_o J + \gamma_o}{F} \, dJ \tag{3.20}$$

Integrating provides the formula for crack growth which incorporates constraint effects.

$$\Delta a = \frac{\Delta a_{reference}}{F} \tag{3.21}$$

Every point along the crack front had unique values for J and F. Together, the two parameters were used to calculate the crack extension at each point along the front. Once every point on the front had been advanced the appropriate amount, the plastic displacement was incremented, and the process began again at the new load.

Comparison of Computer Output to Experimental Data

It was initially hoped that this computer program could be used to model the 21-6-9 stainless steel surface crack tension specimens that were tested as part of this work, but, as shown in Chapter II, a J-based approach is invalid for this material. As a consequence, this computer program is inappropriate for prediction of crack growth in these stainless steel specimens.

While this program is admittedly inappropriate for modeling the fracture behavior in these stainless steel surface crack specimens, it is convenient to use the material data developed in testing these specimens to test the general behavior of the program. The purpose for using the data from the stainless steel specimens is simply to check the program for instability, discontinuities, or any other obvious shortcomings.

The results of three computer simulations are shown in Figure 3.2, 3.3, and 3.4. These figures compare the actual test results to the computer simulation for surface crack tension specimens SC16, SC11, and SC4, respectively. These surface crack specimens were chosen because they were all tested to a point past their maximum attainable load and they all exhibited significant crack growth. More specifically, these three specimens were chosen because their different
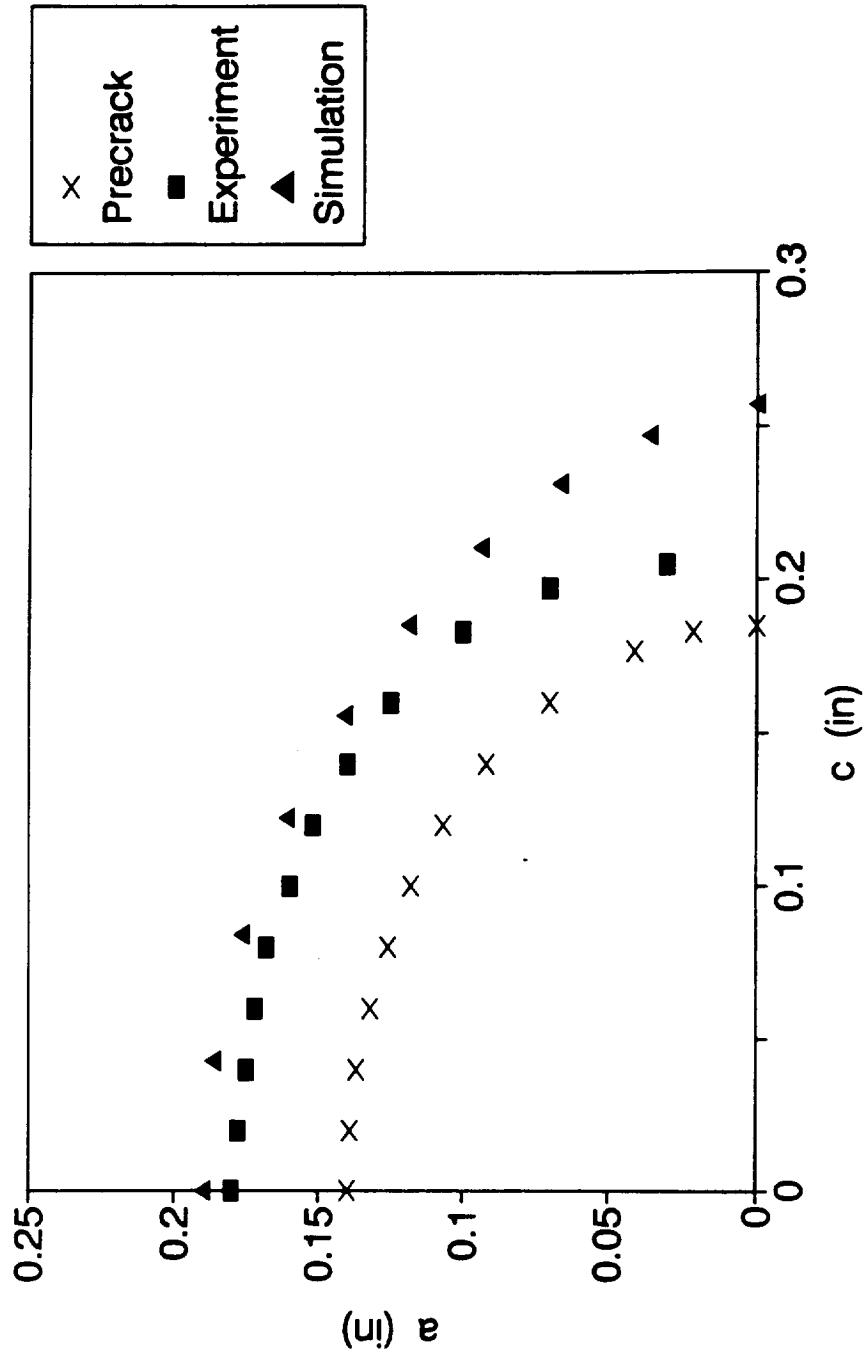
Figure 3.2: Comparison of Simulation to Test Data for SC16

Figure 3.3: Comparison of Simulation to Test Data for SC11
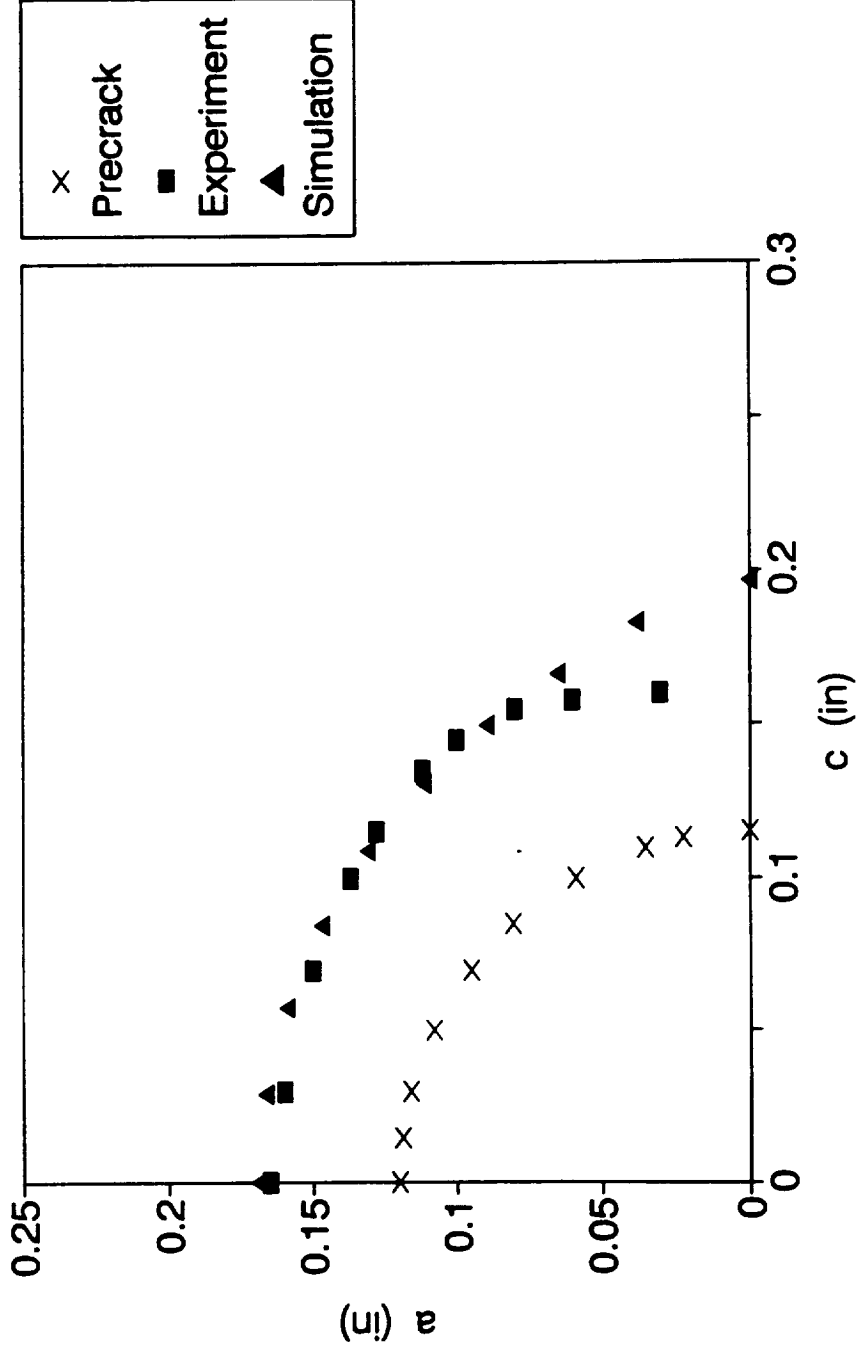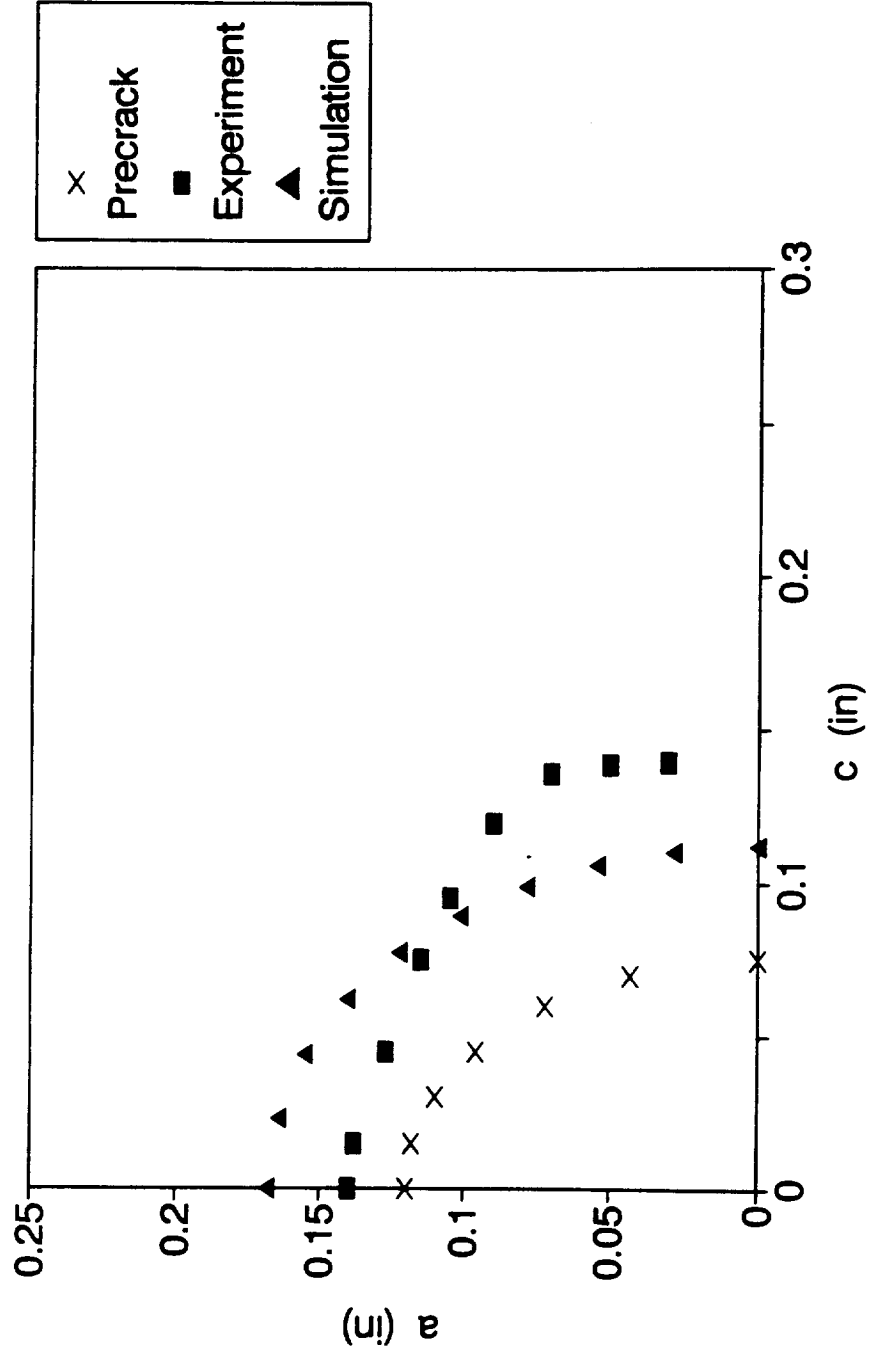
Figure 3.4: Comparison of Simulation to Test Data for SC4

aspect ratios. This allows an analysis of the performance of the computer program over a wide range of aspect ratios.

Discussion and Conclusions

The results of the computer simulation using the data from the stainless steel surface crack tests shows that the program performs as expected. The new crack fronts calculated by the program do not exhibit any discontinuities or instability problems. In order to effectively evaluate the accuracy of the program, it would be necessary to compare the predicted results to the experimental results obtained from a set of surface crack specimens tested under J-dominant conditions.

The experimental results presented in Chapter II show that the growth of these cracks is a deformation process. The photographs of these same specimens in Chapter II show the extensive plastic deformation around the crack mouth and at the back surface. The fact that the maximum loads for these specimens can be accurately predicted from deformation theory serves to reinforcing the assessment that a fracture mechanics based simulation for this material is inappropriate.

It is not possible to judge the simulation results based on a comparison with the stainless steel surface crack

specimens tested here. To make a definitive judgement on the accuracy of the simulation, it would be necessary to compare results for a material that was known to be under J-dominant testing conditions.

REFERENCES

1) Duga, J.J. et al, "The Economic Effects of Fracture in the United States." NBS Special Publication 647-2, United States Department of Commerce, Washington D.C., March 1983.

2) Westergaard, H. M., "Bearing Pressures and Cracks." *Journal of Applied Mechanics*, Vol. 6, 1939, pp A49-A53.

3) Irwin, G.R., "Fracture Dynamics." *Fracturing of Metals*, American Society for Metals, Cleveland, 1948, pp. 147-166.

4) Griffith, A.A. "The Phenomena of Rupture and Flow in Solids." *Philosophical Transactions*, Series A, Vol 221, 1920, pp. 163-198.

5) Inglis, C.E., "Stresses in a Plate Due to the Presence of Cracks and Sharp Corners." *Transactions of the Institute of Naval Architects*, Vol. 55, 1913, pp. 219-241.

6) Irwin, G.R., "The Crack Extension Force for a Part-Through Crack in a Plate." *Journal of Applied Mechanics*, 1962, pp. 651-654.

7) Newman, J.C., Jr. and I.S. Raju, "Stress-Intensity Factor Equation For Cracks in a Plate." ASTM STP 791, American Society for Testing and Materials, 1983, pp. I-238 - I-265.

8) Rice, J.R., "A Path-Independent Integral and the Approximate Analysis of Strain Concentration by Notches and Cracks." *Journal of Applied Mechanics*, Vol. 35, 1968, pp. 379-383.

9) Cherepanov, G.P., "Crack Propagation in Continuous Media." *Journal of Applied Mathematics and Mechanics Translation*, Vol. 31, 1967, pg. 564.

10) Hutchinson, J.W., "Singular Behavior at the End of a Tensile Crack Tip in a Hardening Material." *Journal of the Mechanics and Physics of Solids*, Vol. 16, 1968, pp. 13-31.

11) Rice, J.R. and G.F. Rosengren, "Plane Strain Deformation Near a Crack Tip in a Hardening Material." *Journal of the Mechanics and Physics of Solids*, Vol. 16, 1968, pp. 1-12.

12) Rice, J.R., W.J. Drugan, and T.L. Sham, "Elastic-Plastic Analysis of Growing Cracks." ASTM STP 700, American Society for Testing and Materials, 1980, pp. 189-221.

13) Ernst, H.A., "Material Resistance and Instability Beyond J-Controlled Crack Growth." ASTM STP 803, American Society for Testing and Materials, 1983, pp. I-191 - I-213.

14) Ernst, H.A., "Resistance Curve Analysis of Surface Cracks", Martin Marietta Manned Space Systems Contract SC-273276, Annual Report-Fiscal Year 1991.

15) Sheldon, J.W., "Growth of Semi-Elliptical Cracks in Ductile Materials," Georgia Institute of Technology, Thesis-June 1992.

16) McCabe, D.E., H.A. Ernst, and J.C. Newman, Jr., "Application of Elastic and Elastic-Plastic Fracture Mechanics Methods to Surface Flaws," Interim Report to Martin Marietta Corporation, March 1991.

17) "Standard Test Method for Determining J-R Curves," ASTM Standard E-1152-87, 1989 Annual Book of ASTM Standards, American Society for Testing and Materials, Vol. 3.01, 1989, pp 487-511.

18) Tada, H., P.C. Paris, and G.R. Irwin. The Stress Analysis of Cracks Handbook, Del Research Corporation. Hellertown, PA. 1973.

19) Ernst, H.A, and E.A. Pollitz. "Fracture Toughness of Surveillance Specimens." Report No. RP-2975-10. Electric Power Research Institute. Palo Alto, CA, 1989.

20) Begley, J.A., and J.D. Landes. "Serendipity and the J-Integral," *International Journal of Fracture Mechanics*, 12, pp 764-766. 1976.

21) Curtin, W., and H.A. Ernst, Thesis work in progress. Georgia Institute of Technology. 1992.

22) Kumar, V., German, M.D., and Shih, C.F., "An Engineering Approach for Elastic-Plastic Fracture Analysis." EPRI Report NP-1931, Electric Power Research Institute, Palo Alto, CA, 1981.

23) Ernst, H.A. "Analysis of Surface Cracks," Final Report, Martin Marrietta SC-273183, May 1991.

24) Dodds, R.H., and M.T. Kirk, Civil Engineering Studies, SRS 353, University of Illinois, July 1989.

25) McClung, R.C. et al, "Growth of Cracks During Large Elastic-Plastic Loading Cycles," XXIII National Symposium on Fracture Mechanics, TX, 1991.

26) McCabe, D.E., "Flaw Growth Analysis for 2219-T87 Aluminum Pressure Vessel Welds," Material Engineering Associates, MEA-2321, 1988.

27) Kordish, H., and E. Sommers, "Three Dimensional Effects Affecting the Precision of Lifetime Predictions," ASTM STP 969, 1988, pp 73-87.

28) Sommers, E. and D. Aurich, "On the Effect of Constraint on Ductile Fracture."

29) Ernst, H.A, P.J. Rush and D.E. McCabe, "Resistance Curve Analysis of Surface Cracks," Presented *ASTM Symposium: Twenty-forth National Symposium on Fracture Mechanics*, Gatlinburg, TN, 1992.

CHAPTER III

FINITE ELEMENT INVESTIGATION OF
CONSTRAINT PARAMETER

Introduction

Constraint is defined as the degree of crack tip stress triaxiality and is commonly quantified by the higher order crack tip stress and displacement terms (i.e. by T-stress or Q). Therefore, the elastic-plastic near tip fields are characterized by two parameters, J and a constraint parameter. The goal of the finite element analysis (FEA) investigation was to determine the coefficients of the higher order crack tip stress and displacement terms. As a subsequent step, the coefficients of the higher order terms were compared to the earlier proposed constraint parameter, $(L_a)^{-1}$. The finite element investigation for this work is just the first step in a larger finite element investigation. That is, this work has started the development of an FEA data base containing the values of the higher order stress and displacement term coefficients. Future finite element investigation to determine these higher order coefficients shall include many other geometries. For example, three-dimensional finite element models of planar specimens will be developed and investigated. Upon completion of all FEA work the coefficients shall be used to compare various constraint

parameters -- including $(L_{al})^{-1}$, q, Q, T-stress, and others -- to the higher order terms.

The coefficients of the higher order stress and displacement terms represent one part of a larger database which shall also include information on various constraint parameters and experimental results. The FEA results are an important part of the database; however, experimental results are critical to the evaluation of a constraint parameter. Experiments are very important because of the processes which lead to fracture. Ductile crack growth occurs due to micro void nucleation, growth, and coalescence. FEA cannot account for the processes which lead to ductile crack growth. Therefore, both experimental and FEA results are required in order to judge the ability of a second fracture parameter to characterize constraint. Each parameter shall be scrutinized upon completion of the entire database.

Three types of FEA models were developed for this study -- a two-dimensional linear elastic center crack tension (CCT) model, a two dimensional elastic plastic CCT model and a three-dimensional linear elastic surface crack tension (SCT) model. Since this study has concentrated on elastic-plastic three dimensional cracks both a three dimensional model and an elastic plastic model were developed for the initial part of the finite element constraint parameter investigation.

Finite Element Models

Linear Elastic CCT Model

All finite element work done for this study utilized ABAQUS software [28]. The linear elastic CCT model consists of a two dimensional plane strain mesh using two planes of symmetry (Figure 3.1). That is, only one quarter of
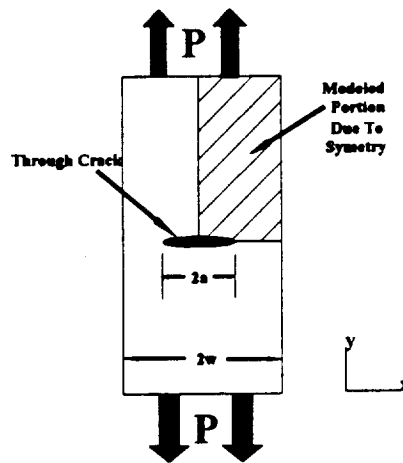
Figure 3.1: Center Crack Tension Model

the specimen was modeled due to symmetry considerations. The mesh contains 8-node biquadratic hybrid elements with reduced integration. The model consisted of 392 elements and was loaded in tension. A plot of the mesh and a sample of the ABAQUS input file are shown in appendix A.* A total of five CCT meshes were developed for the analysis. The crack length over width ratio (a/w) varied from 0.25 to 0.75 for the five meshes (Figure 3.1). For consistency purposes, the same element arrangement near the crack tip was used for all five models. In order to correctly model the $1/\sqrt{r}$ stress singularity for the linear

---

*Appendix A not included

elastic case, quarter point node elements [29] were used at the crack tip and all crack tip nodes were tied together. The element size (radial direction) at the crack tip was 0.0006e for the a/w=0.75 mesh where e=w-a.

Linear Elastic SCT Model

The linear elastic SCT model consisted of a three dimensional mesh using two planes of symmetry (Figure 3.2). The mesh contains 20-node
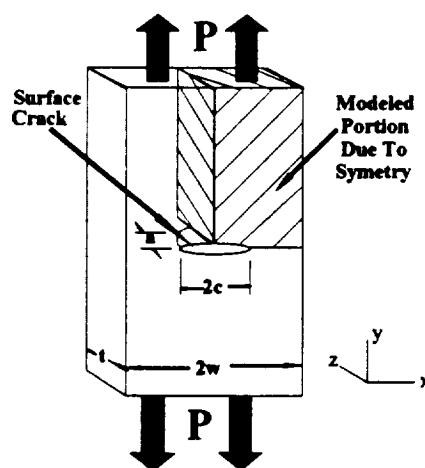
Figure 3.2: Surface Crack Tension Model

biquadratic displacement hybrid brick elements with reduced integration. The model consisted of 1764 elements and was loaded in tension. A plot of the mesh and a sample of the ABAQUS input file are shown in appendix B.* In order to correctly model the $1/\sqrt{r}$ stress singularity for the linear elastic case, quarter point node elements were used at the crack tip and all crack tip nodes were tied together [29]. The element size at the crack tip (radial direction) at

Appendix B not included

$\phi=90°$ was 0.0024d where d=t-a. The modeled surface crack displays a shape of a/c=1.0 and a/t=0.5 (Figure 3.2). The modeled specimen thickness (t) was 1.0 inch and the half width (w) was 2.0 inches.

Elastic Plastic CCT Model

The elastic plastic CCT mesh was identical to the linear elastic CCT mesh except for some adjustments. In order to model the r stress singularity for the elastic plastic analysis, quarter point node elements were not used at the crack tip and the crack tip nodes were not tied together. This allows for the crack tip to blunt for the elastic plastic case. The Ramberg-Osgood non-linear material deformation model was utilized for the elastic-plastic CCT model. In one dimension the Ramberg-Osgood model is,

$$\frac{\varepsilon}{\varepsilon_0} = \frac{\sigma}{\sigma_0} + \alpha\left(\frac{\sigma}{\sigma_0}\right)^n \qquad (3.1)$$

where,

$$\varepsilon_0 = \frac{\sigma_0}{E}$$

and E is Young's modulus. The stress, strain, and yield strength are designated by σ, ε, and σ_0 respectively. The material dependent constants α and n are the yield offset and hardening exponent. The material properties used in the model are displayed in table 3.1. These constants correspond to the properties of a typical low carbon steel. The element size (x direction) at the crack tip was 0.001e for the a/w=0.75 mesh where e=w-a (Figure 3.1). Similar to the linear elastic model, various a/w values were analyzed for the elastic plastic CCT case. Each model was loaded in three steps. The first load step went up to 70%

of limit load. The second step went up to 85% of limit load and the third step went up to 100% of limit load. A sample of an ABAQUS input file is shown in appendix C.

Table 3.1: Material Properties of a Typical Low Carbon Steel

MATERIAL PROPERTY	VALUE
Young's Modulus (E)	30.0 E6 [psi]
Yield Offset (α)	0.5
Strain Hardening Exponent (n)	5
Yield Strength (σ_0)	40,000 [psi]
Flow Stress (σ_f)	50,000 [psi]

Theoretical Background

In order to calculate the coefficients, the dependence on r must be determined for each of the higher order terms in the crack tip stress and displacement series (Figure 3.3). Williams [30] and Westergaard [2] have developed methodologies to determine the higher order terms dependence on r for linear elastic material properties. Sharma and Aravas [32] and Li and Wang [31] have formulated the higher order terms using an asymptotic analysis for a Ramberg-Osgood hardening material.
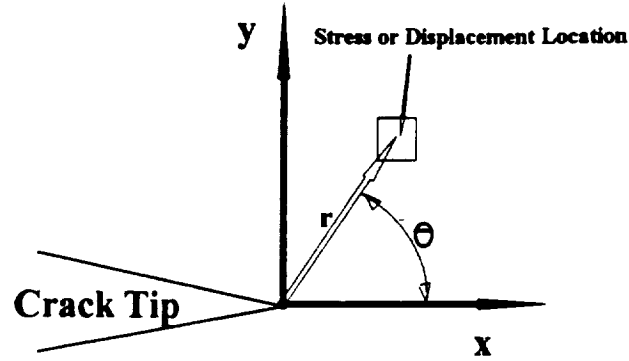
Figure 3.3: The In-plane Crack Tip Stress and Displacement Locations

Linear Elastic Background

For the linear elastic case, the format of the higher order stress and displacement fields can be formulated using two early approaches developed by Williams [30] and Westergaard [2]. Williams derived expressions for the crack tip stress and displacement fields by the eigenfunction expansion method. Utilizing this method for a symmetric stress distribution (mode I) in an infinite body with traction free crack faces, the crack tip stresses at $\theta=0°$ and the crack tip displacements at $\theta=180°$ were derived. The results follow:

$$\sigma_{xx}(r,0^0) = \left[-\frac{3}{4}(b_1 + b_3)\right]r^{-\frac{1}{2}} + T_x + \left[\frac{15}{4}(b_1 + b_3)\right]r^{\frac{1}{2}} + \ldots \tag{3.2}$$

$$\sigma_{yy}(r,0^0) = \left[-\frac{3}{4}(b_1 + b_3)\right]r^{-\frac{1}{2}} + T_y + \left[\frac{15}{4}(b_1 + b_3)\right]r^{\frac{1}{2}} + \ldots \tag{3.3}$$

$$u_y(r,180^0) = \frac{1}{2\mu}\left\{\left[\frac{3}{2}b_1 + \left(\frac{7}{2} - 4H\right)b_3\right]r^{\frac{1}{2}} + \left[\frac{5}{2}b_1 + \left(\frac{9}{5} - 4H\right)b_3\right]r^{\frac{3}{2}} + ...\right\} \quad (3.4)$$

where T_x, T_y, b_1 and b_3 are constants that depend upon geometry and loading conditions. H is defined as $v/(1+v)$. Poissons ratio is v and μ is the shear modulus. Williams [30] showed that T_x and T_y are zero for $\theta=0^o$ provided that the crack faces are traction free. However, more recent investigators have determined that T_x should not be zero [21]. Notice that the $r^{1/2}$ term in equations 3.2 and 3.3 and the $r^{1/2}$ term in equation 3.4 both depend on b_1 and b_3.

Westergaard [2] was the first to demonstrate that the crack tip stress fields can be derived for certain geometries by introducing an analytic function, $Z(z)$, where $z=x+iy$ and $i = \sqrt{-1}$. The normal stresses and displacements utilizing the Z function are,

$$\sigma_{xx} = \operatorname{Re} Z - y \operatorname{Im} Z' \qquad (3.5)$$

$$\sigma_{yy} = \operatorname{Re} Z + y \operatorname{Im} Z' \qquad (3.6)$$

$$u_y = \frac{1-v}{\mu}\operatorname{Im} \overline{Z} - \frac{y \operatorname{Re} Z}{2\mu} \qquad (3.7)$$

where the bar over Z indicates integration with respect to z. Z is considered a function of the form,

$$Z = \frac{c_0 + c_1 z + c_2 z^2 + ...}{\sqrt{z}} \qquad (3.8)$$

where the c's are complex numbers.

The coefficients of the $r^{1/2}$ terms in equations 3.2 and 3.3 were defined as γ_x and γ_y, respectively. The coefficient of the $r^{1/2}$ term in equation 3.4 was defined as B. The relationship between the γ's and B for a two dimensional

linear elastic stress state was determined using the Westergaard stress function. For mode I loading and y=0, the second terms on the right hand side of equations 3.5 and 3.6 drop out. Note that $\gamma_x = \gamma_y$ when y=0. After expansion of the complex numbers, evaluation of the normal stress at $\theta = 0^\circ$, and evaluation of the displacements at $\theta = 180^\circ$, the relationship between γ and B was determined for a two dimensional cracked body. This relationship was found to be,

$$B = -\gamma \left(\frac{4}{3E'} \right) \qquad (3.9)$$

where E'=E for plane stress and E'=E/(1-v^2) for plane strain. For the linear elastic models a normalized B was defined as,

$$B^* = B \frac{E}{K} \sqrt{\frac{\pi}{8}} \qquad (3.10)$$

and a normalized γ as,

$$\gamma^* = \gamma \frac{\sqrt{2\pi}}{K} \qquad (3.11)$$

where K is the stress intensity factor. By combining equations 3.9 to 3.11, the relationship between B^* and γ^* was determined as,

$$B^* = -\frac{1}{3} \gamma^* \qquad (3.12)$$

Rice [38] introduced the boundary layer approach to determine the crack tip stress and displacement fields. The boundary layer approach assumes that the boundary value stresses along the crack face are given by the extension of validity of the singular term in the elastic stress solution (Equation 1.1) to large

values of r and small scale yielding. Larsson and Carlsson [21] introduced the modified boundary layer formulation for the crack tip stress fields. They included a constant T-stress term with the singular term in the boundary layer stress field formulation (T_x in equation 3.2). For a two dimensional infinite body Larsson and Carlsson determined that only the σ_{xx} T-stress term (T_x) was non-zero. However, Nakamura and Parks [31] have determined that three T-stress terms are present in linear elastic three dimensional cracked bodies. They determined that the σ_{xx}, σ_{zz}, and τ_{xz} crack tip stress fields required non-zero T-stress terms for regions behind the crack tip. For a two dimensional elastic-plastic cracked body, O'Dowd and Shih have demonstrated the existence of constant higher order terms in both the σ_{xx} and σ_{yy} fields [22]. They introduced these higher order stress terms using the Q parameter.

Elastic-Plastic Background

For the elastic-plastic analysis, the format of the higher order stress and displacement fields have been formulated by Sharma and Aravas [32] and Li and Wang [33]. These researchers considered a two-dimensional crack problem in a homogenous Ramberg-Osgood elastic-plastic material. The first two terms of the crack tip stress series and the first three terms of the displacement series were formulated by assuming an asymptotic expansion for the stress terms in the form of,

$$\frac{\sigma_{ij}(r,\theta)}{\sigma_0} = r^s \sigma_{ij}^{(0)}(\theta) + r^t \sigma_{ij}^{(1)}(\theta) + \dots \tag{3.13}$$

as r→0 and s < t. Substituting equation 3.13 into the governing equations, the first two terms in the stress and the first three terms in the displacement fields were determined as,

$$\sigma_{ij}(r,\theta) = \sigma_0 \left(\frac{J}{\alpha \varepsilon_0 \sigma_0 I_n} \right)^{1/(n+1)} \tilde{\sigma}_{ij}^{(0)}(\theta) r^{-1/(n+1)} + \sigma_0 Q_0 \left(\frac{\sigma_0}{J} \right)^{t} \tilde{\sigma}_{ij}^{(1)}(\theta) r^{t} + \dots \quad (3.14)$$

$$u_i(r,\theta) = \alpha \varepsilon_0 \left(\frac{J}{\alpha \varepsilon_0 \sigma_0 I_n} \right)^{n/(n+1)} \tilde{u}_i^{(0)}(\theta) r^{1/(n+1)}$$

$$+ \alpha \varepsilon_0 \left(\frac{Q_0}{(J/\sigma_0)^t} \right) \left(\frac{J}{\alpha \varepsilon_0 \sigma_0 I_n} \right)^{(n-1)/(n+1)} \tilde{u}_i^{(1)}(\theta) r^{s(n-1)+t+1} + \varepsilon^{s(0)} \tilde{u}_i^{(2)}(\theta) r^{s+1} + \dots \quad (3.15)$$

where Q_0 is a dimensionless constant that controls the magnitude of the second terms, s = -1/(n+1), and $\varepsilon^{s(0)}$ is an elastic strain resulting from the singular stress term. The governing equations include equilibrium, compatibility, and constitutive equations. The formulation of equations 3.14 and 3.15 neglect the effects of specimen geometry and far field loading and assume that the higher order terms are separable in r and θ. Using a Galerkin finite element technique t was determined to be 0.055 [32] for a two dimensional crack in plane strain with a material strain hardening exponent of 5.

Procedure

The field values of the normal crack tip stresses (σ_{xx} and σ_{yy}) along r at θ=0° and the crack mouth opening displacements (u_y) along r at θ=180° were calculated by each of the finite element models (Figure 3.3). The coefficients

of each higher order term in the crack tip stress and displacement series were determined by curve fitting the FEA data.

Linear Elastic Procedure

The following formats which are similar to equations 3.2 through 3.4 were utilized to curve fit the crack tip stress and displacement fields calculated by FEA for all linear elastic models:

$$\sigma_{xx}(r,0^0) = D_x r^{-\frac{1}{2}} + T_x + \gamma_x r^{\frac{1}{2}} \tag{3.16}$$

$$\sigma_{yy}(r,0^0) = D_y r^{-\frac{1}{2}} + T_y + \gamma_y r^{\frac{1}{2}} \tag{3.17}$$

$$u_y(r,180^0) = Ar^{\frac{1}{2}} + Br^{\frac{3}{2}} \tag{3.18}$$

where r is the distance from the crack tip. The first terms ($r^{1/2}$ terms in equations 3.16 and 3.17 and $r^{1/2}$ term in equation 3.18) were subtracted from the field values determined by FEA. The remaining higher order terms were curve fit using a least squares methodology. The curve fits yielded values for the coefficients T_x, γ_x, T_y, γ_y, and B. Note that the modified boundary layer approach was used to curve fit the higher order terms [21].

The range near the crack tip over which the stresses and displacements were curve fit needed to be determined. For the linear elastic models, the element stresses and nodal displacements (field values) very close to the crack tip which were affected by the quarter point node elements were omitted from the curve fitted data. For the linear elastic CCT model, the curve fitting range

did not significantly affect the values of the coefficients. However, a criterion was used to determine the outer bound of the curve fitted data. The outer bound was determined using the T-stress. T-stress is the normal stress in the x-direction acting on the crack face at $\theta=180°$ [21]. The linear elastic CCT finite element analysis determined that σ_{xx} was constant over almost the entire crack face. This T-stress value at $\theta=180°$ was then compared to the T_x values from curve fits extending over various distances from the crack tip at $\theta=0°$. The value of T_x varied, although not significantly, depending upon the distance from the crack tip over which the higher order σ_{xx} terms were curve fit. Therefore, the curve fit range which displayed the same T_x value as the T-stress value along the crack face at $\theta=180°$ was used to determine the coefficients in equation 3.16 for the linear elastic CCT model. The same curve fit range was then used for the higher order terms in equations 3.17 and 3.18.

For the linear elastic SCT model, the in-plane T-stress at $\theta=180°$ was constant over much of the crack face. However, this T-stress did not coincide with the curve fitted T_x values ($\theta=0°$) possibly because of the three dimensional stress state. That is, the out-of-plane stresses may have affected the T-stress values. Therefore, the outer bound was determined as the distance from the crack tip over which the curve fitted coefficients best represented the FEA field values close to the crack tip. The curve fitting outer bound was determined to be approximately 0.2a for all elliptical angles, where a is the surface crack depth.

After the successful defense of this thesis, an error with the curve fitting format of equation 3.17 was discovered. The T_y term should not be included in

the curve fits since it would invalidate the traction boundary conditions along the crack face at θ = 180°. The term was found to be zero for the linear elastic CCT model curve fits. However, T_y was included in the curve fits for the linear elastic SCT model. The inclusion of T_y is incorrect. See the Discussion section of Chapter III for further information pertaining to the incorrect format.

Elastic-Plastic Procedure

The following formats which are similar to the asymptotic solutions of equations 3.14 and 3.15 were utilized to curve fit the crack tip stress and displacement fields for the elastic-plastic models:

$$\sigma_{xx}(r,0^0) = D_{ep,x} r^{-1/(n+1)} + Q_x r^t \qquad (3.19)$$

$$\sigma_{yy}(r,0^0) = D_{ep,y} r^{-1/(n+1)} + Q_y r^t \qquad (3.20)$$

$$u_y(r,180^0) = A_{ep} r^{1/(n+1)} + B_{ep} r^{s(n-1)+t+1} + C_{ep} r^{s+1} \qquad (3.21)$$

where r is the distance from the crack tip, s = -1/(n+1), and t = 0.055 for a two-dimensional crack in plane strain with n=5. Note that the strain hardening exponent does affect the exponent of r in all of the terms in equations 3.19 to 3.21. The HRR terms ($r^{-1/(n+1)}$ terms in equations 3.19 and 3.20 and $r^{1/(n+1)}$ term in equation 3.21) were subtracted from the field values determined by FEA. The remaining higher order terms were curve fitted using a least squares methodology to determine the values of the coefficients Q_x, Q_y, B_{ep}, and C_{ep}.

In developing a one or two parameter fracture methodology, one has to assume that the asymptotic solution on which the criterion is based provides and accurate description of the near tip stresses over distances that are sufficiently larger than the fracture process zone [32]. Hutchinson [34] suggests that one condition for a valid fracture methodology is,

$$R > 3\delta_t$$

where R is the radius of the zone of dominance of the methodology's crack tip stress solution and is sufficiently larger than the fracture process zone. The crack tip opening is designated by δ_t. Shih [35] has shown that the crack tip opening can be determined by,

$$\delta_t = d_n \frac{J}{\sigma_0}$$

where d_n is approximately equal to 0.5 for n=10 and 0.2 for n=3 [35]. By interpolation the approximate value of d_n for n=5 is 0.3. By substitution of δ_t, Hutchinson's condition becomes,

$$R > 3d_n \frac{J}{\sigma_0}$$

Therefore, R extends a distance $r/(J/\sigma_0) \approx 1.0$ from the crack tip when n=5. The radial distance from the crack tip is designated by r. The data inside R was omitted when curve fitting the elastic-plastic CCT stress and displacement data. The outer curve fit bound was $r/(J/\sigma_0) = 15$. The outer bound is sufficiently larger than R and is the approximate extent of the crack tip plastic zone for all models.

Constraint Parameter Procedure

In order to compare with the higher order term coefficients $(L_a)^{-1}$ was calculated at constant load by,

$$(L_{el})^{-1} = \frac{\Delta G}{G_{ave}\Delta a}\bigg|_P = \frac{(G^{i+1} - G^i)}{G_{ave}(a^{i+1} - a^i)}\bigg|_P \qquad (3.22)$$

where G is the energy release rate and a is the crack length. Incremental steps are designated by i+1 and i. That is, a^{i+1} corresponds to an in-plane crack size slightly larger than a^i. In order to attain values for G^{i+1}, all FEA models were modified so that the crack length was slightly larger than the original model. G_{ave} was defined as the average value of G^{i+1} and G^i or,

$$G_{ave} = \frac{G^{i+1} + G^i}{2} \qquad (3.23)$$

The values of G were calculated by ABAQUS [28] using the internal J-integral subroutine which calculates G using the domain integral method for all linear elastic models. For the elastic plastic CCT models G was calculated as J_{el} using the EPRI [36] estimation scheme (see Equations 3.32-3.35).

Results

The coefficients were plotted as a function of a/w for the CCT models and elliptical angle (ϕ) for the SCT model. In addition, the coefficients were compared with $(L_{el})^{-1}$.

Linear Elastic CCT Model Coefficients

G was calculated by ABAQUS using the domain integral method for each of the linear elastic finite element models. The ABAQUS value of G was within 1% of the handbook [24] value for all linear elastic CCT models.

The crack tip displacement field values at $\theta=180^o$ were determined using the linear elastic finite element models for a/w's ranging from 0.25 to 0.75. A sample of the crack tip displacements along with the singularity displacements ($Ar^{1/2}$ term only) is shown in figure 3.4. After subtracting the singularity term in the displacement series, where for plane strain,

$$A(\theta = 180^0) = \frac{K}{\mu}\sqrt{\frac{2}{\pi}}(1-v) \qquad (3.24)$$

the value of B was determined by curve fitting for each crack size, where μ is the shear modulus. Note that B is the coefficient of the $r^{3/2}$ term in the displacement series defined by equation 3.18. B was then normalized as B* by use of equation 3.10. The results show an increasing trend with increasing a/w (Figure 3.5). The normalized coefficient values are shown in table 3.2.
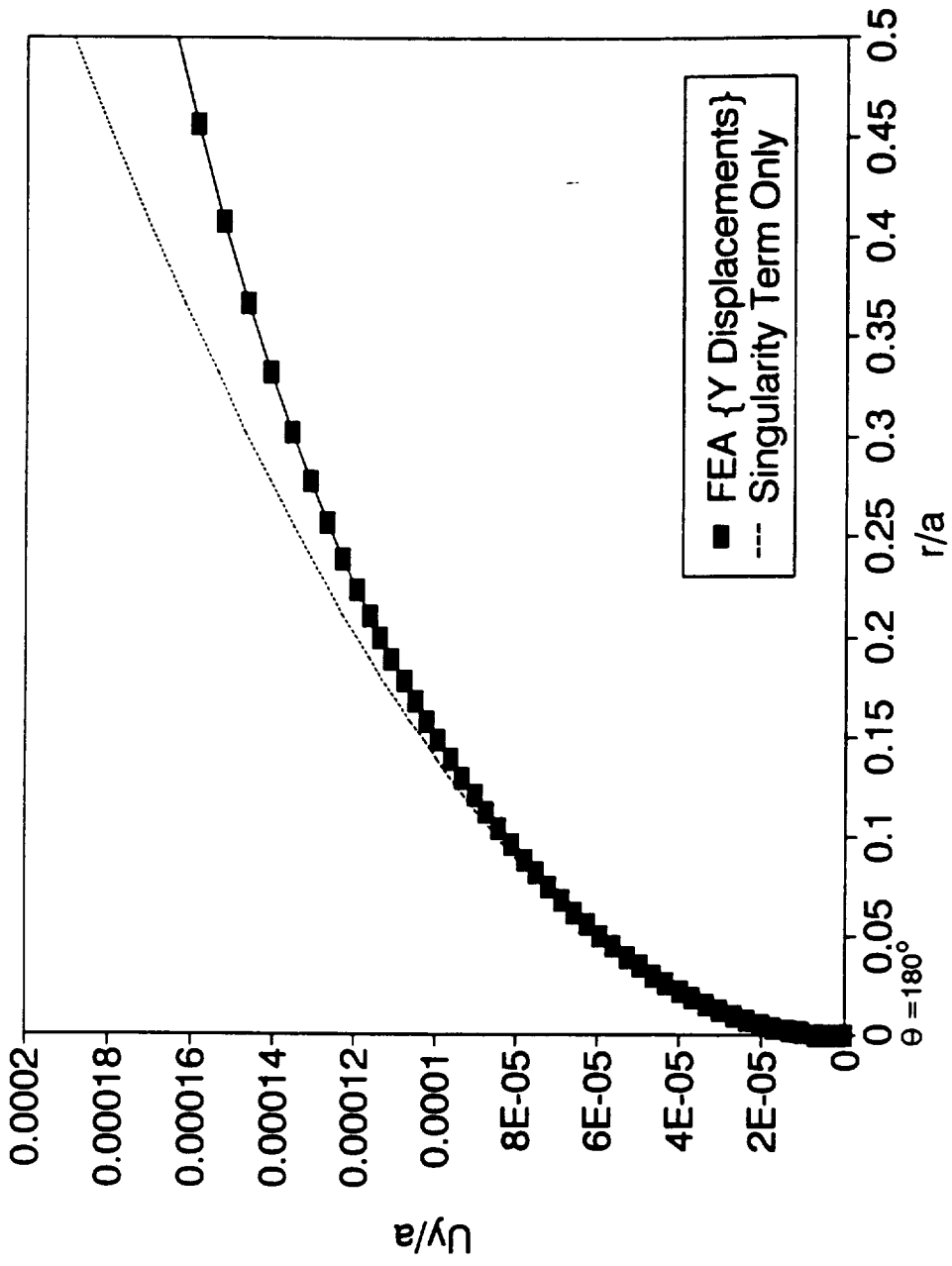
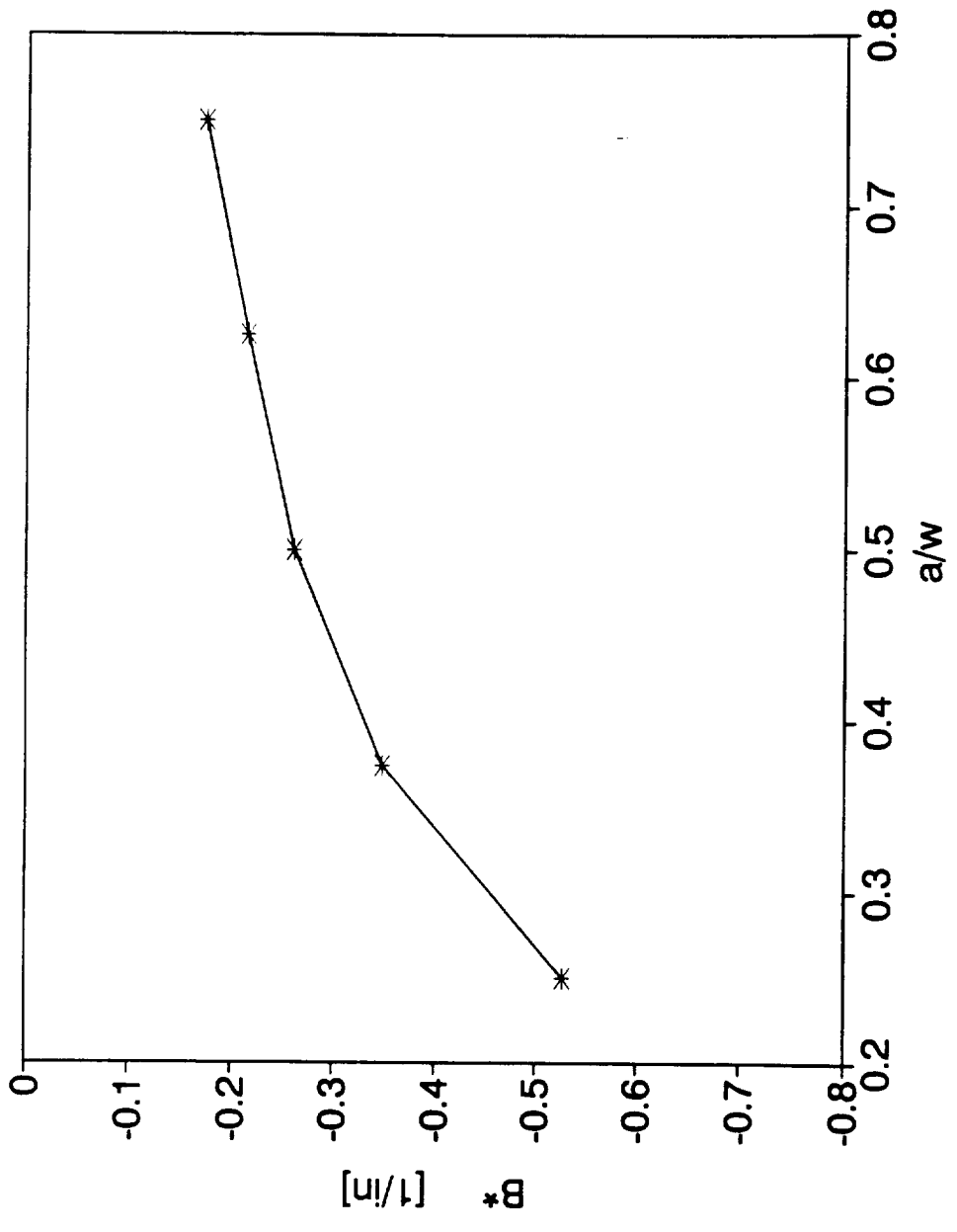Figure 3.4: Crack Tip Displacements for Linear Elastic CCT Model (a/w=0.25)

Figure 3.5: Variation of B* with Crack Length for Linear Elastic CCT Model

Table 3.2: Higher Order Term Coefficients For Linear Elastic CCT Model

a/w	B*	T_x^*	γ_x^*	γ_y^*	$(L_{el})^{-1}$
0.25	-0.5275	-0.6152	1.396	1.415	2.328
0.375	-0.3482	-0.3962	0.939	0.972	1.894
0.50	-0.2615	-0.2820	0.671	0.748	1.832
0.625	-0.2157	-0.2117	0.462	0.603	1.951
0.75	-0.1737	-0.1576	0.079	0.372	2.520

The crack tip normal stress values in both the x and y directions at $\theta=0^\circ$ were also recorded from the linear elastic CCT finite element analysis. The finite element values along with the singularity values are shown in figure 3.6. The differences between the FEA and singularity values of the crack tip stresses are due to the low constraint CCT geometry. That is, the crack tip stresses deviate from the singular values for low constraint geometries. The singularity terms, $D_x r^{-1/2}$ and $D_y r^{-1/2}$, where

$$D_x(\theta = 0^0) = D_y(\theta = 0^0) = \frac{K}{\sqrt{2\pi}} \qquad (3.25)$$

were subtracted from the FEA field values of σ_{xx} and σ_{yy}, respectively. The form of equations 3.16 and 3.17 were used to curve fit the remaining higher order terms in order to determine T_x, T_y, γ_x, and γ_y values. γ_x and γ_y were normalized using equation 3.11. T_x and T_y were normalized using,
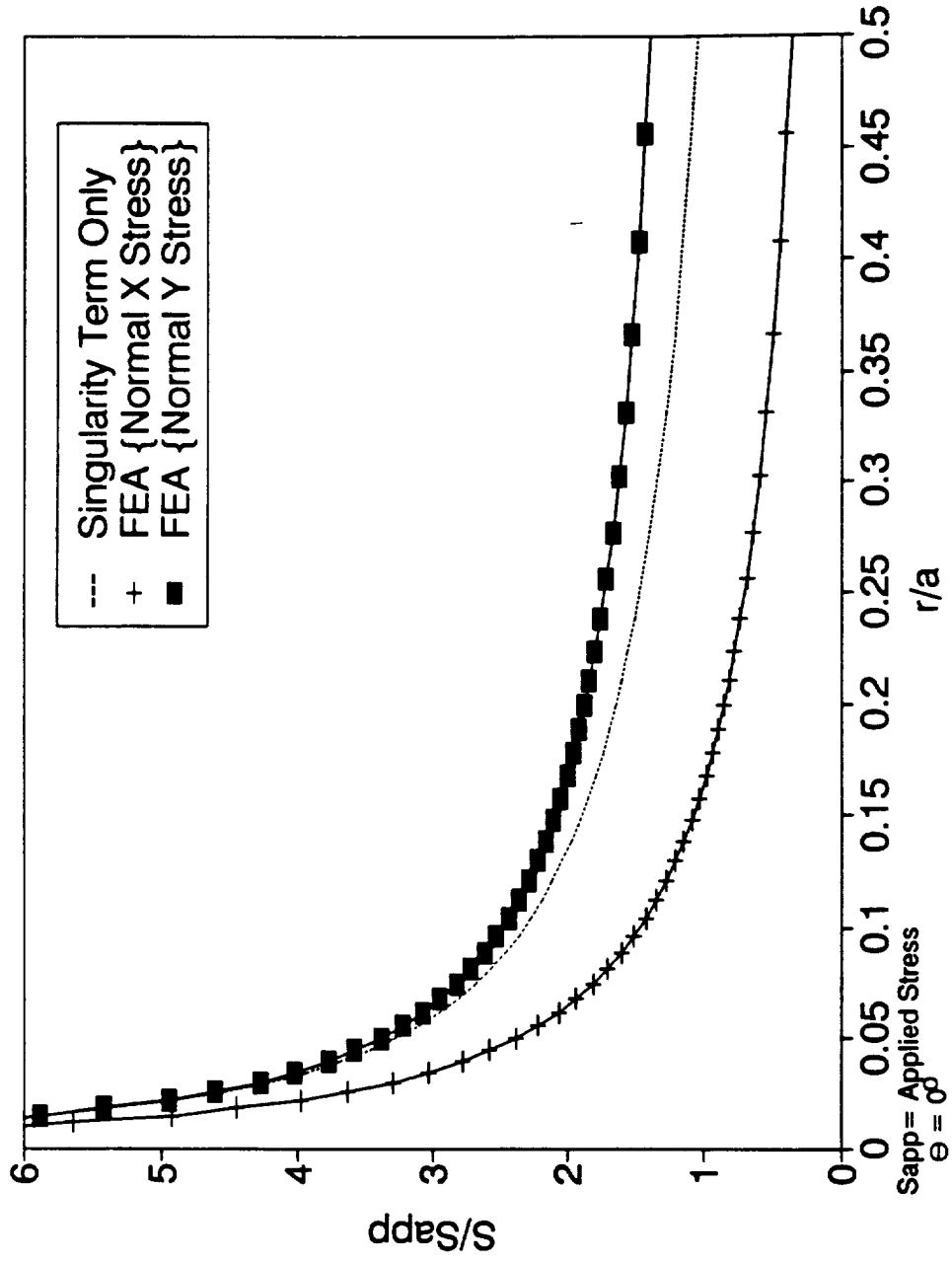
$$T_i^* = T_i \frac{\sigma_{app}}{K^2} \qquad (3.26)$$

Figure 3.6: Crack Tip Stresses for Linear Elastic CCT Model (a/w=0.25)

where σ_{app} is the applied tensile stress. The curve fits determined that T_y was zero for all crack lengths. This is consistent with the Larsson and Carlsson modified boundary layer approach for a two dimensional linear elastic stress state. That is, Larsson and Carlsson defined T_y as zero in equation 2.19. The values of T_x^*, γ_x^*, and γ_y^* are plotted versus crack length in figure 3.7 and their values are shown in table 3.2.

Linear Elastic SCT Model Coefficients

G_I values for the SCT model were calculated along the crack front by ABAQUS. These values of G_I compared well with the numerical equations for G_I developed by Newman and Raju (Equation 1.6). Figure 3.8 compares these values of G_I.

The displacements and stresses calculated by FEA were transformed to the local in-plane coordinate systems at elliptical angles (ϕ) ranging from 0° to 90° (see Figure 1.4). The local in-plane coordinate system is shown in figure 3.3 and is always perpendicular to the crack front.

The crack tip displacement field values at $\theta=180^\circ$ were determined using the three dimensional linear elastic finite element model for elliptical angles of 0°, 22.5°, 45°, 67.5°, and 90°. An example of the FEA displacement field plotted versus distance from the crack tip is shown in figure 3.9. The first (singularity) term could not be subtracted from the FEA displacements because it is dependent on the unknown out-of-plane stress state (i.e. plane stress or plane strain). Along the front of a semi-elliptical surface crack the out-of-plane stress state varies from approximately a state of plane stress at the surface ($\phi=0^\circ$) to an
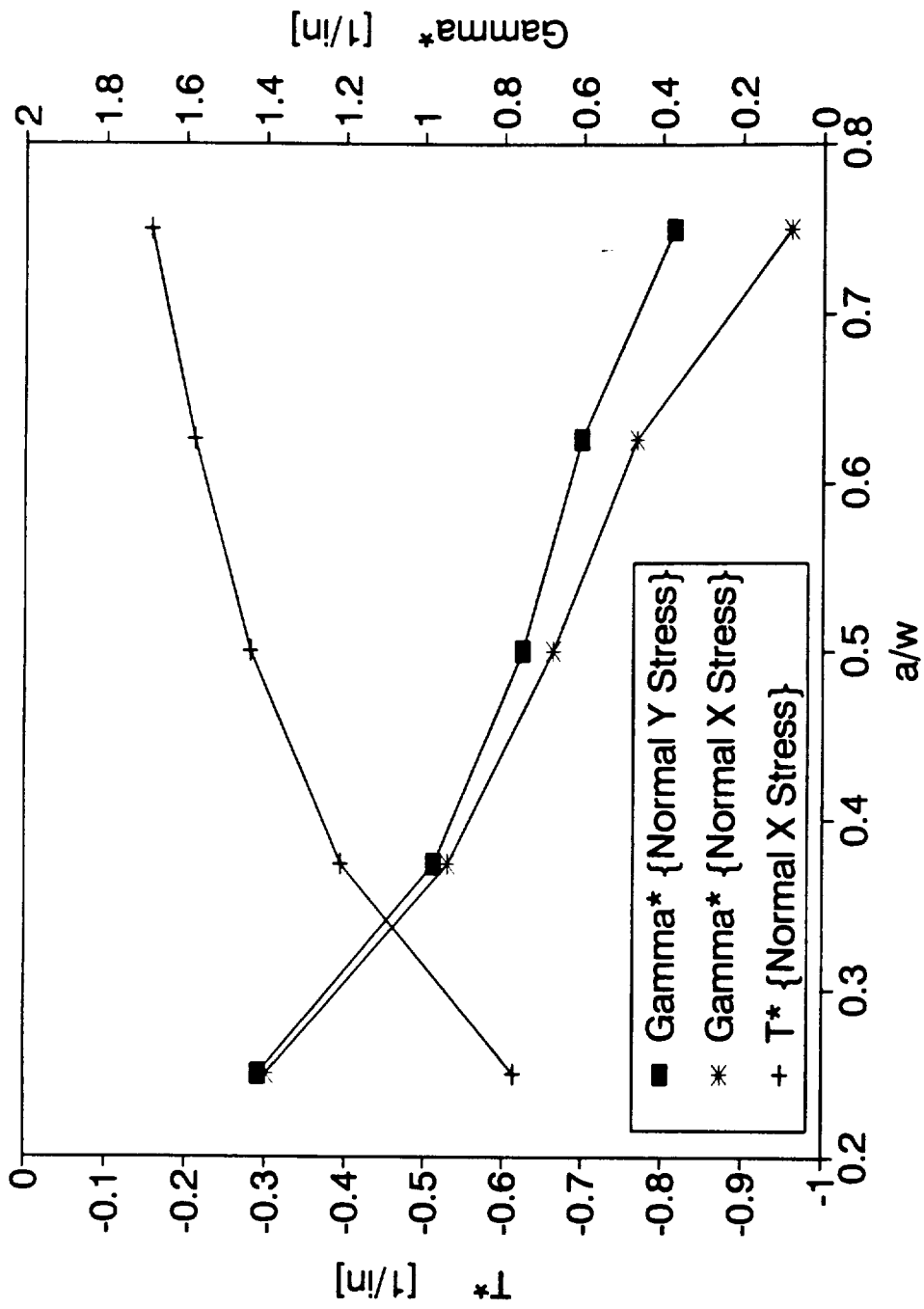
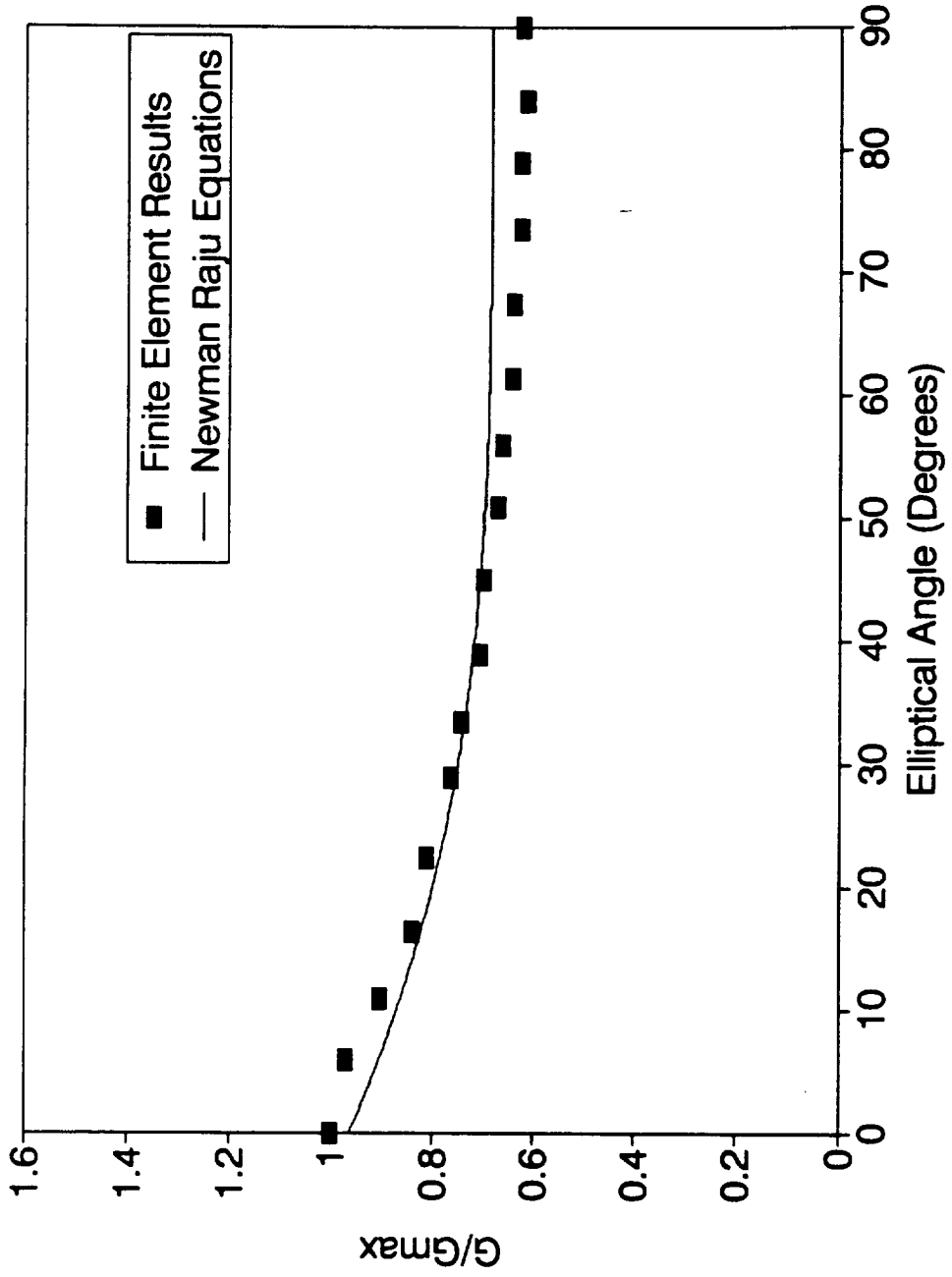Figure 3.7: Higher Order Stress Term Coefficients for the Linear Elastic CCT Model

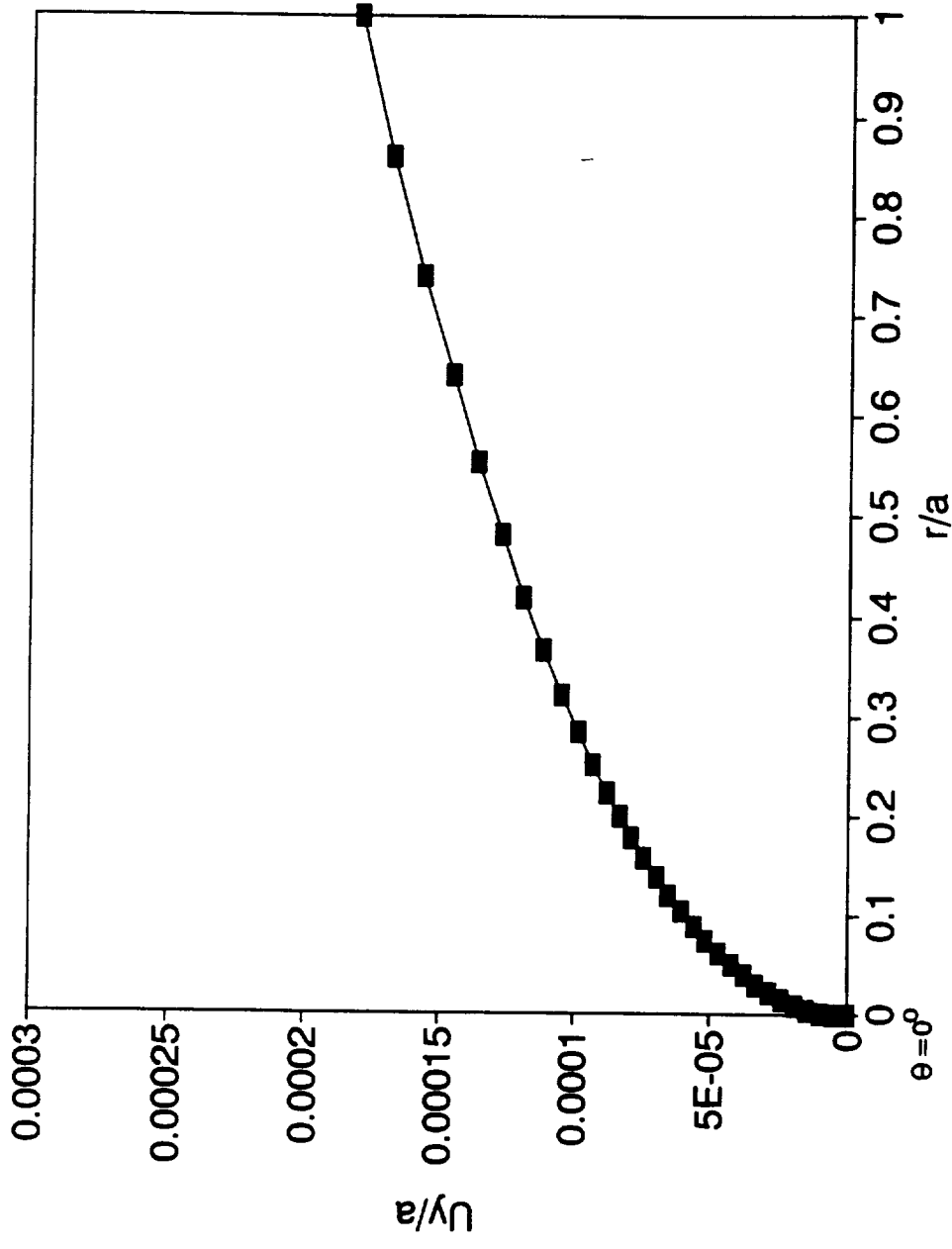Figure 3.8: Energy Release Rate for 3-D SCT Model

Figure 3.9: Crack Tip Displacements for Linear Elastic SCT Model ($\phi = 45°$)

approximate state of plane strain at $\phi=90°$. Therefore both A and B were determined at each elliptical angle by curve fitting where Note that A and B are displacement series coefficients defined by equation 3.18. The values of A determined by curve fitting were close to the plane stress value of A at $\phi=0°$ and to the plane strain value of A at $\phi=90°$. The coefficient, B, was then normalized as B* by use of equation 3.10. The results show an increasing trend with increasing elliptical angle (Figure 3.10). The normalized coefficient values are shown in table 3.3. A possible source of error is introduced when determining the value of A by curve fitting. Error may be introduced because the A term is the dominant term in the two term series. Therefore, relatively small changes in A can introduce significant changes in B.

The crack tip normal stress values in both the local x and y directions at $\theta=0°$ were also recorded from the linear elastic SCT finite element analysis. An example of these stresses versus distance from the crack tip is shown in figure 3.11. The singularity terms, $D_x r^{1/2}$ and $D_y r^{1/2}$ were subtracted from the FEA field values of σ_{xx} and σ_{yy}, respectively. Local values of the stress intensity factor, K_I, were used to calculate the singularity terms of equation 3.25. The form of equations 3.16 and 3.18 were used to curve fit the remaining higher order terms in order to determine T_x, T_y, γ_x, and γ_y values. The coefficients, γ_x and γ_y, were normalized using equation 3.11 and T_x and T_y were normalized using equation 3.26. The values of T_x^*, T_y^*, γ_x^*, and γ_y^* are plotted versus elliptical angle in figure 3.12 and are shown in table 3.3. Note that after the successful defense of this thesis the curve fitting format used to determine T_y^* and γ_y^* was found to be incorrect. See the Discussion at the end of Chapter III for more information.
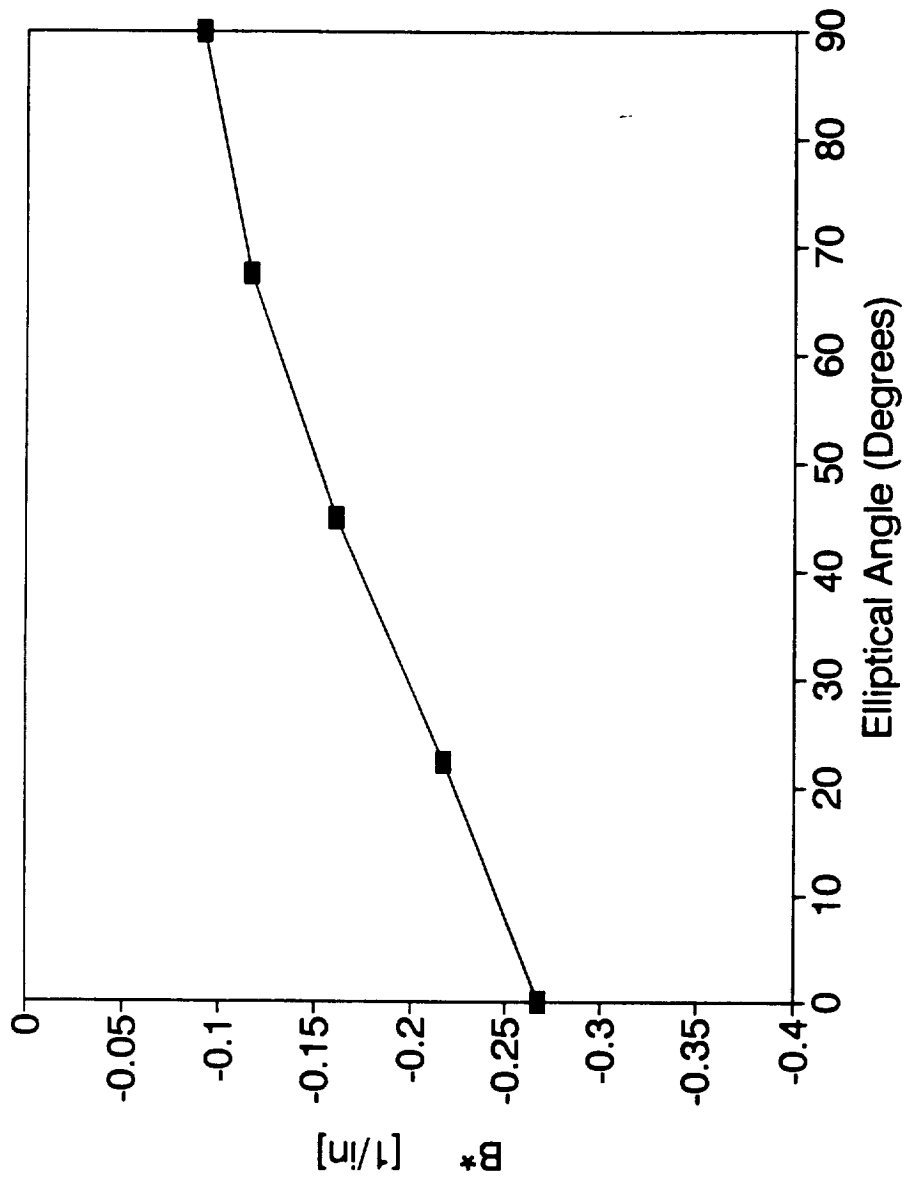
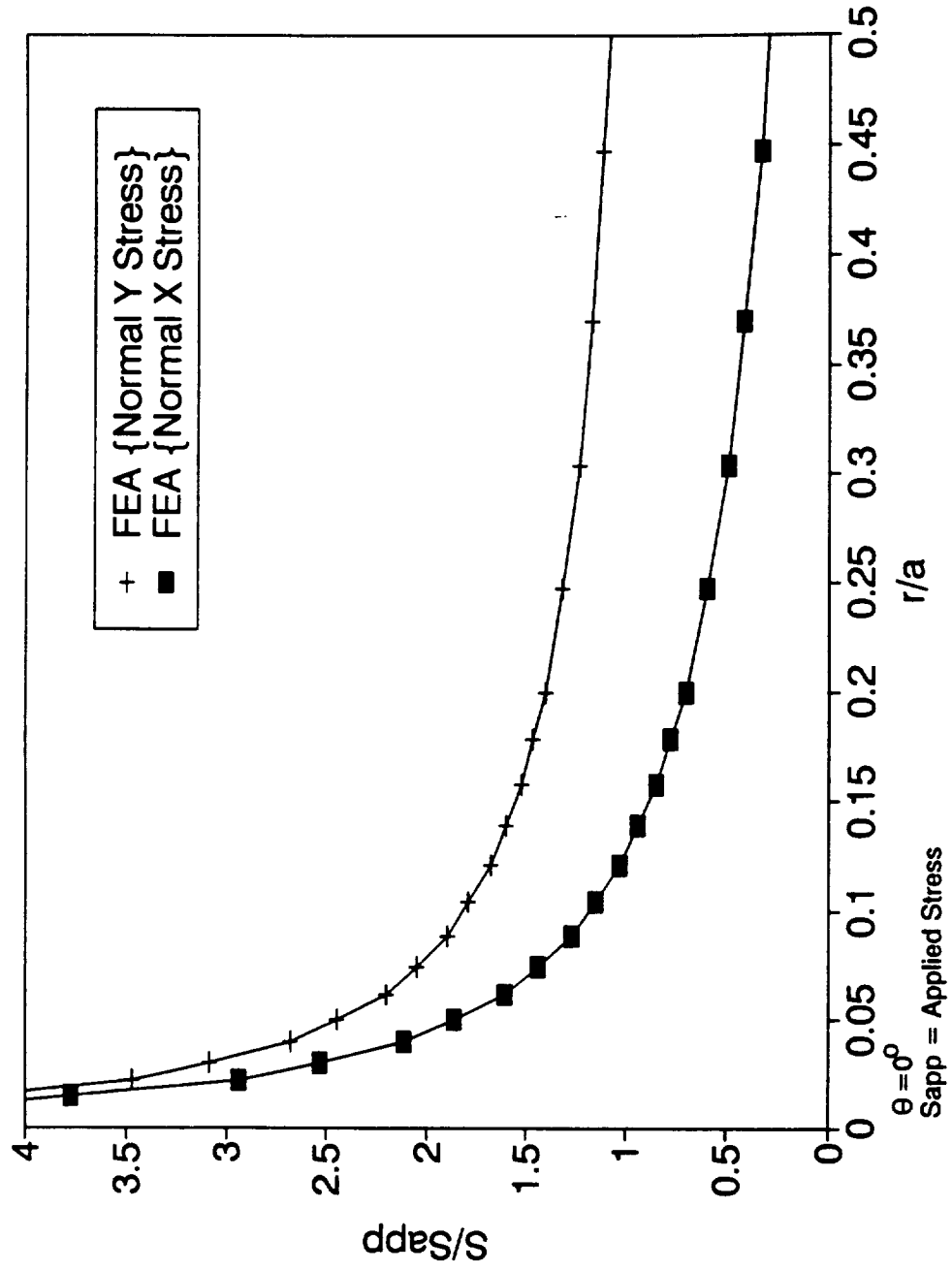Figure 3.10: Variation of B* with Elliptical Angle for Linear Elastic SCT Model

Figure 3.11: Crack Tip Stresses for Linear Elastic SCT Model ($\phi=45°$)
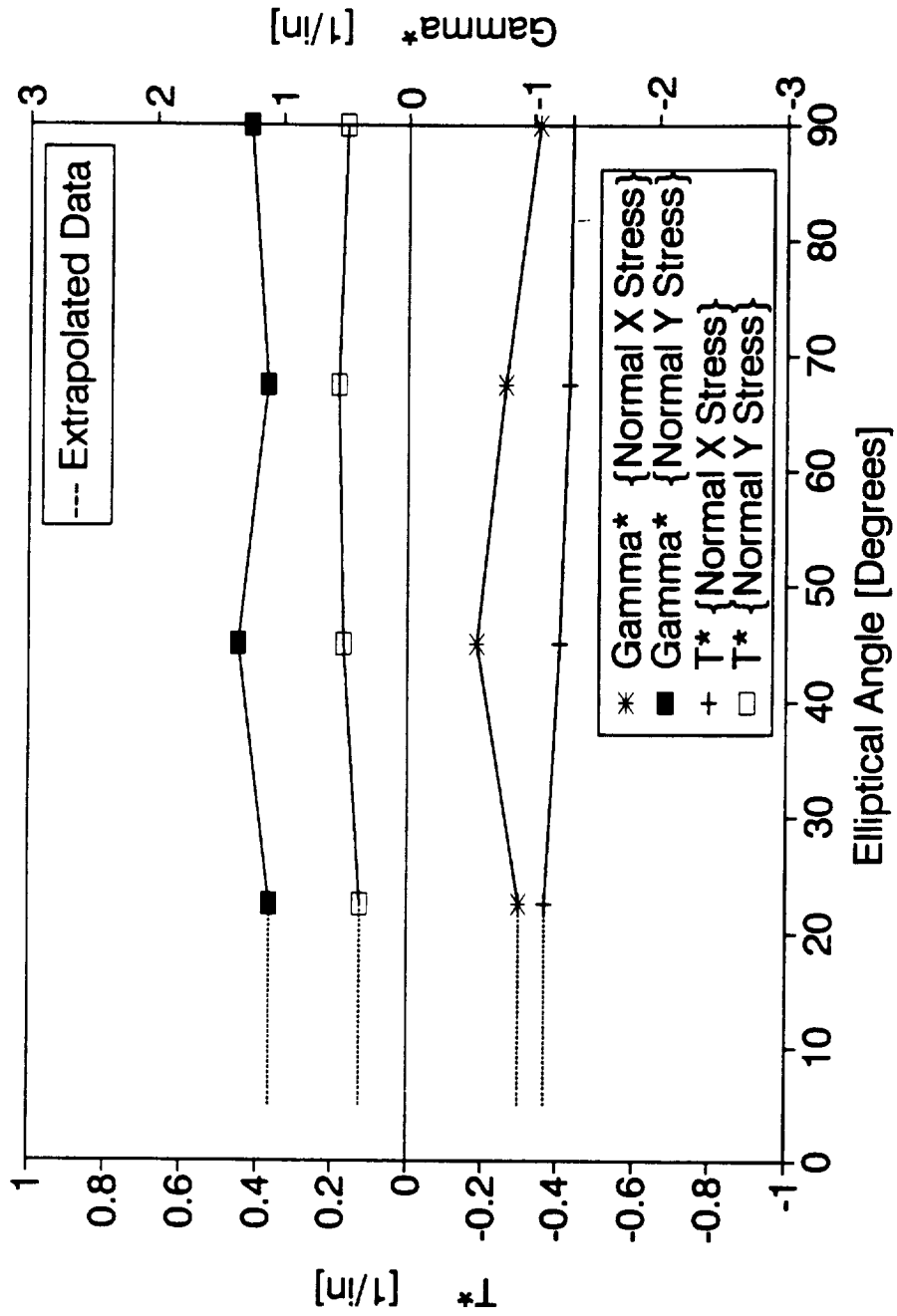
Figure 3.12: Higher Order Stress Term Coefficients for the Linear Elastic SCT Model

Table 3.3: Higher Order Term Coefficients for Linear Elastic SCT Model

ϕ	B^*	T_x^*	T_y^*	γ_x^*	γ_y^*	$(L_a)^{-1}$
$0°$	-0.2672	-1.1519	-0.2457	3.6601	4.4192	3.055
$22.5°$	-0.2175	-0.3677	0.1258	-0.8967	1.0986	2.621
$45°$	-0.1614	-0.4080	0.1700	-0.5552	1.3473	2.275
$67.5°$	-0.1163	-0.4295	0.1849	-0.7787	1.1209	2.014
$90°$	-0.0920	-0.4360	0.1640	-1.0449	1.2546	1.910

Accurate stress values at $\phi=0°$ were not obtained from the SCT model because the finite element mesh was not fine enough in the z direction to account for surface effects. Therefore, the values of T^* and γ^* were extrapolated between the elliptical angles of $0°$ and $22.5°$ in figure 3.12. In addition, a possible source of error was introduced during the evaluation of the singular stress terms. The local values of G_1 were calculated by ABAQUS. In order to determine K_1, from G_1, knowledge of the out-of-plane stress state is required, but is unknown. Therefore, the condition of plane stress was assumed during the evaluation of the singular stress terms for the SCT model.

Elastic-Plastic CCT Model Coefficients

All coefficients were determined for the elastic-plastic CCT models at 70% of limit load (P_o). The total J was calculated by ABAQUS using the domain integral method for each model. The total J values were within 5% to 10% of the EPRI estimation scheme [36] values of J for all models. The plastic

zone size determined by the equivalent stress being equal to σ_0 at $\theta=180°$ was observed to extend between $r/(J/\sigma_0) = 13$ and $r/(J/\sigma_0) = 20$ for all elastic-plastic models where r is the distance from the crack tip.

The crack tip displacement field values at $\theta=180°$ were determined using the elastic-plastic finite element models for a/w's ranging from 0.25 to 0.75. An example of the crack tip displacements versus distance from the crack tip is shown in figure 3.13. After subtracting the HRR term ($A_{ep}r^{1/(n+1)}$ in Equation 3.21) from the FEA displacements, where

$$A_{ep}(\theta = 180°) = \alpha\varepsilon_0\left(\frac{J}{\alpha\varepsilon_0\sigma_0 I_n}\right)^{n/(n+1)}\tilde{u}_y(180°) \qquad (3.27)$$

the value of B_{ep} and C_{ep} were determined by curve fitting. In equation 3.27, α and n are the yield offset and strain hardening exponent respectively. I_n is an integration constant where $I_n = 5.0$ for plane strain [37]. The material yield strength is designated by σ_0 and $\varepsilon_0 = \sigma_0/E$. J was calculated by ABAQUS and $\tilde{u}_y(180°) = 2.3678$ [37]. B_{ep} and C_{ep} were then normalized where,

$$B_{ep}* = \frac{B_{ep}}{\alpha\varepsilon_0\left(\dfrac{\sigma_0}{J}\right)^t\left(\dfrac{J}{\alpha\varepsilon_0\sigma_0 I_n}\right)^{(n-1)/(n+1)}}\left(\frac{1}{(J/\sigma_0)}\right) \qquad (3.28)$$

$$C_{ep}* = \frac{C_{ep}}{\alpha\varepsilon_0\left(\dfrac{\sigma_0}{J}\right)^t\left(\dfrac{J}{\alpha\varepsilon_0\sigma_0 I_n}\right)^{1/(n+1)}}\left(\frac{1}{(J/\sigma_0)}\right) \qquad (3.29)$$

The coefficients, $B_{ep}*$ and $C_{ep}*$, versus a/w are plotted in figure 3.14. The normalized values are shown in table 3.4. B_{ep} and C_{ep} were normalized by the
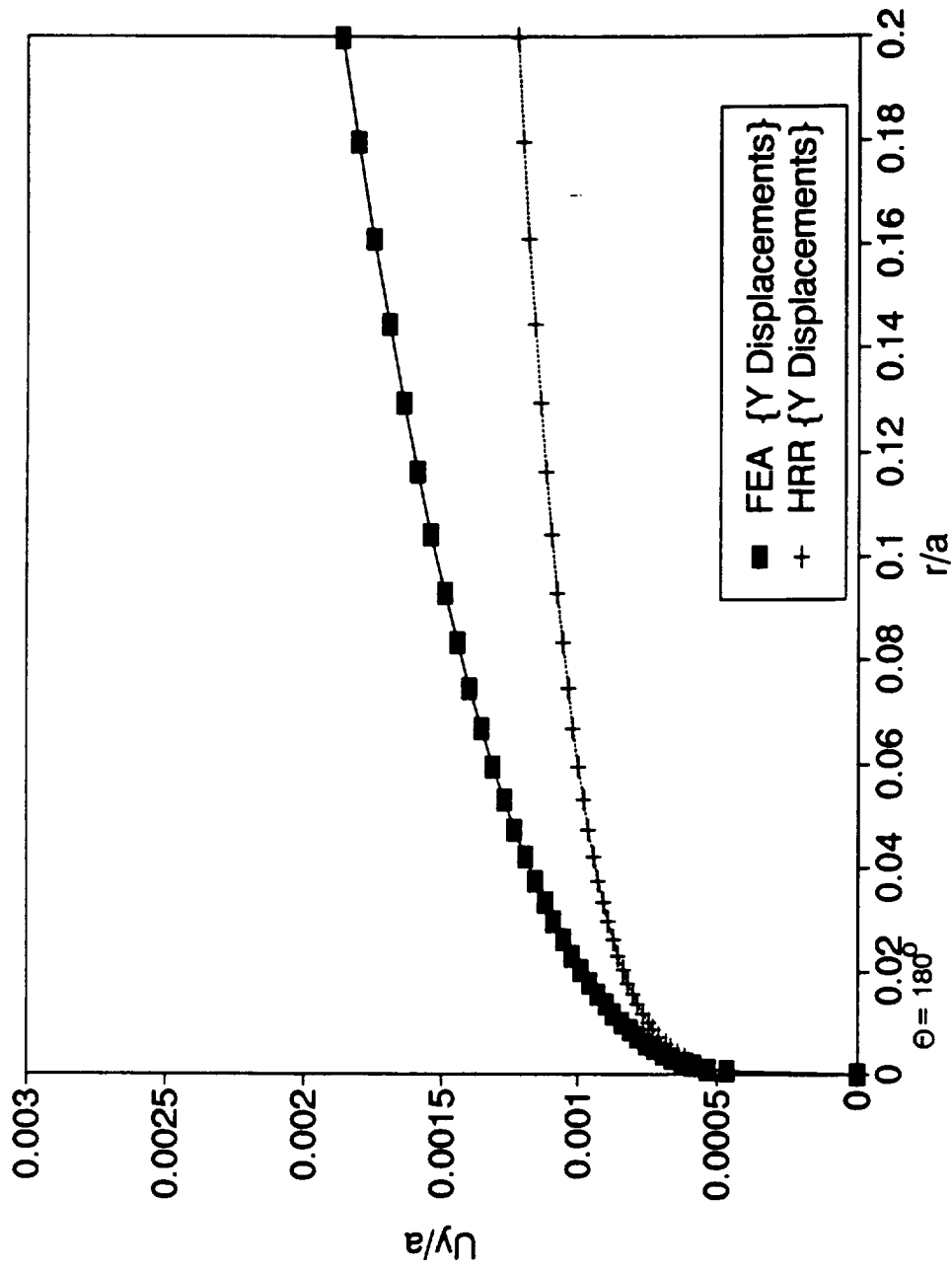
Figure 3.13: Crack Tip Displacements for Elastic-Plastic CCT Model (a/w=0.25)
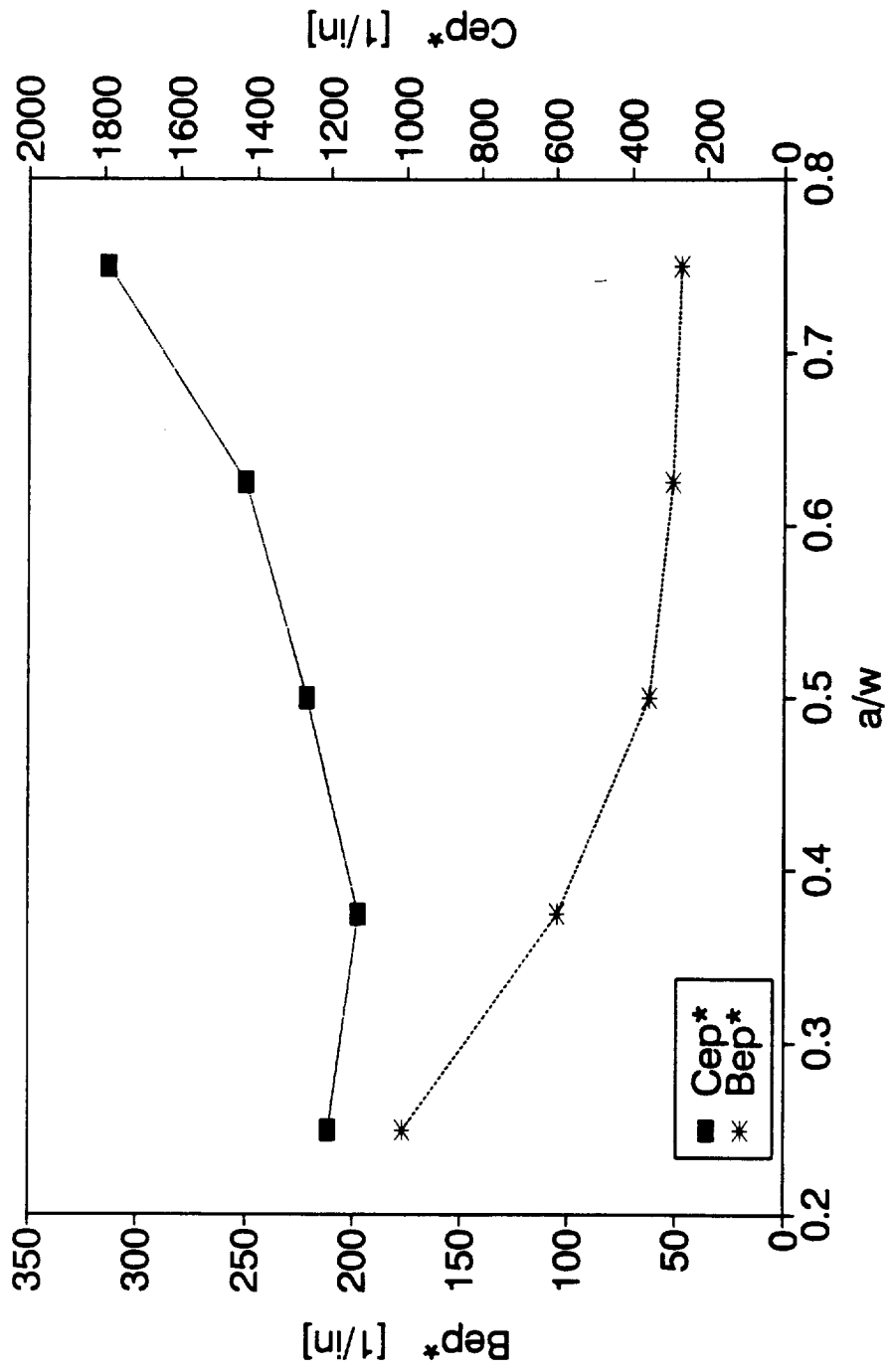
Figure 3.14: Higher Order Displacement Term Coefficients for the
Elastic-Plastic CCT Model

coefficients of the respective terms in equation 3.17 to obtain a dimensionless value. An additional $1/(J/\sigma_0)$ term was then included to obtain normalized units of [1/length]. The units of $(L_{el})^{-1}$ are also [1/length].

Table 3.4: Higher Order Term Coefficients For Elastic-Plastic CCT Model

a/w	$B_{cp}*$	$C_{cp}*$	Q_x*	Q_y*	$(L_{el})^{-1}$
0.25	176.62	1206.2	-1583.8	-1391.9	2.30
0.375	104.21	1129.4	-1284.7	-1149.2	1.90
0.50	61.83	1265.5	-1311.3	-1213.5	1.90
0.625	51.40	1429.9	-1447.5	-1370.9	2.13
0.75	46.81	1793.5	-1868.8	-1809.7	2.82

The crack tip normal stress values in both the x and y directions at $\theta=0°$ were also recorded from the elastic-plastic CCT finite element analysis. An example of the normal stresses versus distance from the crack tip (r) is shown in figure 3.15. The HRR terms, $D_{cp,x}r^{-1/(n+1)}$ and $D_{cp,y}r^{-1/(n+1)}$, where

$$D_{cp,i}(\theta = 0°) = \left(\frac{J}{\alpha\varepsilon_0\sigma_0 I_n}\right)^{1/(n+1)} \tilde{\sigma}_i(0°) \qquad (3.30)$$

were subtracted from the FEA field values of σ_{xx} and σ_{yy}, respectively. The values of the functions of theta were $\tilde{\sigma}_{xx}(0°) = 1.6836$ and $\tilde{\sigma}_{yy}(0°) = 2.2172$ [37]. The form of equations 3.19 and 3.20 were used to determine Q_x and Q_y by curve fitting. All Q's were normalized in a similar fashion as B_{cp} using,
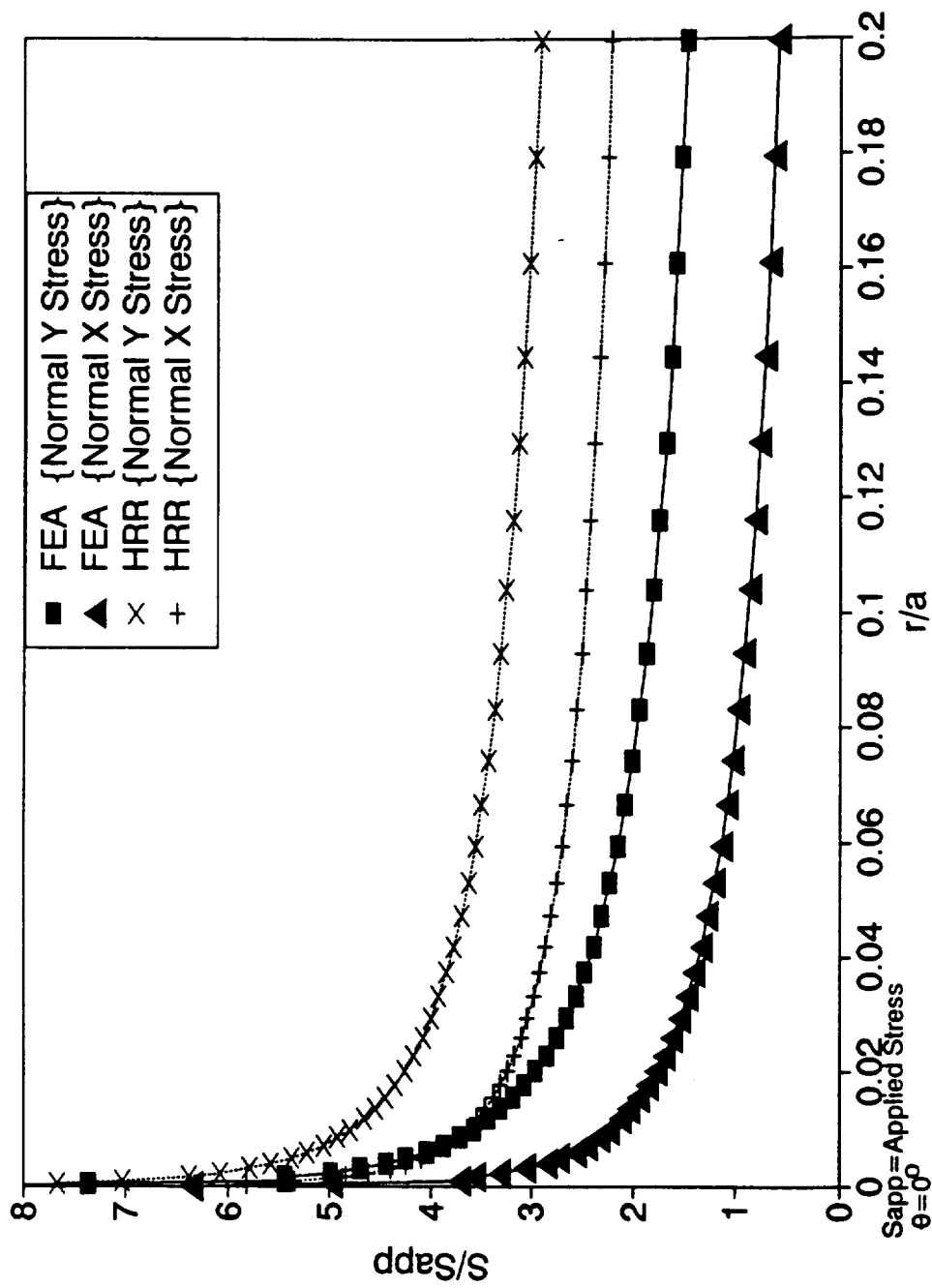
Figure 3.15: Crack Tip Stresses for Elastic-Plastic CCT Model (a/w=0.25)

$$Q_i^* = \frac{Q_i}{\sigma_0 \left(\dfrac{\sigma_0}{J}\right)^i} \left(\frac{1}{(J/\sigma_0)}\right) \qquad (3.31)$$

The values of Q_x^* and Q_y^* are plotted versus crack length in figure 3.16 and are shown in table 3.4. Both Q_x and Q_y were found to be non-zero quantities and similar in magnitude. This is consistent with the findings of O'Dowd and Shih [22]. These researchers introduced a Q parameter in order to extend J based fracture mechanics to include low constraint geometries. The Q parameter quantifies constraint by representing the second term in the near tip stress fields. Their investigation determined that the higher order stress terms ($Q_x r$ and $Q_y r$ in equations 3.21 and 3.22) were approximately constant but did show a slight dependence on r for stresses in the forward sector of the plastic zone ($-90° < \theta < 90°$). The present findings also demonstrated that the higher order stress terms showed only a slight dependence on r.

Constraint Parameter Comparison

The coefficients of the higher order crack tip stress and displacement terms were plotted with $(L_{el})^{-1}$ for each of the finite element models. These figures were developed as one part of a growing database of information on crack tip constraint. The database also includes information on additional constraint parameters and experimental results of various fracture geometries. The ability of these parameters to characterize constraint shall be scrutinized upon the completion of the entire database.

$(L_{el})^{-1}$ was calculated for each of the linear elastic CCT models. B* was then compared to $(L_{el})^{-1}$. Figure 3.17 and 3.18 show that -B* and -T* display
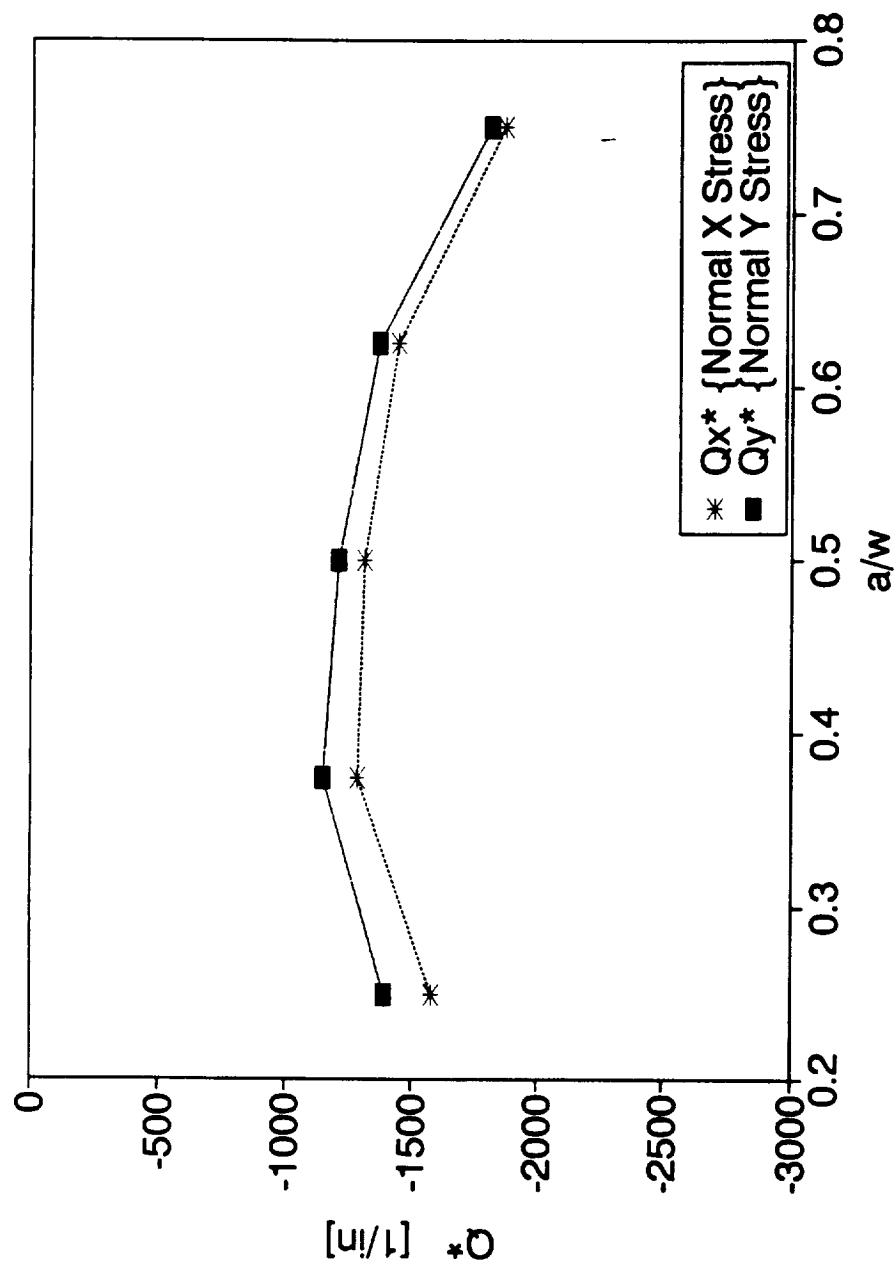
Figure 3.16: Higher Order Stress Term Coefficients for Elastic-Plastic CCT Model
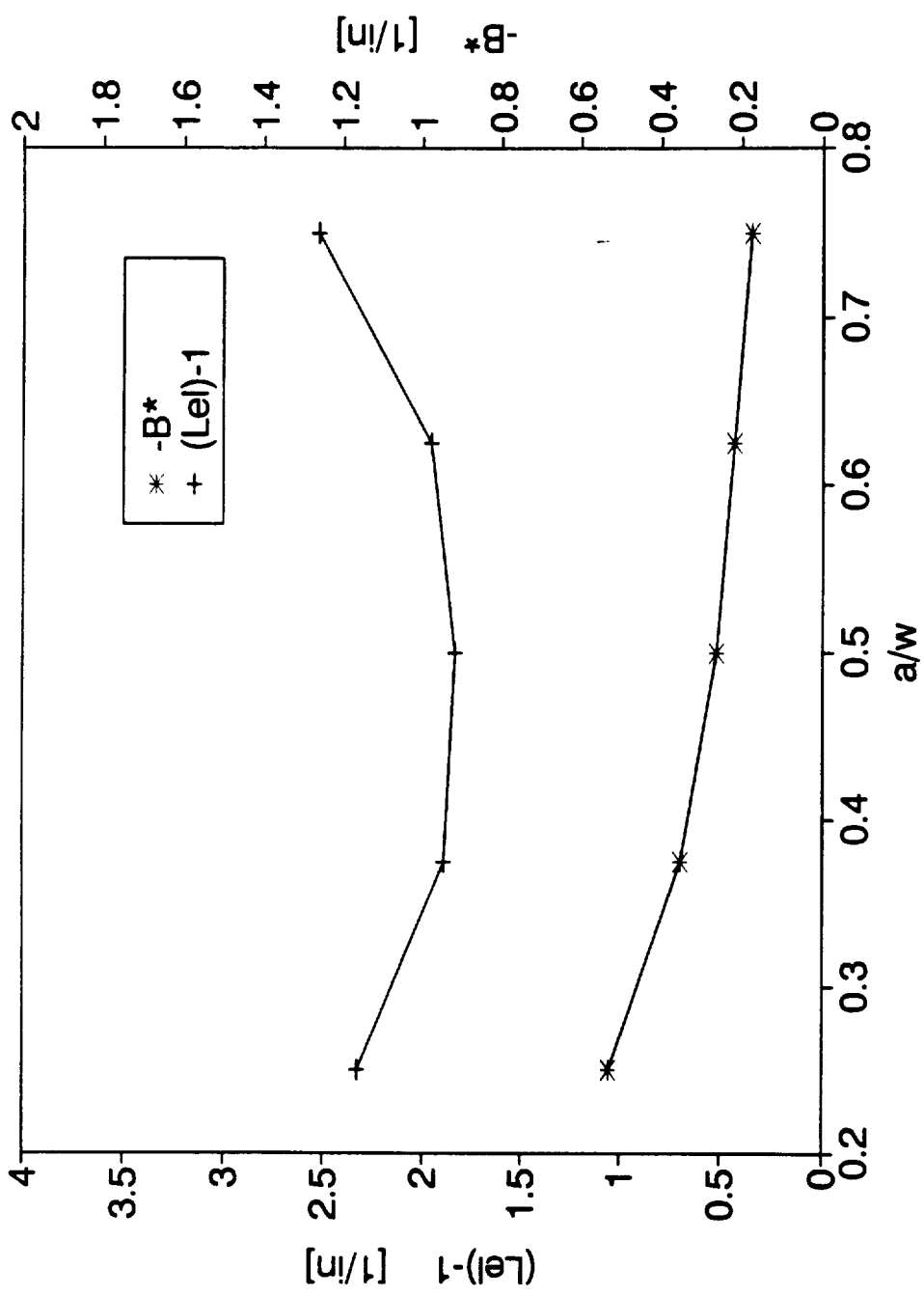
Figure 3.17: (Lel)-1 and -B* for Linear Elastic CCT Model
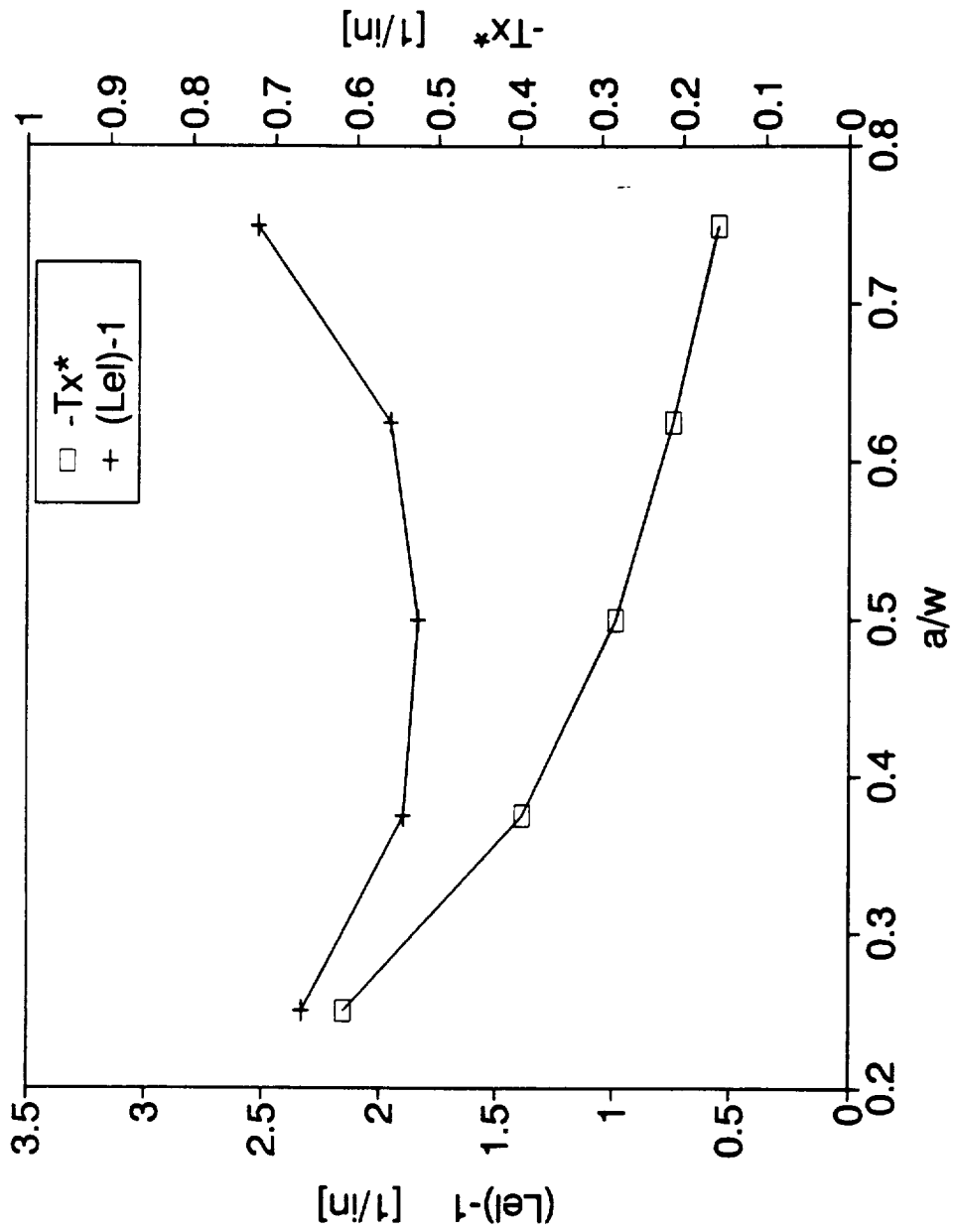
Figure 3.18: (Lel)-1 and -Tx* for Linear Elastic CCT Model

similar trends when plotted with $(L_{el})^{-1}$ from a/w=0.25 to a/w=0.5, but at higher values of a/w the trends diverge. Figure 3.19 displays γ_x^* and γ_y^* with $(L_{el})^{-1}$.

For the linear elastic SCT model, local values of the proposed constraint parameter were calculated by incrementing the size of the crack and applying equation 3.22. Local values of virtual crack extension perpendicular to the original crack front were used to calculate $(L_{el})^{-1}$. Figure 3.20 displays similar trends for -B* and $(L_{el})^{-1}$. Accurate stress values at $\phi=0°$ were not obtained from the SCT model because the finite element mesh was not fine enough in the z direction to account for surface effects. Therefore, the values of T* and γ^* were extrapolated between the elliptical angles of $0°$ and $22.5°$ in figures 3.21 and 3.22. T_x^* and $-T_y^*$ show similar trends with the proposed constraint parameter when plotted as a function of elliptical angle (Figure 3.21). Figure 3.22 compares γ_x^* and γ_y^* with $(L_{el})^{-1}$, but a similar trend was not found. Note that an error was found with the higher order stress term coefficients for the SCT model which is explained in the Discussion of Chapter III.

For the elastic-plastic models, the linear elastic portion of J (G or J_{el}) was calculated using the EPRI [36] estimation scheme, where

$$J_{el} = \frac{(1 - v^2)K^2(a_{\it eff})}{E} \qquad (3.32)$$

and,

$$a_{\it eff} = a + \frac{1}{1+(P/P_0)^2}\frac{1}{\beta\pi}\left(\frac{n-1}{n+1}\right)\left(\frac{K(a)}{\sigma_0}\right)^2 \qquad (3.33)$$

$$P_0 = \frac{4}{\sqrt{3}}tb\sigma_f \qquad (3.34)$$
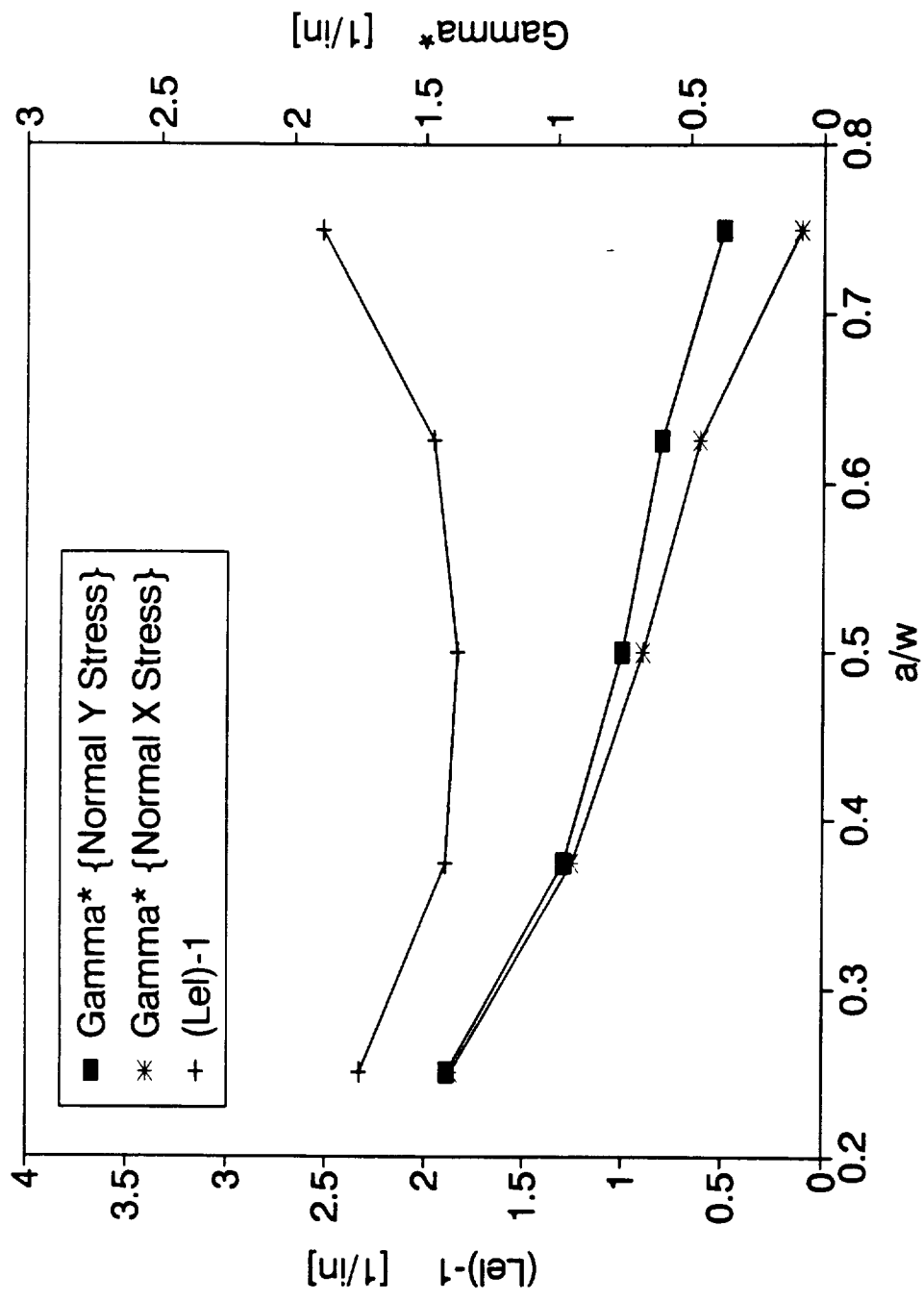
Figure 3.19: (Lel)-1 and Gamma* for Linear Elastic CCT Model
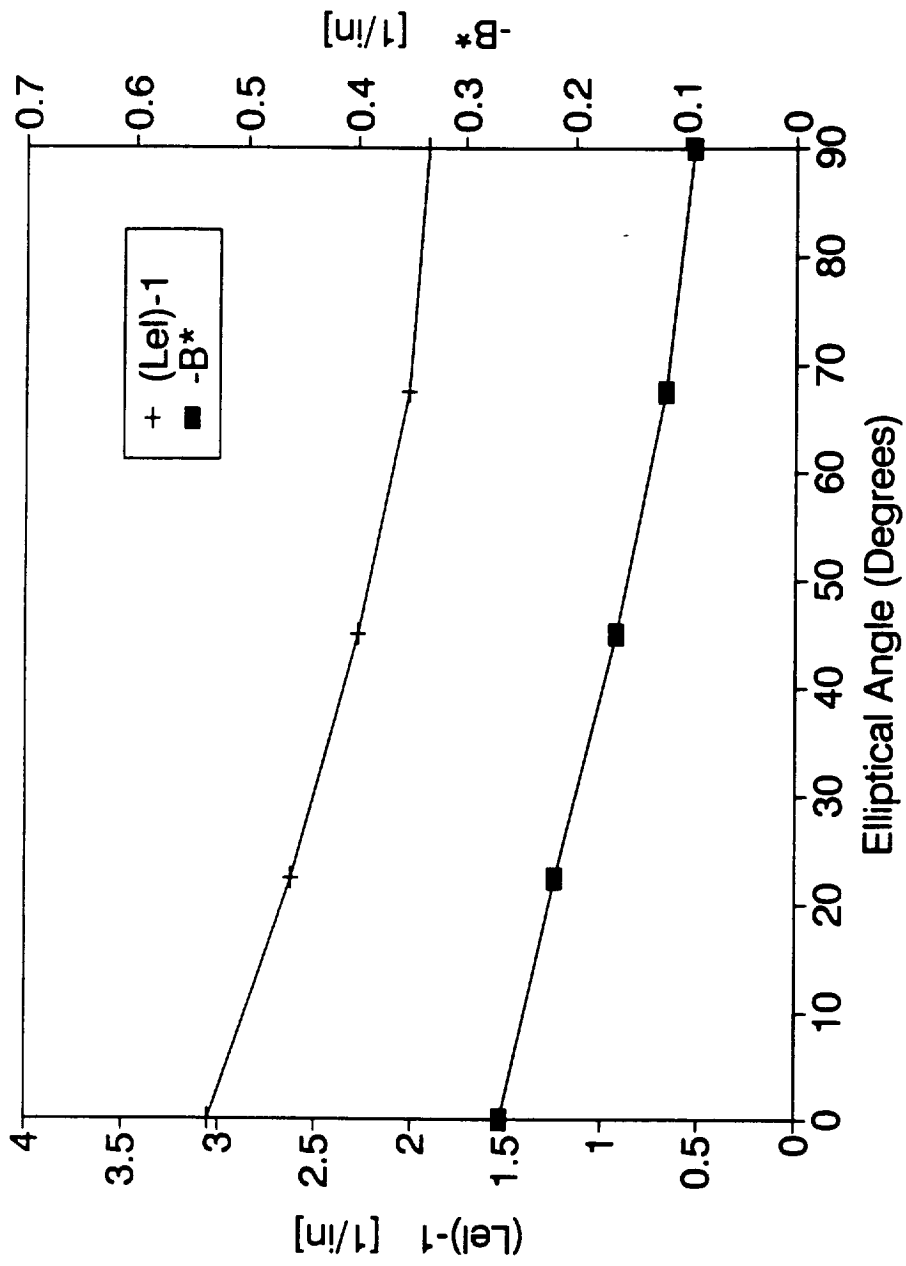
Figure 3.20: (Lel)-1 and B* for Linear Elastic SCT Model
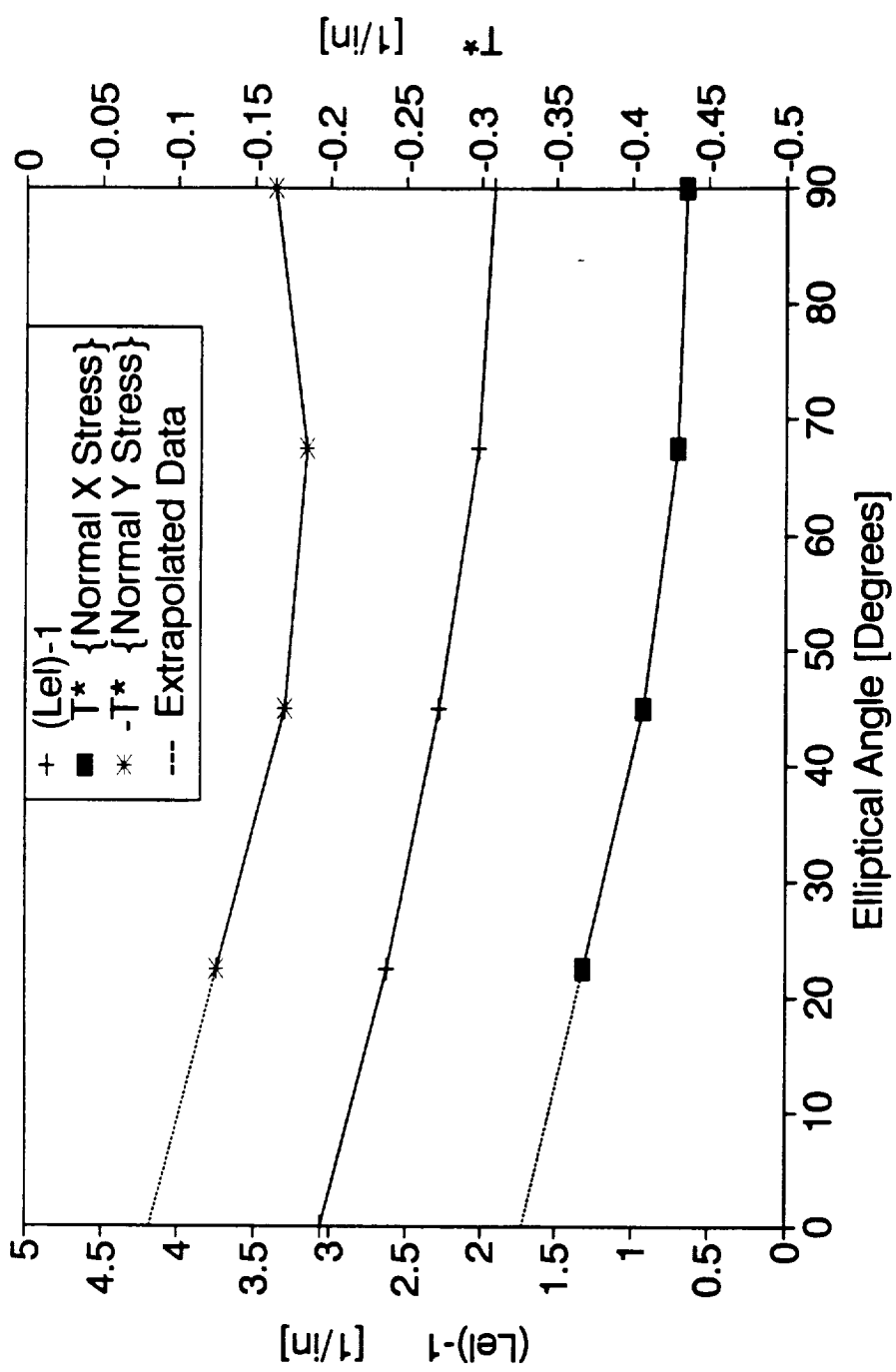
Figure 3.21: (Lel)-1 and T* for Linear Elastic SCT Model
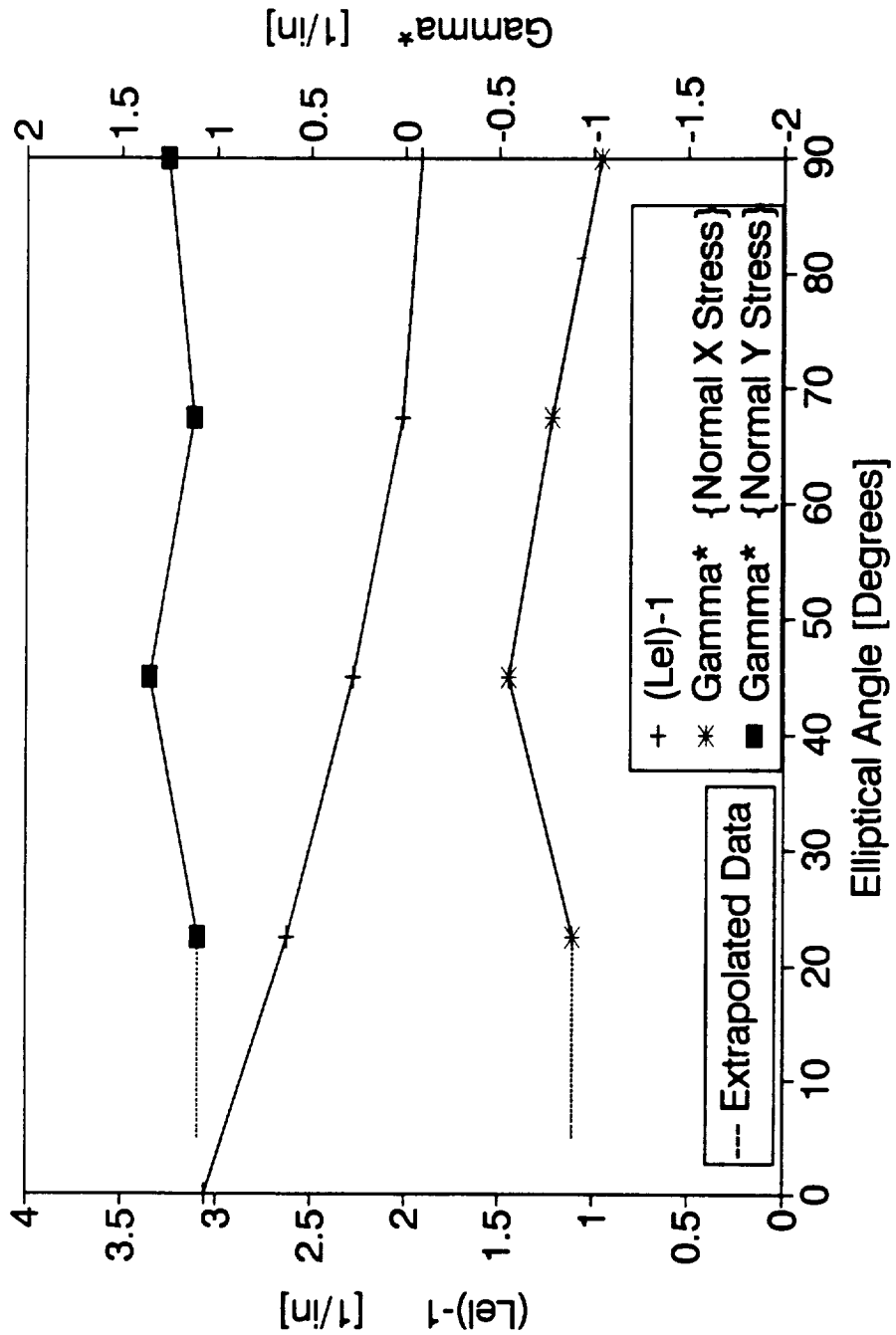
Figure 3.22: (Lel)-1 and Gamma* for Linear Elastic SCT Model

$$\sigma_f = \frac{\sigma_{ut} + \sigma_0}{2} \qquad\qquad (3.35)$$

where $\beta=6$ for plane strain, P is the total applied load, and n is the strain hardening exponent. The specimen thickness, length of the remaining ligament, ultimate tensile strength, and yield strength are designated by t, b, σ_{ut}, and σ_0 respectively. Loaded to 70% of limit load (P_0), the ABAQUS calculated total J values deviated from the EPRI J_{el} values by 15% to 35%. Therefore, 15% to 35% of the total J was due to plasticity (J_{pl}). For the elastic-plastic CCT model, $B_{ep}{}^*$ and $C_{ep}{}^*$ were then plotted with $(L_{el})^{-1}$ in figure 3.23 and 3.24, respectively. Figure 3.25 displays $Q_x{}^*$ and $Q_y{}^*$ with the proposed constraint parameter.

Discussion

The coefficients of the higher order terms developed from the linear elastic CCT model were compared with higher order term relationships derived using the eigenfunction expansion method [3,30] and the Westergaard [3] Z function (Equation 3.12). As predicted by the eigenfunction expansion and the Z function methods, $\gamma_x{}^*$ is virtually equal to $\gamma_y{}^*$ in our numerical results. However, the values begin to deviate at higher a/w's; additional higher order stress terms are possibly required with larger cracks since the finite body effects (at the surface) become more significant. The relationship determined by the Westergaard approach (Equation 3.12) between γ^* and B^* was: $B^*=(-1/3)\gamma_x{}^*=(-1/3)\gamma_y{}^*$. However, the FEA results (with a/w$\leq$0.5) indicate a
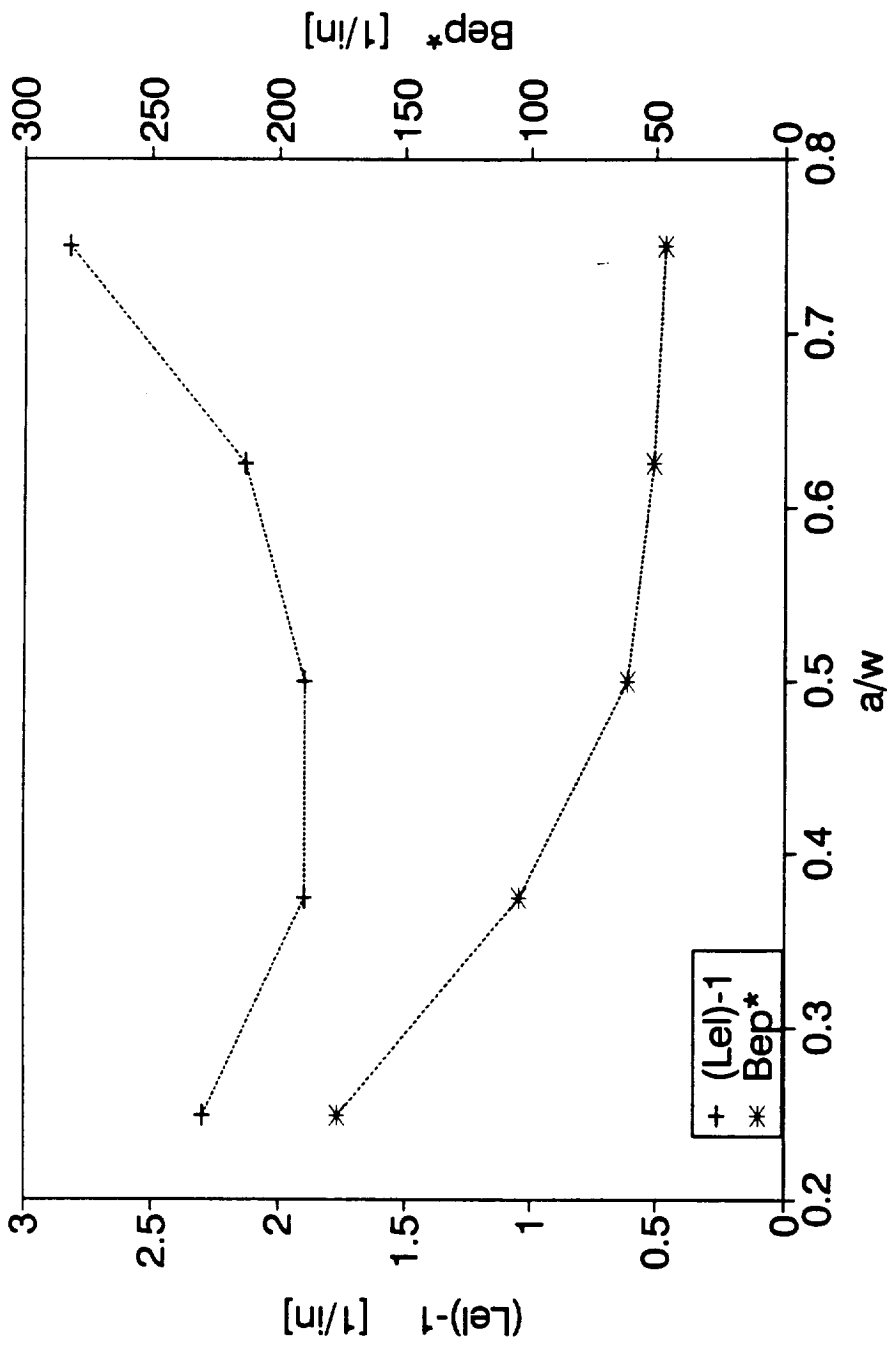
Figure 3.23: (Lel)-1 and Bep* for Elastic-Plastic CCT Model
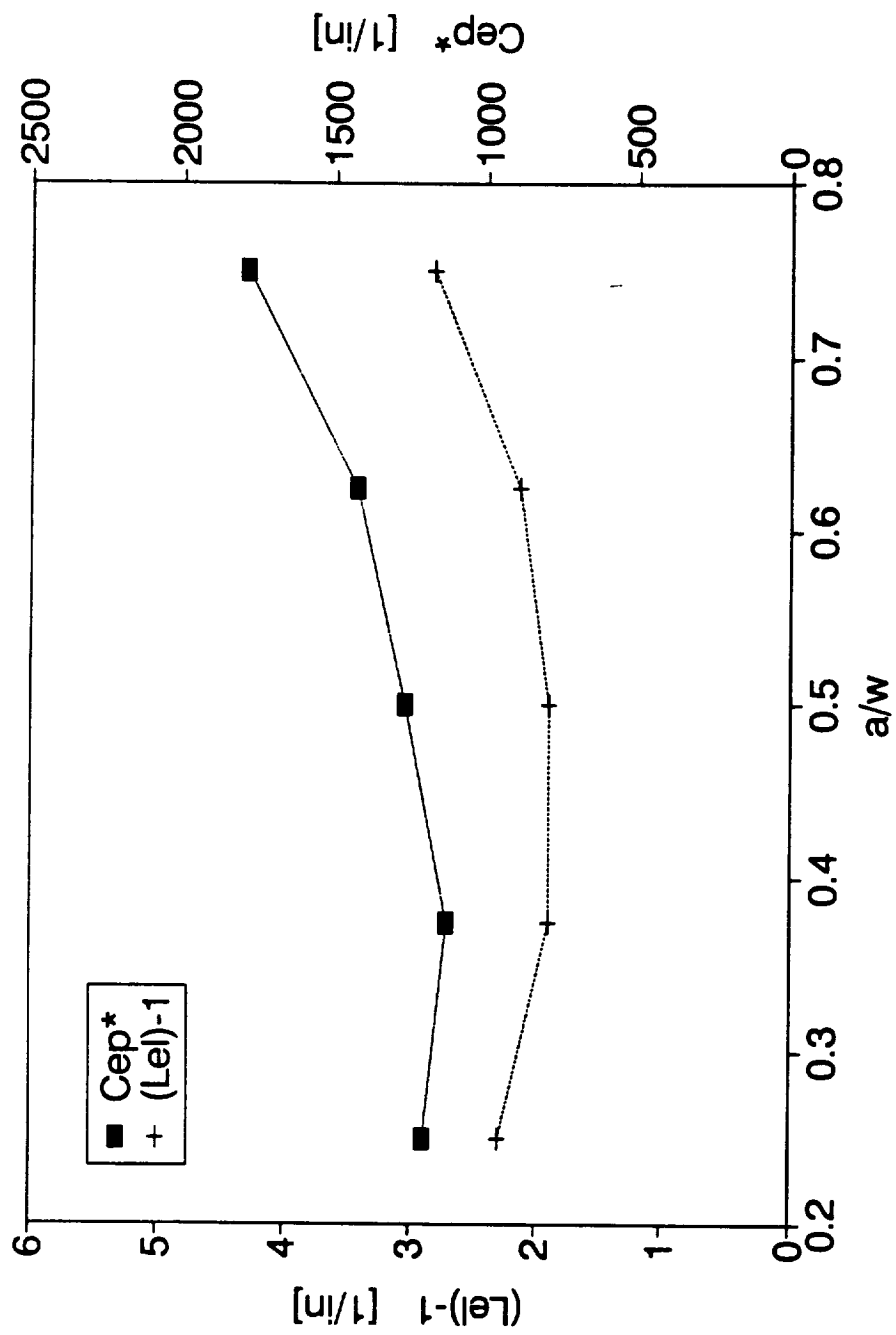
Figure 3.24: (Lel)-1 and Cep* for Elastic-Plastic CCT Model
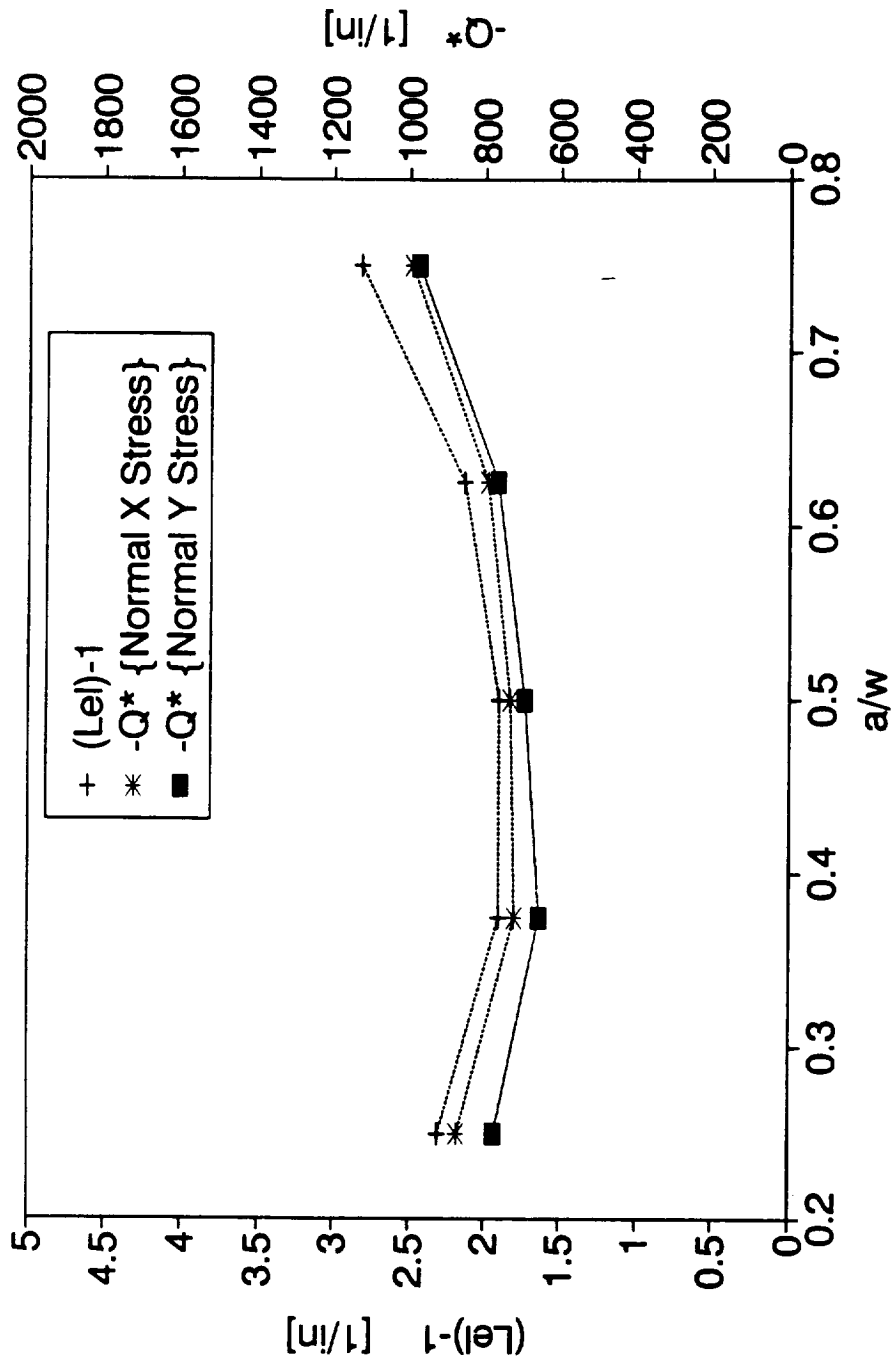
Figure 3.25: (Lel)-1 and the Higher Order Stress Coefficients for Elastic-Plastic CCT Model

relationship of the form: $B^* \approx -0.37\gamma_x^* \approx -0.37\gamma_y^*$. The difference in the two results could be attributed to finite body effects.

After the successful defense of this thesis, the curve fitting format of equation 3.17 was found to be incorrect. The T_y term was included when curve fitting the higher order σ_{yy} terms for the linear elastic SCT model. However, the T_y term should not have been included in the curve fits since it would invalidate the traction boundary conditions along the crack face. The term was not found to be zero, as it was in the linear elastic CCT model, because the higher order σ_{yy} terms converged to a finite stress value at the crack tip as r→0. The most likely explanation for the finite value convergence is the inaccuracy of the singular σ_{yy} term calculation. An assumption on the out-of-plane stress state was made during the calculation of the singular term in order to convert the energy release rate, G_I, calculated by ABAQUS [28] to the stress intensity factor, K_I; after converting, K_I was then used to calculate the singular stress terms. Perhaps a better procedure to determine the singular stress term includes iteratively offsetting the higher order σ_{yy} terms by T_y. That is, determine the higher order σ_{yy} term coefficients using the out-of-plane stress state assumption. Then, add T_y to the singular stress term to determine the value of an iterative singular stress term. At this point, the iterative singular stress term is subtracted from the FEA stresses to obtain iterative values of the higher order σ_{yy} stress terms. The iterative higher order terms can be curve fit in order to obtain iterative values for T_y and γ_y. Repeat the previous steps until the iterative singular σ_{yy} term converges and T_y=0. After convergence, a more accurate value for K_I can be calculated using the singular stress term. This value of K_I should

then be used to calculate the singular σ_{xx} term and the first term in the displacement series, so that the higher order σ_{xx} and u_y term coefficients can be determined. In addition, perhaps a similar iterative procedure could be utilized to bring the higher order term coefficients of the linear elastic CCT model (a/w=0.625,0.75) into agreement with equation 3.12.

The Q values for the elastic-plastic CCT model were determined by curve fitting the two-term stress series expansion (Equations 3.19 and 3.20). The two terms yielded good representations of the crack tip stresses over the curve fitted range $1 < r/(J/\sigma_0) < 15$. Sharma and Aravas [32] used this two term series in their asymptotic analysis of crack tip fields. However, they also stated that at the distances $r/(J/\sigma_0)=2$ and $r/(J/\sigma_0)=5$ from the crack tip additional terms in the asymptotic stress expansion (Equation 3.13) may be needed for an accurate representation of the stress field in front of the crack tip.

The second and third order terms were required for curve fitting the elastic-plastic displacements. The Sharma and Aravas and Li and Wang analyses both state that the second order term $(B_{cp}r^{(n-1)r+1})$ does not account for the effects of elasticity. The third order displacement term is a function of the elastic strain resulting from the singular (HRR) stress term. Therefore, with the second and third order terms included, excellent agreement between the FEA field values and the curve fitting constants were obtained for the displacement fields.

The similar trends observed between C_{cp}^* and $(L_{sl})^{-1}$ in figure 3.24 and Q^* and $(L_{sl})^{-1}$ in figure 3.25 are significant developments. The similar trend suggests that C_{cp}^*, Q^*, and $(L_{sl})^{-1}$ are related. Of course, an implicit relationship

exists between the terms in the crack tip stress, strain and displacement series. Therefore, if a relationship does exist between $(L_{el})^{-1}$ and the higher order terms, $(L_{el})^{-1}$ can be considered a second fracture parameter (i.e. constraint parameter). However, an extensive analytical study of the higher order term coefficients is required in order to develop a relationship with $(L_{el})^{-1}$.

$(L_{el})^{-1}$ is a parameter associated with the higher order strain/displacement terms for a linear elastic stress state. C_{ep}^{*} is a function of the elastic strain/displacement resulting from the HRR term in the stress series. Therefore, the similar trend between C_{ep}^{*} and $(L_{el})^{-1}$ suggests that constraint parameters may be separable in elastic and plastic components by relating these separate terms to different higher order terms in the stress, strain, or displacement series. However, finite geometry effects have not been accounted for in the comparison between C_{ep}^{*} and $(L_{el})^{-1}$. In addition, experimental results must be implemented in the investigation before concluding that $(L_{el})^{-1}$ is a valid constraint parameter for general use. Nevertheless, the possible relationship with the higher order stress and displacement terms suggests a bright future for $(L_{el})^{-1}$ as a constraint parameter.

REFERENCES

[1] Anderson, T.L., <u>Fracture Mechanics Fundamentals and Applications</u>, CRC Press Inc., Boca Raton, FL, 1991.

[2] Westergaard, H.M., "Bearing Pressures and Cracks", *Journal of Applied Mechanics*, Vol. 6, 1939, pp. 49-53.

[3] Williams, M.L., "Stress Singularities Resulting From Various Boundary Conditions in Angular Corners of Plates in Extension," *Journal of Applied Mechanics*, 1952, pp. 526-528.

[4] Irwin, G.R., "The Crack Extension Force for a Part-Through Crack in a Plate," *Journal of Applied Mechanics*, 1962, pp. 651-654.

[5] Newman, J.C. and Raju, I.S., "Stress-Intensity Factor Equation for Cracks in Three-Dimensional Finite Bodies," ASTM STP 791, American Society for Testing and Materials, 1983, pp. I285-I265.

[6] Griffith, A.A., "The Phenomena of Rupture and Flow in Solids." *Philosophical Transactions*, Series A, Vol. 221, 1920, pp.163-198.

[7] Inglis, C.E., "Stresses in a Plate Due to the Presence of Cracks and Sharp Corners." *Transactions of the Institute of Naval Architects*, Vol. 55, 1913, pp. 219-241.

[8] Irwin, G.R., "Plastic Zone Near a Crack and Fracture Toughness," *Proceedings: Seventh Sagamore Conference*, 1960, pp. IV-63.

[9] Rice, J.R. "A Path Independent Integral and the Approximate Analysis of Strain Concentration by Notches and Cracks." *Journal of Strain Analysis*, Vol. 1, 1966, pp. 145-153.

[10] Hutchinson, J.W., "Singular Behavior at the End of a Tensile Crack Tip in a Hardening Material." *Journal of the Mechanics and Physics of Solids*, Vol. 16, 1968, pp. 13-31.

[11] Rice, J.R. and Rosengren, G.F., "Plane Strain Deformation near a Crack Tip in a Power-Law Hardening Material." *Journal of the Mechanics and Physics of Solids*, Vol. 16, 1968, pp. 1-12.

[12] Hutchinson, J.W. and Paris, P.C., "Stability Analysis of J-Controlled Crack Growth," ASTM STP 668, American Society of Testing and Materials, 1979, pp. 37-64.

[13] Ernst, H.A., "Material Resistance and Instability Beyond J-Controlled Crack Growth," ASTM STP 803, American Society for Testing and Materials, 1983, pp. I191-I213.

[14] Ernst, H.A., "Further Developments on the Modified J-Integral," ASTM STP 995, American Society for Testing and Materials, 1989, pp. 306-319.

[15] Parks, D.M., and Wang, Y.Y., "Elastic-Plastic Analysis of Part-Through Surface Cracks." *Analytical, Numerical, and Experimental Aspects of Three-Dimensional Fracture Processes*, ASME AMD-91, American Society of Mechanical Engineers, New York, 1988, pp. 19-32.

[16] McCabe, D.E., "Flaw Growth Analysis for 2219-T87 Aluminum Pressure Vessel Welds", Materials Engineering Associates, MEA-2321, 1988.

[17] Ernst, H.A., "Resistance Curve Analysis of Surface Cracks", Martin Marietta Manned Space Systems Contract SC-273276, Annual Report-Fiscal Year 1991.

[18] Sommers, E., and Aurich, D., "On the Effect of Constraint on Ductile Fracture."

[19] Kordisch, H., and Sommers, E., "Three-Dimensional Effects Affecting the Precision of Lifetime Predictions," ASTM STP 969, 1988, pp. 73-87.

[20]   McClintock, F.A., "A Criterion for Ductile Fracture by the Growth of Holes", *Journal of Applied Mechanics*, Vol. 35, 1968, pp 73-87.

[21]   Larsson, S.G. and Carlsson, A.J., "Influence of Non-Singular Stress Terms and Specimen Geometry on Small-Scale Yielding at Crack Tips in Elastic-Plastic Materials", *Journal of Mechanics and Physics of Solids*, Vol. 23, 1973, pp 263-277.

[22]   O'Dowd, N.P. and Shih, C.F., "Family of Crack-Tip Fields Characterized by a Triaxiality Parameter: Parts I and II", *Journal of Mechanics and Physics of Solids*, 1991.

[23]   McClintock, F.A., "Plasticity Aspects of Fracture," *Fracture: An Advances Treatise*, Vol. 3, Academic Press, New York, 1971, pp. 47-225.

[24]   Tada, H., Paris, P.C., and Irwin, G.R., "The Stress Analysis of Cracks Handbook", Del Research Corporation, St. Louis, MO, 1976.

[25]   Begley, J.A., and Landes, J.D., "The J-Integral as a Fracture Criterion," ASTM STP 514, American Society for Testing and Materials, 1972, pp. 1- 20.

[26]   Richardson, D.E., "A New Biaxial Stress Failure Criterion," Ph.D. Thesis, Clemson University, August, 1991.

[27]   Betegon, C., and Hancock, J.W., "Two Parameter Characterization of Elastic-Plastic Crack Tip Fields." *Journal of Applied Mechanics*, 1991.

[28]   ABAQUS USER'S MANUAL, Hibbitt, Karlsson & Sorensen, Inc., 1988.

[29]   Barsoum, R.S., "On the Use of Isoparametric Finite Elements in Linear Elastic Fracture Mechanics," *International Journal of Numerical Methods in Engineering*, Vol. 10, 1976, pp. 25-37.

[30]   Williams, M.L., "On the Stress Distribution at the Base of a Stationary Crack." *Journal of Applied Mechanics*, Vol. 24, 1957, pp. 109-114.

[31] Nakamura, T., and Parks, D.M., "Determination of Elastic T-Stress Along Three-Dimensional Crack Fronts Using An Interaction Integral," *International Journal of Solids and Structures*, Vol. 29, No. 13, 1992, pp. 1597-1611.

[32] Sharma, S.M., and Aravas, N., "Determination of Higher-Order Terms in Asymptotic Elastoplastic Crack Tip Solutions," *Journal of the Mechanics and Physics of Solids*, Vol. 39, No. 8, pp. 1043-1072.

[33] Li, Y., and Wang, Z., "Higher-Order Asymptotic Field of Tensile Plane-Strain Non-Linear Crack Problems," Scientia Sinica, Vol. XXIX, No. 9, pp. 941-955, September, 1986.

[34] Hutchinson, J.W., "Fundamentals of the Phenomenological Theory of Non-Linear Fracture Mechanics," *Journal of Applied Mechanics*, Vol. 50, 1983, pp. 1042-1051.

[35] Shih, C.F., "Relationship Between the J-Integral and the Crack Opening Displacement for Stationary and Extending Cracks," *Journal of the Mechanics and Physics of Solids*, Vol. 29, 1981, pp. 305-326.

[36] Kumar, V., German, M.D., Shih, C.F., "An Engineering Approach for Elastic-Plastic Fracture Analysis," Electric Power Research Institute, Palo Alto, CA, EPRI Report NP-1931, Project 1237-1, July 1981.

[37] Symington, M., Shih, C.F., and Ortiz, M., Brown University Report, MRG/DMR-8714665/1, 1988.

[38] Rice, J.R., Fracture (edited by Liebowitz, H.), Vol. 2, Mathematical Fundamentals, p. 191, Academic Press, New York.

CHAPTER IV

EFFORTS TO CHARACTERIZE THREE-DIMENSIONAL EFFECTS OBSERVABLE IN TWO DIMENSIONAL FRACTURE SPECIMENS.

by D. Lambert and H. Ernst

4.1. Introduction

The underlying purpose of this research is to develop a methodology which would allow the characterization of three-dimensional (3D) effects in fracture. This characterization should include:

(1) geometric effects arising from crack front curvatures (curvatures are present, for example, with surface cracks),

(2) geometric effects related to thickness and ligament length (the gross sizing details that affect the three-dimensionality of the state of stress at the crack tip), and

(3) loading geometry effects (including three-dimensionality of the far field stress arising from the character of applied loads, and, especially the gradient of the far-field stress arising from differing ratios of bending-to-tension).

Two-dimensional (2D) or *planar* specimens have been observed to generate different fracture resistance curves when different

thicknesses are tested. Specifically discussed here are J_MR curves that use the J-modified parameter as developed by Ernst [4.1,4.2][1]. Different configurations have been shown to support a differing degree of triaxiality of the stress field in the vicinity of the crack front, where the fracture process is occurring. The degree of stress field triaxiality that is exhibited is referred to as the *constraint*. The J_MR curves are a result of the different, *averaged* constraint in each specimen. Even though the configurations are considered to be planar, curvatures can develop in crack fronts that result from fracture in the presence of a gradient of the constraint within the specimen. Thus, the complexities that occur in the most general cases of fracture appear in the simplest cases of planar specimens. Ultimately, to evaluate fracture resistance retaining a planar analogy requires that the crack front fall within specific limits of straightness.

Since, 3D stress fields are present in planar configurations, an effort to map the crack face separation *profiles* of a variety of geometries as a function of the position within the cross-section has been proposed. The crack tip opening displacement (CTOD) is a linear function of the J-integral [4.3]. Profiling represents an extension of that functional relationship.

One goal of the overall research program is to test a wide variety of planar specimens, varying the thickness and length of the initial remaining ligament, as well as the bending-to-tension

---

[1]Numbers in brackets refer to the references at the end of the paper

ratio due to the nature of the applied load to produce significant changes in fracture behavior. The results will be compared using the ligament dimensions as variables, and finite-element analysis will be used to evaluate the triaxiality of the stress field. Although other parameters might be used, one parameter being considered to quantify the stress field triaxiality is h:

$$h = \frac{\sigma_{mean}}{\sigma_{vM}}$$
(4.1)

Here, σ_{mean} is the mean stress and σ_{vM} is von Mises equivalent stress. Ultimately, this approach is expected to produce parameters and fracture behavior that can be generalized to the 3D cases that are of the most interest.

4.2 Introduction to Profiling

The displacement of the faces of a crack are a function of the loading and of the position. Using a two dimensional analogy, the displacement of a point along a crack face within an elastic body was given by Tada, et al [4.4]:

$$v_{el} = \frac{4\sqrt{2}}{E'\sqrt{\pi}} K \sqrt{r}$$
(4.2)

Here, v_{el} is the "y"-directed elastic displacement at position r, measured from the crack tip to the point in question, E' is the equivalent modulus (E'=E for plane stress, E'=E/(1-v^2) for plane strain, v is Poisson's ratio). The loading is specified in the presence of a flaw by K, the stress intensity parameter. This displacement relationship has a square-root of r form.

Hutchinson [4.5] and Rice and Rosengren [4.6] developed a similar form for plastic response that follows Ramberg-Osgood deformation characteristics, i.e.:

$$\frac{\varepsilon}{\varepsilon_o} = \alpha (\frac{\sigma}{\sigma_o})^n \qquad (4.3)$$

In this equation, ε and σ are the equivalent strain and stress and ε_o, σ_o and n are material constants. The form of the displacement is as follows:

$$v_{pl} = k \cdot J_{pl}^{\frac{n}{n+1}} r^{\frac{1}{n+1}} \qquad (4.4)$$

This equation is written for a non-growing crack, and v_{pl} is the the displacement of the body, assuming Ramberg-Osgood type deformation, and k includes the functionality with regards to the constraint, i.e., plane stress or plane strain condition. Looking at the equations (4.2) and (4.4), the constraint appears

in the coefficient E' for the linear elastic case and in the coefficient k for the plastic case. Thus, the separation at various points through the ligament thickness could be expected to reflect that difference in constraint that arises with the depth into the thickness. It may also provide a measure of that constraint.

Since the development above is for a non-growing crack situation, differences that occur between the theoretical elastic plus plastic displacements and the displacement profile of an actual growing crack near the crack tip might provide a fracture criterion on that local level.

4.3 Profiling Matrix and Details

One objective in the research was to characterize the separation between the surfaces of cracks. This separation *profile* is a function of the level of J and of the position within the ligament. In this case the position would include the distance from the load-line, x, in the direction of crack growth, and the depth beneath the surface in the thickness direction, z.

The primary effort in the past six months has been to characterize the crack face separation of selected specimens. The specimen identities and the corresponding configurations appear in Table 4.1, below. Data was generated for a total of six compact tension (CT) specimens and three center-crack tension (CCT) specimens. The CCT configuration produces two crack

Table 4.1: Matrix of Specimens Profiled

(W, B, and b are in inches, a/W is nondimensional)

Spec	Config	W	B	b	a/W	Remarks	No of Profs
E2	1T-CT	2	1/2	1	.5	Baseline Specimen	8
81	1T-CT	2	1/2	.5	.75	Larger Init. a/W	8
51	1T-CT	2	1/4	1	.5	Thinner Section	5
C9	1T-CT	2	.85	1	.5	Thicker Section	13
82	1T-CT	2	1/2	1	.5	Multi-Specimen	8
84	1T-CT	2	1/2	1	.5	Multi-Specimen	8
08	1T-CT 20%SG	2	1/2	.8	.6	Side-Grooved	8
D6	CCT	1	1/2	.5	.5	Tension	2×8
55	CCT	1	1/8	.5	.5	Tension, Thin	2×3
B9	CCT	1	.85	.5	.5	Tension, Thick	2×9

profiles per specimen, and thus the total number of crack fronts observed is thirteen. Profiles were made of the AL6061-T651 in every case: the IN718-STA1 material has proven too hard to polish in the same fashion as the aluminum. Epoxy infused into the gap of the crack was effective in producing a well-defined crack profile for the aluminum, but the profiles of the nickel were rounded and poorly-defined. Until the techniques have been modified to overcome the rounding, the profiling was suspended for the nickel.

After mounting the specimens in epoxy, the exposed surface was polished to provide a surface profile. After recording the profile, 0.025- to 0.035-inches was removed by grinding and polishing to produce the next profile to be recorded. This was continued for each specimen into the center of the cross-section.

```
14440 REM ---------------------------------------------------------
15000 REM          dJ/da CALCULATION
15001 REM
15100 REM TRANSFER ARRAYS SO EXISTING SUBROUTINES CAN BE USED
15105 REM
15110 FOR DUM=0 TO NUM:JT(DUM)=J(DUM):XT(DUM)=X(DUM):YT(DUM)=Y(DUM):NXT(D
DUM):NYT(DUM)=NY(DUM):NEXT DUM
15120 REM ---------------------------------------------------------
15150 REM   CALCULATE NORMAL TO EQUIVALENT ELLIPSE
15155 FOR DUM=1 TO NUM-1
15160 YD(DUM)=-X(DUM)*A*(1-(X(DUM)/C(DUM))^2)^-.5/C(DUM)^2
15162 PX=-YD(DUM):PY=1
15164 HYP=(1+PX^2)^.5
15166 NX(DUM)=PX/HYP
15168 NY(DUM)=PY/HYP
15195 NEXT DUM
15200 REM   CALCULATE COORDINATES OF POINTS AHEAD OF FRONT
15210 FOR DUM=0 TO NUM
15220 X(DUM)=XT(DUM)+NX(DUM)*(T/2500)
15230 Y(DUM)=YT(DUM)+NY(DUM)*(T/2500)
15240 NEXT DUM
15241 A=Y(NUM)
15242 REM ---------------------------------------------------------
15245 REM CALCULATION OF EFFECTIVE C'S SUCH THAT NORMALS ARE EQUAL
15250 FOR DUM=1 TO NUM-1
15255 C(DUM)=(X(DUM)^2/(1-(Y(DUM)/A)^2))^.5
15260 NEXT DUM
15265 C(NUM)=C(NUM-1):REM BECAUSE C AT THE TOP IS UNDEFINED
15270 C(0)=X(0):REM BY DEFINITION
15301 REM ---------------------------------------------------------
15302 REM          CALCULATE ELLIPTICAL ANGLES
15304 GOSUB 12000
15310 REM ---------------------------------------------------------
15320 REM                    CALCULATE G'S
15330 GOSUB 8000
15340 REM ---------------------------------------------------------
15350 REM                    CALCULATE J'S  ·
15355 GOSUB 8500
15360 REM ---------------------------------------------------------
15363 REM CALCULATE dJ/da FROM INCREMENTAL GROWTH OF EQUIV. FRONTS
15364 REM
15365 FOR DUM=0 TO NUM:JDA(DUM)=(JT(DUM)-J(DUM))/(T/2500):NEXT DUM
15390 REM ---------------------------------------------------------
15400 REM CALCULATE dJ/da FROM MASTER R-CURVE
15410 FOR DUM=0 TO NUM
15420 JDAM(DUM)=3*ALPA*J(DUM)^2+2*BETA*J(DUM)+GMMA
15425 JDAM(DUM)=1/JDAM(DUM)
15430 NEXT DUM
15450 FOR DUM=0 TO NUM
15455 F(DUM)=JDA(DUM)/JDAM(DUM)
15456 IF F(DUM)<1 THEN F(DUM)=1:REM BY DEFINITION F CANNOT BE LESS THAN 1
15460 NEXT DUM
15500 REM TRANSFER BACK ARRAYS
15510 FOR DUM=0 TO NUM:J(DUM)=JT(DUM):Y(DUM)=YT(DUM):X(DUM)=XT(DUM):NX(DUM
DUM):NY(DUM)=NYT(DUM):NEXT DUM
15600 RETURN
```

```
10020 C(DUM)=((X(DUM)^2*A^2)/(A^2-Y(DUM)^2))^.5
10040 NEXT DUM
10050 C(NUM)=C(NUM-1)
.10200 FOR DUM=0 TO NUM
10210 IF C(DUM)>W/2 THEN C(DUM)=W/2:PRINT" C > W/2"
10220 NEXT DUM
10900 RETURN
10998 REM ###########################################################
10999 REM -----------------------------------------------------------
11000 REM            CALCULATION OF Fs AT ONE POINT
11001 REM -----------------------------------------------------------
11002 REM                FOR A/C>1
11100 M1=(C(DUM)/A)^.5*(1+.04*C(DUM)/A)
11150 M2=.2*(C(DUM)/A)^4
11200 M3=-.11*(C(DUM)/A)^4
11250 LG=1+(.1+.35*(C(DUM)/A)*(A/T)^2)*(1-SIN(TH(DUM)))^2
11300 FT=((C(DUM)/A)^2*(SIN(TH(DUM)))^2+(COS(TH(DUM)))^2)^.25
11495 RETURN
11499 REM -----------------------------------------------------------
11500 M1=1.13-9.000001E-02*(C(DUM)/A)
11550 M2=-.54+.89/(.2+A/C(DUM))
11600 M3=.5-1/(.65+A/C(DUM))+14*(1-A/C(DUM))^24
11650 LG=1+(.1+.35*(A/T)^2)*(1-SIN(TH(DUM)))^2
11700 FT=((A/C(DUM))^2*COS(TH(DUM))^2+SIN(TH(DUM))^2)^.25
11900 RETURN
11997 REM ###########################################################
11998 REM
11999 REM -----------------------------------------------------------
12000 REM          CALCULATION ELLIPTICAL ANGLE ALONG THE FRONT
12001 REM -----------------------------------------------------------
12100 FOR DUM=1 TO NUM-1
12110 IF A/C(DUM)<1 OR A/C(DUM)=1 THEN OPP=Y(DUM):ADJ=(A^2-OPP^2)^.5
12115 IF A/C(DUM)>1 THEN ADJ=X(DUM):OPP=(C(DUM)^2-ADJ^2)^.5
12117 IF A/C(DUM)<0 OR X(DUM)>C(DUM) THEN PRINT"A/C OUT OF RANGE":GOTO 500
12120 TH(DUM)=ATN(OPP/ADJ)
12150 NEXT DUM
12400 RETURN                              .
12450 REM ###########################################################
12998 REM
12999 REM -----------------------------------------------------------
13000 REM          CALCULATION OF Dstar
13001 REM -----------------------------------------------------------
13100 FOR DUM=0 TO NUM
13110 XD1=.224*N*W
13120 XD2=PI*BN*(N+1)*(GAVG/SIG^2)
13130 XD3=(A/C(DUM))^(1-PP*N)
13140 XD4=(A/T)^(-2-M*N)
13150 XDS(DUM)=XD1*XD3*XD4/XD2
13160 NEXT DUM
13400 RETURN
13450 REM ###########################################################
14000 REM
14001 REM      INCREMENT PLASTIC DISPLACEMENT
14100 VPL=VPL+IVPL
14105 IF VPL>=VPLM THEN 500
14110 P=W*T*BN*(Y(NUM)/X(0))^PP*(Y(NUM)/T)^M*(VPL/T)^(1/N)
14120 SIG=P/(W*T)
14200 RETURN
14420 JDAM(DUM)=1/JDAM(DUM)
14430 NEXT DUM
```

```
8498 REM
8499 REM ----------------------------------------------------------------
8500 REM                         POINT J CALCULATION
8501 REM ----------------------------------------------------------------
8502 REM
8580 REM                                        FIND GAVG
8590 GTOT=0
8600 FOR DUM=0 TO NUM
8610 GTOT=GTOT+G(DUM)
8620 NEXT DUM
8630 GAVG=GTOT/(NUM+1)
8640 REM
8700 GOSUB 13000
8705 REM
8710 FOR DUM=0 TO NUM
8720 J(DUM)=G(DUM)*(1+XDS(DUM)*(SIG/BN)^(N-1))
8725 NEXT DUM
8995 REM
8996 RETURN
8997 REM ###############################################################
8998 REM
8999 REM ----------------------------------------------------------------
9000 REM                         DELTA-a CALCULATION
9001 REM ----------------------------------------------------------------
9002 REM
9010 FOR DUM = 0 TO NUM
9015 START(DUM)=ADEL(DUM)
9020 ADEL(DUM)=(ALPA*J(DUM)^3+BETA*J(DUM)^2+GMMA*J(DUM))/F(DUM)
9025 IF ADEL(DUM)<START(DUM) THEN ADEL(DUM)=START(DUM)
9026 INCA(DUM)=ADEL(DUM)-START(DUM)
9027 REM
9090 NEXT DUM
9100 REM  MOVING AVERAGE TO SMOOTH OUT INCREMENTAL CRACK EXTENSION
9110 REM
9170 FOR DUM=1 TO NUM-1
9180 INCA(DUM)=(INCA(DUM-1)+INCA(DUM)+INCA(DUM+1))/3
9190 NEXT DUM
9200 INCA(0)=(2*INCA(0)+INCA(1))/3
9210 INCA(NUM)=(2*INCA(NUM)+INCA(NUM-1))/3
9496 RETURN
9497 REM ###############################################################
9498 REM
9499 REM ----------------------------------------------------------------
9500 REM                    ADVANCE THE CRACK FRONT
9501 REM ----------------------------------------------------------------
9502 REM
9510 FOR DUM=0 TO NUM
9520 X(DUM)=XO(DUM)+NX(DUM)*INCA(DUM):XO(DUM)=X(DUM)
9530 Y(DUM)=YO(DUM)+NY(DUM)*INCA(DUM):YO(DUM)=Y(DUM)
9535 IF X(DUM)>W/2 OR Y(DUM)>T THEN PRINT:PRINT"EXCESSIVE CRACK GROWTH"
9540 NEXT DUM
9590 REM
9997 RETURN
9998 REM
9999 REM ----------------------------------------------------------------
10000 REM        CALCULATION OF EFFECTIVE c ALONG CRACK FRONT
10001 REM ----------------------------------------------------------------
10002 REM
10004 A=Y(NUM)
10010 FOR DUM=0 TO NUM-1
```

```
4295 REM ####################################################
5998 REM
5999 REM -----------------------------------------------------
6000 REM                 PLOT THE CRACK FRONT ON SCREEN
6001 REM -----------------------------------------------------
6002 REM
6100 LOCATE 1,1:PRINT:PRINT "LOAD = ";P;" lbf           Vpl = ";VPL;" in
"
6110 REM
6125 LINE (2.6*X(0)/T,Y(0)/T)-(2.6*X(1)/T,Y(1)/T)
6130 FOR DUM = 1 TO NUM-1
6140 LINE (2.6*X(DUM)/T,Y(DUM)/T)-(2.6*X(DUM+1)/T,Y(DUM+1)/T)
6150 NEXT DUM
6996 RETURN
6997 REM ####################################################
6998 REM          .
6999 REM -----------------------------------------------------
7000 REM                 DIRECTION OF CRACK EXTENSION
7001 REM -----------------------------------------------------
7002 REM
7003 NY(0)=0:REM        CONSTRAINS EDGE TO HORIZONTAL FREEDOM
7004 NX(0)=1:REM        CONSTRAINS EDGE TO HORIZONTAL FREEDOM
7005 REM
7006 NX(NUM)=0:REM      CONSTRAINS CENTER TO VERTICAL FREEDOM
7007 NY(NUM)=1:REM      CONSTRAINS CENTER TO VERTICAL FREEDOM
7008 REM
7010 FOR DUM=1 TO NUM-1
7020 IY=Y(DUM+1)-Y(DUM-1):REM   DIFFERENCES IN POSITIONS FOR NEIGHBORING
7025 IX=X(DUM+1)-X(DUM-1):REM   POINTS ON THE CRACK FRONT
7029 REM
7030 PX=IY:REM                  CONVERT TO MEASURE OF SLOPE OF
7035 PY=-IX:REM                 THE PERPENDICULAR
7036 REM
7040 HYP=(PX^2+PY^2)^.5
7045 REM
7050 NX(DUM)=PX/HYP
7060 NY(DUM)=PY/HYP
7065 NEXT DUM
7070 REM
7996 RETURN
7997 REM ####################################################
7998 REM
7999 REM -----------------------------------------------------
8000 REM                      G CALCULATION
8001 REM -----------------------------------------------------
8002 REM
8010 FOR DUM=0 TO NUM
8020 PHI2=(1+1.464*(C(DUM)/A)^1.65):REM                    PHI2
8025 REM
8330 FW=(COS((PI*C(DUM)/W)*(A/T)^.5))^-.5:REM              FW
8335 REM
8400 IF A/C(DUM)>1 THEN GOSUB 11000 ELSE GOSUB 11500:REM M1,M2,M3,LG,FT
8405 REM
8410 FS=(M1+M2*(A/T)^2+M3*(A/T)^4)*LG*FT*FW
8430 REM
8440 K=SIG*FS*(PI*A/PHI2)^.5
8450 G(DUM)=K^2/E
8460 NEXT DUM
8496 RETURN
8497 REM ####################################################
```

```
2350 RETURN
2398 REM
2399 REM -------------------------------------------------------------
2400 REM                      PLATE DIMENSIONS
2401 REM -------------------------------------------------------------
2402 REM
2410 T=.25:REM              PLATE THICKNESS
2420 W=2:REM                PLATE WIDTH
2430 RETURN
2498 REM
2499 REM -------------------------------------------------------------
2500 REM           MATERIAL DEFORMATION PROPERTIES
2501 REM -------------------------------------------------------------
2502 REM
2505 PRINT:PRINT"MATERIAL:  21-6-9 SS"
2510 E=2.84E+07:REM         YOUNG'S MODULUS
2520 BN=110011!
2530 M=-.076
2540 PP=.0383
2550 N=5.75
2960 RETURN
2998 REM
2999 REM -------------------------------------------------------------
3000 REM                    J-dA CURVE INPUT
3001 REM -------------------------------------------------------------
3002 REM
3060 ALPA=7.226487E-14
3070 BETA=-6.2973138D-10
3080 GMMA=.0000040561366#
3150 RETURN
3198 REM
3199 REM -------------------------------------------------------------
3200 REM                    CRACK GEOMETRY
3201 REM -------------------------------------------------------------
3202 REM
3220 PRINT:INPUT "Initial A/T";ADT
3230 IF (ADT>1) OR (ADT=1) THEN GOTO 3220 .
3240 PRINT:INPUT "Initial A/C";ADC
3270 A=ADT*T
3280 C=A/ADC
3290 RETURN
3998 REM
3999 REM -------------------------------------------------------------
4000 REM                   SET-UP THE SCREEN
4001 REM -------------------------------------------------------------
4002 REM
4010 PI=3.14159265359#
4020 PIDT=PI/2
4030 FOR DUM = 0 TO NUM
4040    X(DUM)=C*COS(DUM*PIDT/NUM)
4050    Y(DUM)=A*SIN(DUM*PIDT/NUM)
4060 XO(DUM)=X(DUM):YO(DUM)=Y(DUM)
4070 NEXT DUM
4075 Y(0)=0!:X(NUM)=0!:YO(0)=0:XO(NUM)=0
4170 SCREEN 9
4180 WINDOW (-1,-.25)-(3.8,1.25)
4190 LINE (0,-.25)-(0,1.25)
4200 LINE (-1,0)-(0,0):LINE (2.6*C/T,0)-(3.8,0)
4210 LINE (-1,1)-(3.8,1)
4290 RETURN
```

```
5 CLS:CLEAR:KEY OFF:SCREEN 0
10 DEFINT D
11 DEFDBL A-C,E-Z
12 DIM X(50),Y(50),NX(50),NY(50),ADEL(50),TH(50),NXT(50),NYT(50)
13 DIM G(50),J(50),C(50),EXT(50),START(50),INCA(50),YD(50)
14 DIM XO(50),YO(50),XDS(50),JT(50),XT(50),YT(50),JDA(50),JDAM(50)
15 REM
35 GOSUB 2000:REM            MAXIMUM VPL AND VPL INCREMENT
40 GOSUB 2300:REM            NUMBER OF POINTS ALONG THE CRACK FRONT
45 GOSUB 2400:REM            PLATE DIMENSIONS
50 GOSUB 2500:REM            MATERIAL DEFORMATION PROPERTIES
55 GOSUB 3000:REM            J-R CURVE INPUT
60 GOSUB 3200:REM            CRACK GEOMETRY
65 GOSUB 4000:REM            SCREEN SET-UP
70 REM
71 REM -------------.MAIN LOOP --------------
72 REM
75 GOSUB 6000:REM            PLOT THE CRACK FRONT
81 REM
82      FOR DUM=0 TO NUM
83         J(DUM)=0
84      NEXT DUM
85 GOSUB 14000:REM           INCREMENT THE PLASTIC DISPLACEMENT
86 REM
90 GOSUB 7000:REM            DIRECTION OF CRACK EXTENSION
91 REM
92 GOSUB 10000:REM           CALCULATION OF EFFECTIVE C ALONG FRONT
93 REM
94 GOSUB 12000:REM           CALCULATE ELLIPTICAL ANGLES ALONG THE FRONT
95 REM
96 GOSUB 8000:REM            CALCULATE G ALONG THE CRACK FRONT
97 REM
98 GOSUB 8500:REM            CALCULATE Jtot ALONG THE CRACK FRONT
99 REM
100 GOSUB 15000:REM          CALCULATE dJ/da ALONG FRONT
101 REM
105 GOSUB 9000:REM           DELTA-A      .
106 REM
110 GOSUB 9500:REM           ADVANCE THE CRACK FRONT
111 REM
150 GOTO 75
500 END
501 REM ##################################################################
1998 REM
1999 REM -----------------------------------------------------
2000 REM              VPL AND VPL INCREMENT
2001 REM -----------------------------------------------------
2002 REM
2160 PRINT:INPUT "Enter the Maximum Plastic Displacement (in) ";VPLM
2170 IVPL=VPLM/50
2283 RETURN
2298 REM
2299 REM ------------------------------------------------------------
2300 REM           NUMBER OF POINTS ALONG CRACK FRONT
2301 REM ------------------------------------------------------------
2302 REM
2303 NUM=10
2304 NUM=NUM-1:REM    THIS ACCOUNTS FOR NUMBERING BEGINNING AT 0
2305 REM
2335 TH(0)=0:TH(NUM)=3.14159265359#/2
```

APPENDIX

COMPUTER PROGRAM LISTING

APPENDIX

4.4 Preliminary Results of Profiling

Two of the profiles produced has been included as figures (4.1a and 4.1b) for the sake of discussion. Figure (4.1a) is a profile of a crack taken at the surface. The precrack and the monotonic fracture regions are marked on the figure. Figure (4.1b) shows a profile of the same crack taken at the center of the cross-section. Again, the precrack, and the monotonic fracture regions are shown. The character of the two profiles is quite different. The monotonic fracture region at the surface (figure 4.1a) is at an angle to the precrack region, while that angle is not obvious for the central section (figure 4.1b). To illustrate a second observation, the net displacement has been
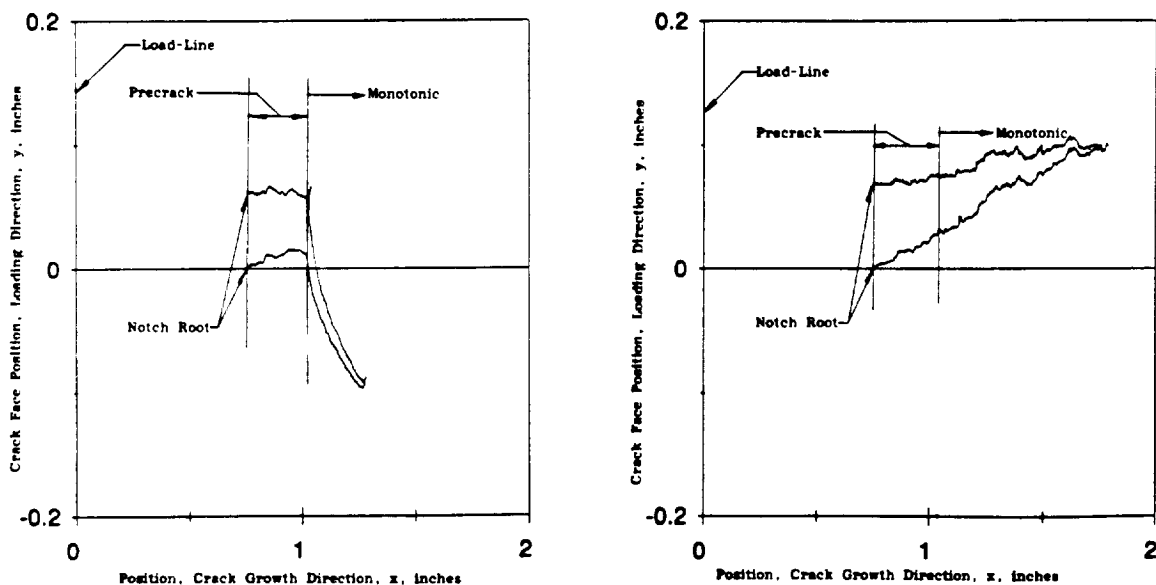
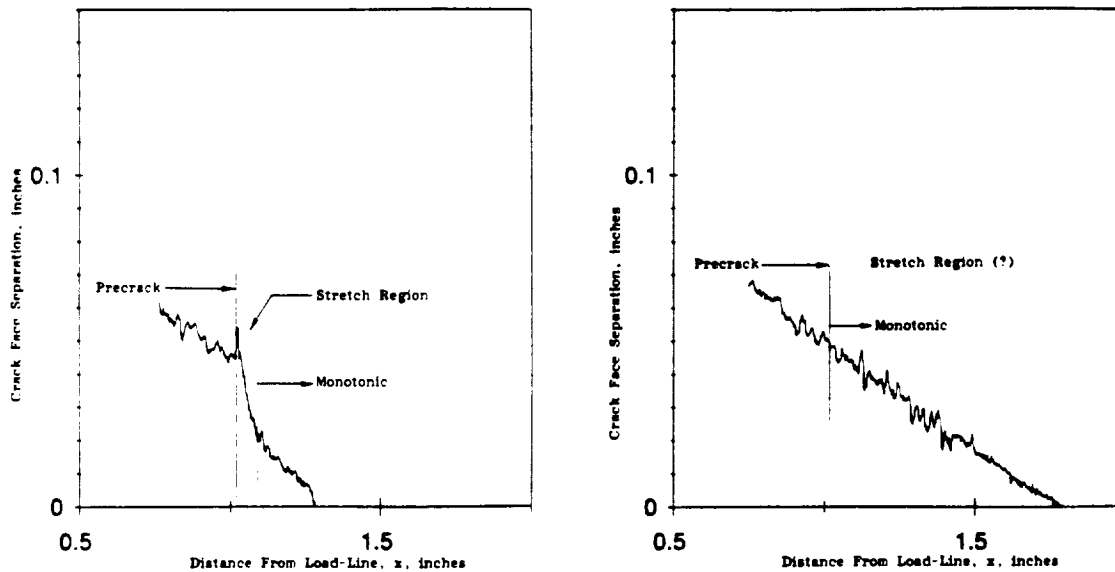Figure 4.1: Typical Crack Face Separation Profiles; (a) at surface, (b) at central cross-section.

Figure 4.2: Typical Crack Separation Plots; (a) at surface, (b) at central cross-section.

calculated as the difference between the y-values of the upper and the lower parts of the profile, and figures (4.2a) and (4.2b) have been included below to register this second observation.

In figures (4.2a) and (4.2b), the precrack region and the monotonic fracture region are again marked. The two separation profiles look dramatically different: a substantial region of stretch exists at the end of the precrack region and the beginning of the monotonic fracture region at the surface. This stretch is not apparent in the central cross-section.

At this time, the profile data is being developed and observations are being made.

4.5 Future Efforts

Profiling continues, and analysis of the profiles and synthesis of an approach to account for the constraint in the crack growth of these "planar" specimens.

4.7 <u>References</u>

[4.1]   H. A. Ernst, "Material Resistance and Instability beyond J-Controlled Crack Growth", *Elastic Plastic Fracture: 2nd Symposium, Volume I-- Inelastic Crack Analysis, ASTM STP 803*, Shih and Gudas, Ed., (1983), Pp. I-191-213.

[4.2]   Ernst, H. A., "Further Developments on the Modified J-Integral", *ASTM STP 995*, (1989), Pp. 306-19.

[4.3]   Rice, J. R., "A Path Independent Integral and the Approximate Analysis of Strain Concentration by Notches and Cracks", *Journal of Applied Mechanics, Transactions of the ASME*, June 1968.

[4.4]   Tada, H., Paris, P. C., and Irwin, G. R., *The Stress Analysis of Cracks Handbook*, Second Edition (1985), Del Research Corp., St. Louis, MO.

[4.5]   Hutchinson, J. W., "Plastic Stress and Strain Fields at the Crack Tip", *Journal of the Mechanics and Physics of Solids*, Vol. 16 (1968), Pp. 337-47.

[4.6]   Rice, J. R., and Rosengren, G. F., "Plane Strain Deformation Near a Crack Tip in a Power-Law Hardening Material", *Journal of the Mechanics and Physics of Solids*, Vol. 16 (1968), Pp. 1-12.